AD_____

Award Number: DAMD17-02-1-0581

TITLE: Analysis of Breast Cell-Lineage Response Differences to Taxol Using a Novel Co-Culture System

PRINCIPAL INVESTIGATOR: Lauren S. Gollahon, Ph.D.
Nathan Collie, Ph.D.

CONTRACTING ORGANIZATION: Texas Tech University
Lubbock, TX 79409

REPORT DATE: June 2005

TYPE OF REPORT: Final

PREPARED FOR: U.S. Army Medical Research and Materiel Command
Fort Detrick, Maryland 21702-5012

# REPORT DOCUMENTATION PAGE

*Form Approved*
*OMB No. 0704-0188*



| 1. REPORT DATE | 2. REPORT TYPE | 3. DATES COVERED |
|---|---|---|
| 01-06-2005 | Final | 1 Apr 2002 – 31 May 2005 |

**4. TITLE AND SUBTITLE**

Analysis of Breast Cell-Lineage Response Differences to Taxol Using a Novel Co-Culture System

**5a. CONTRACT NUMBER**

**5b. GRANT NUMBER**
DAMD17-02-1-0581

**5c. PROGRAM ELEMENT NUMBER**

**6. AUTHOR(S)**
Lauren S. Gollahon, Ph.D.
Nathan Collie, Ph.D.

Email: lauren.gollahon@ttu.edu

**5d. PROJECT NUMBER**

**5e. TASK NUMBER**

**5f. WORK UNIT NUMBER**

**7. PERFORMING ORGANIZATION NAME(S) AND ADDRESS(ES)**

Texas Tech University
Lubbock, TX 79409

**8. PERFORMING ORGANIZATION REPORT NUMBER**

**9. SPONSORING / MONITORING AGENCY NAME(S) AND ADDRESS(ES)**
U.S. Army Medical Research and Materiel Command
Fort Detrick, Maryland 21702-5012

**10. SPONSOR/MONITOR'S ACRONYM(S)**

**11. SPONSOR/MONITOR'S REPORT NUMBER(S)**

**12. DISTRIBUTION / AVAILABILITY STATEMENT**
Approved for Public Release; Distribution Unlimited

**13. SUPPLEMENTARY NOTES**
Original contains colored plates: ALL DTIC reproductions will be in black and white.

**14. ABSTRACT** We have established a new co-culture system in which human mammary epithelial cells (HMEC) and human mammary tumor cells (HMT) are physically grown together. We hypothesized that cells in co-culture (CC) would generate gene expression profiles different from homogeneous cell populations. In this study, cells were incubated with blue or red CellTracker Dyes and co-cultured. Our novel capture system allowed cells to be co-cultured and then quickly separated while maintaining ~90% viability. Using deconvolution microscopy, co-cultured HMEC were observed to form focal, gland-like structures surrounded by TTUderived from an invasive ductal carcinoma. Using a differential trypsinization technique, cell populations were rapidly separated to perform RNA extractions performed (<2 h) in order to obtain expression profiles from still viable cells. RT2 profiler PCR Array (SuperArray) RT-PCR was utilized to analyze differential gene expression between parent cell lines and cells co-cultured. We observed that in co-culture HMEC become more cancerous compared to homogenous parent HMEC and CC - TTUexhibit gene expression profiles considered to be less cancerous that that of parent HMT. Replated CC HMEC have both gene expression profiles of CC HMEC and parent HMEC, but were more similar to CC HMEC. Replated TTU showed similar results.

**15. SUBJECT TERMS**
Breast cancer, co-culture, gene expression profiles, Taxol, transport mechanisms

| 16. SECURITY CLASSIFICATION OF: | | | 17. LIMITATION OF ABSTRACT | 18. NUMBER OF PAGES | 19a. NAME OF RESPONSIBLE PERSON |
|---|---|---|---|---|---|
| a. REPORT | b. ABSTRACT | c. THIS PAGE | | | USAMRMC |
| U | U | U | UU | | 19b. TELEPHONE NUMBER *(include area code)* |

# Table of Contents

INTRODUCTION:

The subject of this research is investigating whether different normal cell types, isolated from primary breast tissue 1) respond differently in co-culture, 2) respond differently in co-culture when exposed to anti-tumor agents, than in homogeneous cell cultures. Our data showed that cells cultured as monolayers demonstrated very different responses to Taxol. The normal epithelial cells were highly sensitive, tumor cell sensitivity was linked to ER status and the stromal (fibroblast) cells were highly resistant. Therefore, we investigated whether normal cells influenced gene expression of breast cancer cells through co-culture interactions. Our hypothesis was that cultured cells allowed to physically interact would exhibit different response and genetic profiles than homogeneous cell cultures. Additionally, we were interested in determining whether these co-culture interactions would influence the cell response to an anti-tumor agent. For this portion, we used the anti-tumor agent Taxol. Once the baseline gene expression profiles were established, we then exposed the cells to Taxol in order to elucidate whether the cells most affected by the anti-tumor agent were the tumor cells, or whether the bystander effect was greater than anticipated, or if physical interactions between the normal and tumor cells conferred a protective mechanism against the anti-tumor agent. Furthermore, our results would show whether normal cells exhibited an inhibitory effect on tumor cells, or vice versa. Therefore we established a novel co-culture system that allowed us to identify and isolate cell types from mixed populations. This was based on three criteria, 1) fluorescent dyes, 2) cell surface antigens, 3) cell adhesion properties. In developing separation and isolation techniques, we also developed a novel, fast, convenient, inexpensive method to separate the cell populations with high accuracy (Du et al, 2006; Wankhede et al, 2006, [1, 2] appended). The scope of this project included co-culturing normal mammary epithelial cells with breast tumor cells, normal mammary epithelial cells with normal mammary stromal cells and tumor cells with normal mammary stromal cells.

A second major portion of this work is devoted to the transport mechanisms of the mammary cells in conjunction to drug delivery and efficacy. An anti-tumor drug delivered to the target tissue by even the most efficient route will fail if the tumor is resistant to that drug. Hence, studies of drug delivery and resistance are reasonable partners in the search for optimal treatment regimes. There are many mechanisms by which tumors become resistant to chemotherapeutic agents. Here, we focus on a clinically important category, that is, multidrug resistance mediated by plasma membrane efflux pumps. Almost 50 members of the ATP-binding cassette (ABC) transporter superfamily are expressed in a wide variety of normal human cells, where they play physiological roles ranging from the defense against xenobiotics to the transport of phospholipids, cholesterol, ions, and a host of other essential solutes [3, 4]. Unfortunately, some of these transporters are expressed in tumor cells, where they confer multidrug resistance by extruding a wide range of chemotherapeutic drugs. Best known among these is P-glycoprotein (P-gp), a 1280 amino-acid, single polypeptide encoded by the human *MDR1* gene [5]. This plasma membrane protein contains two transmembrane domains, each with six membrane-spanning $\alpha$-helices, that mediate substrate binding [6]. In addition, two intracellular nucleotide-binding domains each contain the Walker A and Walker B motifs along with the ABC signature sequence that identifies P-gp as a member of the transporter superfamily. ATP hydrolysis by these domains drives the conformational changes resulting in active solute efflux from the cell [7]. P-gp is expressed in many normal endothelial and epithelial tissues, including the blood-brain and blood-testis barriers, intestine, liver, kidney, and bladder. However, overexpression of P-gp is also common in many neoplasms, contributing to resistance to most of the commonly used anti-tumor drugs (e.g., taxanes, anthracyclines, vinca alkaloids, epipodophyllotoxins). The majority of carcinomas originating in the colon, rectum, pancreas, liver, and kidneys overexpress P-gp intrinsically. Furthermore, when patients become unresponsive to chemotherapy, P-gp overexpression appears in those with breast, ovarian, and small-cell lung cancer and with metastatic gliomas, leukemia, lymphoma, mutiple myeloma [reviewed in 8, 9, 10].

**Body of the Report**

The rationale for this proposed research project stems observations by von Zglinicki et al.,[11, 12]. They reported that hyperoxic conditions (40%) induced a cellular senescent phenotype in lung fibroblasts after 2 weeks in culture. These results prompted us to investigate whether the same phenomenon would be repeated in human mammary stromal (HMS) cells. In addition, we were curious whether human mammary epithelial (HME) cells would respond differently considering their apparent differences in p53 and pRb regulation and function [13-17]. We observed that the stromal cells died after 14 days in culture under hyperoxic conditions (personal observations) as von Zglinicki et al., [11, 12]observed. In contrast to these observations, the normal epithelial cells continued to grow without significant differences from the control cultures. We then incubated spontaneously immortalized HME cells [15] as well as immortalization-induced corresponding HME/HMS cells [13, 16, 18]under hyperoxic conditions. As expected there was no difference in the growth rates of the immortal HME cells regardless of the mechanism of immortalization. Interestingly, the immortal HMS cells also did not show any decrease in growth rates. These results suggested that there is an inherent difference in the way epithelial cells and stromal cells respond to DNA damage and that upon immortalization, the stromal cells acquire a mechanism to bypass the cell cycle regulation to DNA damage conditions observed in the mortal HMS cells.

We had previously co-cultured HME/HMS cells separated by a microporous filter. A medium that supports both cells at >80% normal growth was developed. During these co-culture experiments, the density of HME to HMS cells was observed to enhance the growth of HMS cells. The converse experiment showed that HME cell growth was independent of HMS cell density. However, the cells were never in physical contact. Other studies [19-22] show that fibroblast cells may participate in either cancer inhibition or progression. Co-culture experiments showed that stromal cells had an inhibitory effect to both epithelial and tumor cell growth [20]. Thus interactions between HME and HMS cells may enhance regulatory mechanisms and/or DNA damage control. If this assumption is correct, then there may be functional differences in gene expression between cell types that have a synergistic effect. Not only would cells with DNA directly affected start repair, but there may also be signaling between cells that would initiate repair mechanisms. In a co-culture study by Dong-Le Bourhis et al., (1997) [20], they found evidence to suggest a tumor-growth-regulatory mechanism exhibited by HME and HMS cells collectively. Therefore we investigated the effects of co-culture as a function of physical interactions. A methodology previously not well developed.

***Task I. Co-culture human mammary epithelial (HME) cells and corresponding human mammary stromal (HMS) cells under control conditions and in the presence of Taxol: (Year 1).***
**1a.** Determine growth patterns for concurrent cultures of control and treated HME - HMS cells using fluorescent microscopy. (Months 1 -- 6).

***Task 2.*** **Co-culture normal HMS cells with corresponding tumor cells under control conditions and in the presence of Taxol: (Year 2):**
2a. Determine growth patterns for concurrent cultures of control and treated HMS - tumor cells using fluorescent microscopy. (Months 12 - 18).

***Task 3.*** **Co-culture normal HME cells with corresponding tumor cells under control conditions and in the presence of Taxol: (Year 3):**
3a. Determine growth patterns for concurrent cultures of control and treated HME - tumor cells using fluorescent microscopy. (Months 24 - 30).

**These experiments were performed concurrently and thus are reported concurrently.**

***Cells and Cell Culture.*** Generally, cultured cells are in monolayers. In addition, when cells are first isolated from primary tissues, different media types are used to distinguish cell-lineage specific growth, i.e. epithelial cells grow well is serum-free media plus supplements, whereas fibroblast (stromal cells) grow well in serum supplemented DMEM

[15].Tumors cells vary between different basal formulas but are also serum supplemented [23]. Figure 1 shows the different cell types and their characteristic morphologies once they have been isolated and grown in a specific medium. If the media are switched between the epithelial and stromal or tumor cells, it has been our experience that cell viability deceases significantly [24]. Therefore, the goal of these experiments was to demonstrate that a medium could be formulated which allowed the co-culture of two different cell lineages with >80%viability retained. Figure 2 shows the growth curves for the cells in the optimized medium formulation. The medium formulation was determined to consist of serum-free fibroblast basal medium (FBM - Clonetics) and supplements from the MCDB 170 mammary epithelial medium formulation [15]. Cell culture experiments with HME, HMS and tumor cells showed growth curves with >80% viability for all the cell types. It would appear that the supplemental bovine pituitary extract and the addition of insulin, transferrin and hydrocortisone were sufficient to sustain cell growth. Originally epidermal growth factor was included in the formulation. Initial culture experimental results suggested fibroblast growth factor was also needed and was therefore added to the medium in order to encourage HMS cell growth.

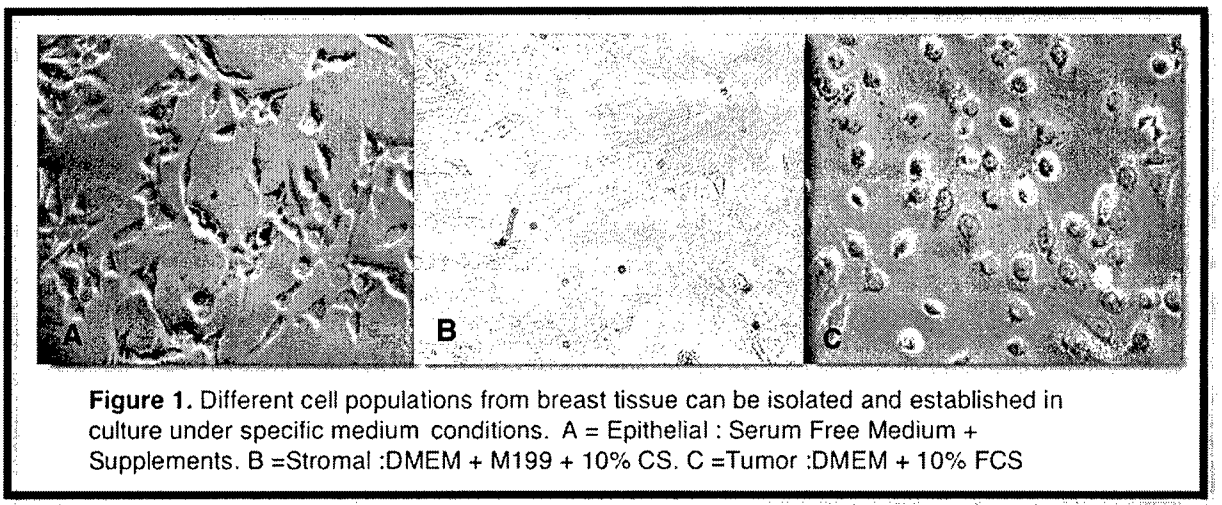


**Figure 1.** Different cell populations from breast tissue can be isolated and established in culture under specific medium conditions. A = Epithelial : Serum Free Medium + Supplements. B =Stromal :DMEM + M199 + 10% CS. C =Tumor :DMEM + 10% FCS

*Cell culture:* Human mammary cells used for this project were obtained from patients undergoing breast cancer surgery. Tissues adjacent to areas of surgical resection were harvested and enzymatically dispersed into primary cultures (for complete review of the cell line history, please see [15]. The nomenclature consists of the type of cell followed by the patient number eg. HME 50 indicates human mammary epithelial cell derived from patient # 50. Subclones have been further indicated by clone number eg. HMS 50-5. Retrovirally infected cells used to obtain immortalized cells are indicated by cell type followed by the introduced gene of interest. All infections are performed using human papilloma virus type 16 (HPV type 16) under the transcriptional regulation of the moloney murine leukemia virus (MMLV) promoter sequence (12). The HPV E6 and E7 proteins have been shown to bind and inactivate p53 and pRb respectively [25]. While the mortal cells have limited replicative potential in culture and senesce at ~50 pdl, the same cells when immortalized with E6/E7 have unlimited replicative potential. Spontaneously immortalized cells denoted 'e' have unlimited replicative potential in culture. These were also used for the study.

*HME cells-* HME 50-5, HME50-5e, HME 50-5 16E6, HME 50-5 E6/E7 were used. HME 50 cells have obtained from a patient with Li-Fraumeni syndrome (LFS). LFS patients have a germ line mutation of p53 and show multiple primary tumors beginning very early in their life [26]. The study focused on these cells because of the comprehensive sets of cells that were available (mortal, spontaneously immortalized and induced immortalized). All the HME cells were grown in serum-free MCDB-170 media (Life technologies) supplemented with 0.4% bovine pituitary extract (BPE), 5 μg/ml insulin, 10 ng/ml epidermal growth factor (EGF), 0.5 μg/ml hydrocortisone, 5μg/ml transferrin and 25 μg/ml gentamycin sulfate [15].

*HMS cells-* HMS cells used for the study had the same origin as HME 50. They were separated from the tissue using enzymatic dispersion, followed by selective growth using 10% FBS (fetal bovine serum) supplemented media. This media prevents the growth of mammary epithelial cells while promoting the growth of stromal cells. The nomenclature is the same as HME cells. The cells used were HMS 50 and HMS 50 16E6/E7. HMS 50 16E6 transfected cells were not used because inactivation of both pRb and p53 is required for immortalization in fibroblasts [27]. The mortal cells senesced at ~ PDL 55. All HMS cells were cultured in DMEM-XSG media consisting of 4 parts of DMEM (Dulbecco's modified Eagle media) and 1 part of medium-199 supplemented with 10% CCS (cosmic calf serum-Hyclone) and 25 μg/ml gentamycin sulfate.

*Tumor cells-* The institution of origin followed by the patient number was used for naming the tumor cells. TTU-1 and SCC -1419 were used for this study. Both have been derived from invasive mammary ductal carcinoma. SCC 1419

is ER+/PR- and TTU-1 is ER-. Both cell lines have undergone transformation as evidenced by aneuploidy and foci formation and require serum for maintenance *in vitro [23].* Cells were grown in DMEM with 10% FBS and 25 μg/ml gentamycin sulfate at 37° C under 5% $CO_2$.

*Taxol Treatment-* Taxol (Sigma) was dissolved in DMSO as per the manufacturer's instructions and diluted further to working concentration using medical grade saline and stored at -20° C. The concentrations made were $10^{-2}$ M, $10^{-3}$M and $10^{-4}$ M. Cells were allowed to grow for 48 hours under normal conditions followed by treatment with media containing Taxol. Taxol concentrations used were 2.54 x $10^{-6}$ M and 2.21 x $10^{-7}$ M. These concentrations were chosen based on previous studies and on the mean plasma level of Taxol in patients who had received a 24 hours infusion schedule [28-31]. Following 48 hours treatment with Taxol, cells were grown in media without Taxol for the indicated length of study.

*Cell Counting-* Cells were counted using a Coulter Counter (model ZI). Two methods were used for counting. The first one, involved aspiration of media followed by rinsing with buffered saline solution, treatment with trypsin-EDTA for 2 minutes, followed by aspiration and incubation at 37° C/ 5mins. The cells were then collected in media and counted. The second method involved incubation with trypsin at 37°/ 5 mins following the rinsing. Trypsin was then collected and the cells were counted.

**Live/Dead Assay-** Cell viability following treatment with Taxol was done using the live/dead viability assay (Molecular Probes). Viable cells emit green fluorescence at an excitation of 495 nm whereas the dead cells show intense red fluorescence on excitation at the same wavelength. Assays were performed as per the manufacturer's direction. Cells were visualized using inverted fluorescence microscope (Olympus BH-2) and photographs taken using Kodak film. Nonviable cells seemed to have lost adherence to the plate and were lost on aspiration before staining and hence not visualized in the assay. Statistical analysis using Bio-Tech fluorescence micro-plate reader and KC4 software package was therefore used to show that the ratio of live to dead cells was similar to the cell counts for the same.

**Statistical analysis-** Analysis and interpretation of data from cell counts and microplate fluorescence reading was done using one way ANOVA included in the SPSS statistical software package.

**Time dependence on cell viability experiment-** A time course experiment was conducted to see if shorter exposure time had any effect. Cells were counted and assayed at 0, 3, 6, 24 and 48 hours.

Studies in our lab [32] showed that HME cell strains 32 and 50 were highly sensitive to Taxol exposure followed by the tumor cells. Surprisingly, Taxol did not significantly affect corresponding HMS 32 and 50 cells. These cells were obtained from normal tissue outside the area of resection. The 50 series originated from a patient with Li-Fraumeni Syndrome. This condition is characterized by a germ line mutation in the p53 allele [26].The 32 series were obtained from a patient undergoing a reduction mammoplasty [16, 18]. Both cell strains have been previously characterized [15, 16, 18]. Normal diploid cells and cells induced to immortalize with human papillomavirus (HPV) type 16 E6E7 and/or HPV 16 E6 were analyzed for cellular response to Taxol. The HME 50 series also gave rise to a spontaneously immortalized cell line [15]. In addition to the HME and HMS cells, we analyzed two breast tumor-derived cell lines. TTU-1 originated from a patient undergoing radical mastectomy and was diagnosed as an invasive ductal carcinoma. The primary culture was established prior to this study in our laboratory. The second tumor cell line, SCC 1419, was established from a patient undergoing resection for an invasive ductal carcinoma. We have previously characterized this tumor cell line [23]. Thus, corresponding normal mortal, spontaneous immortal and induced immortal cells (non-transformed) were studies as well as the two distinct breast tumor cell lines.

Corresponding strains of HME and HMS cells (designated HME 50, or HMS 50) transfected with GFPs were co-cultured. Original tissue samples were obtained from areas outside the margin of resection in patients undergoing breast cancer surgery. Life span in culture for these cells was previously characterized [23] as well as population homogeneity. Freshly resected tissue was mechanically and enzymatically dispersed with a mixture of hyaluronidase and collagenase as previously described [15, 18, 23]. After the initial separation, cultures were established in either a serum-free medium (MCDB170) or a DMEM based medium supplemented with fetal bovine serum. The primary cultures were then assayed for cell specific markers. Cytokeratin 14 and 18 were used to distinguish between populations of luminal epithelial and myoepithelial cells (data not shown). Alpha actin and vimentin antibodies were used to distinguish fibroblast cells from epithelial cells (data not shown). In addition to these preliminary cell characterization studies, epithelial cultures were fed with FBS-based medium and fibroblasts with MCDB 170 supplemented medium. As expected, the cells died in the medium formulated specifically for their counterparts. The

HME cell populations described above were primarily composed of myoepithelial cells [15, 18, 23] and personal observations).

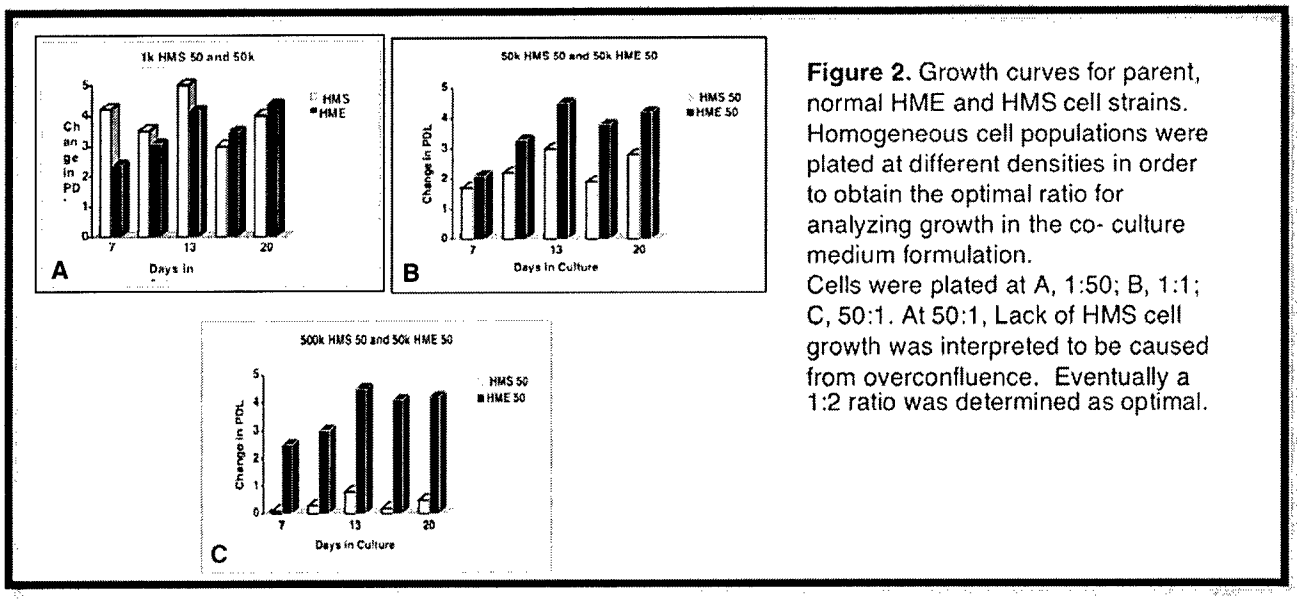


**Figure 2.** Growth curves for parent, normal HME and HMS cell strains. Homogeneous cell populations were plated at different densities in order to obtain the optimal ratio for analyzing growth in the co- culture medium formulation. Cells were plated at A, 1:50; B, 1:1; C, 50:1. At 50:1, Lack of HMS cell growth was interpreted to be caused from overconfluence. Eventually a 1:2 ratio was determined as optimal.

***Cell Viability Studies.*** Determination of programmed cell death. The LIVE/DEAD viability/cytotoxicity Kit (Molecular Probes) was utilized as a measure of cell death. This assay will show the percent of cell death in the mortal and immortal HME and HMS cultures. This detection kit is based on simultaneous criteria of plasma membrane integrity and intracellular esterase activity. Calcein AM is a cell permeant that is enzymatically converted to intensely fluorescent calcein (530nm) in viable cells. The second dye, (EthD-1), an ethidium homodimer, intercalates into the DNA of cells with plasma membrane disruption, and fluoresces intense red (>600 nm). We have previously optimized the concentrations for these stains at, 0.5 μM calcein AM and 5.0 μM EthD-1. Random fields of vision were photographed on an Olympus BH2 inverted microscope using Kodak Elite print film. For this study, parallel cell cultures will be counted using the Coulter Counter™ and stained using the viability assay. Representative fields of vision will be photographed for the stained cell cultures.

Live/dead cell populations were determined by photomicrography and cell counts. For cells in co-culture, the cells were first isoleated based on GFP emissions, then stained by cell surface antigens and confirmed by CellTracker dye. Finally, they were assayed for viability. Parallel cultures were photographed before and after population mixing. For this task, we utilized deconvolution microscopy in lieu of confocal microscopy. The rationale was twofold. First, the dichroric filters allowed us a broader range in which to observe the FP variants. Secondly, deconvolution microscopy employs bright white light filtered to produce the desired wavelengths. As a result, there is no laser to harm the cells and they remain viable longer.

*HME Cells.* Cell viability was determined after 48h Taxol exposure using three treatment groups CTRL (No Taxol), Low ($2.21 \times 10^{-7}$ M Taxol) and High ($2.54 \times 10^{-6}$ M Taxol). Cell counts showed significant differences ($P \leq 0.05$) between the three treatment groups in the ANOVA for all of the HME 50 series. Similar statistical results were obtained from fluorescence ratios using the LIVE/DEAD cell viability assay (Molecular Probes) measured by microplate reader. Representative graphs of cell counts and plate reader results are shown in Figures 3 A and B, respectively. The one-way ANOVA also showed significant differences in cell counts between treatment groups in all HME cells regardless of strain. In addition to the observed differences in the number of viable cells, differences in cellular morphology between the treatment groups were also observed. The most striking was evident between the control group and the high dose treatment group.

*HMS Cells.* Cell viability was determined for HMS cells after 48h treatment with Taxol using the same concentrations previously described for the HME cells. Viable cells were counted and results were analyzed for both HMS 50 and HMS 50 16E6E7 cell types. Surprisingly, no significant difference between the three treatment groups was demonstrated. Fluorescence emission data taken from the LIVE/DEAD assay also showed no significant difference between cell types. Fewer replicates of the HMS cells were performed due to the problems of

cells becoming over-confluent and detaching from the plate before either counts or Live/Dead assays could be performed. The fact that the cells became over-confluent (personal observations) confirms the data that was obtained reflects the true response of these cells to Taxol. Figure 4 show representative HMS 50 cell counts and fluorescence emissions statistical analyses.

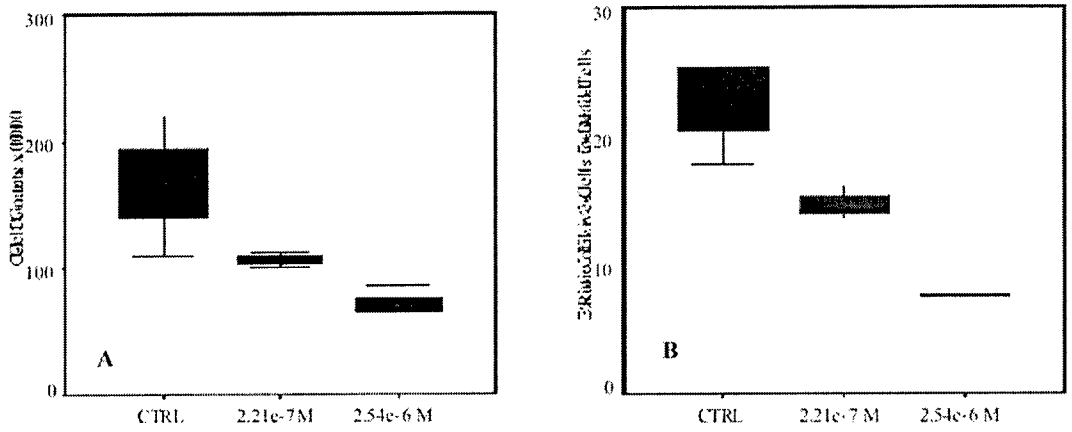


**Figure 3.** Representative graphs of HME cell viability after 48h Taxol exposure. A) Cell counts were obtained using a Coulter Counter. B) Fluorescence emissions were obtained using the LIVE/DEAD cell viability assay and measure red using a Bio-Tek fluorescence plate reader. Treatment groups: CTRL (No Taxol), Low ($2.21x10^{-7}$ M Taxol) and High ($2.54x10^{-6}$ M Taxol).

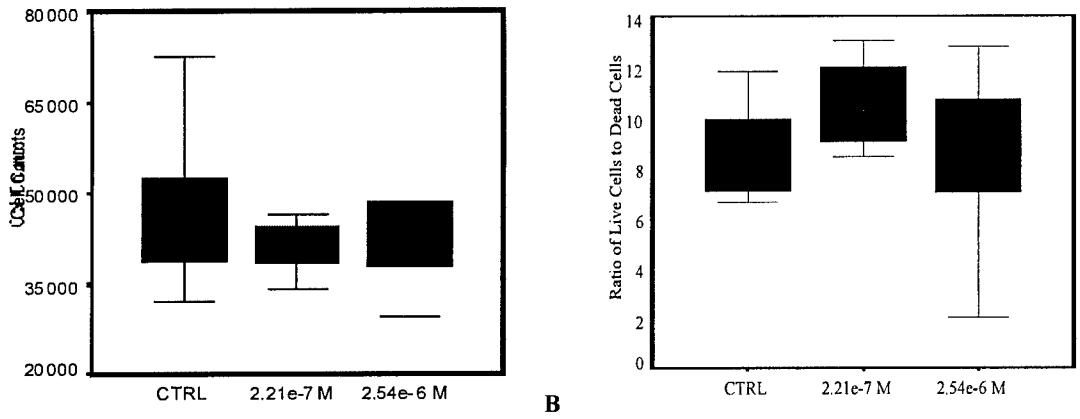


**Figure 4.** HMS cell viability statistics after 48h Taxol exposure. A) Cell counts were obtained using a Coulter Counter. B) Fluorescence emissions were obtained using the LIVE/DEAD cell viability assay and measuring red fluorescence using a Bio-Tek fluorescence plate reader. Treatment groups: CTRL (No Taxol), Low ($2.21x10^{-7}$M Taxol), High ($2.54x10^{-6}$M Taxol).

*Tumor Cells.* The tumor cell lines tested, TTU-1 and SCC 1419 showed varying degrees of sensitivity to Taxol. The differences in growth rates correlated with expected sensitivity to Taxol. TTU-1, which grew faster under normal culture conditions was much more sensitive to Taxol treatment versus SCC 1419. For both cell lines, cell counts and fluorescence readings paralleled each other, as was the case for both HME and HMS cells. Figures 5A and B are graphical representations of TTU-1 and SCC 1419 sensitivity to Taxol, respectively. Fluorescence microscopy results for both TTU-1 and SCC 1419 paralleled the cell counts and data from the fluorescence microplate reader. Death patterns were similar to those observed in the HME cells following treatment. Interestingly, there appeared to be foci formation of viable cells developing in the TTU-1 cells following exposure to Taxol. Figure 6 is a representative photomicrograph of TTU-1 cell viability following exposure to Taxol for 48h.

*Cell viability and morphology.* Cell counts showed significant differences ($P \leq 0.05$) between the control, low and high Taxol treatment group in ANOVA for all of the HME 50 series. Similar statistical results were obtained from fluorescence ratio using the LIVE/DEAD assay measured by the microplate reader. Representative graphs of cell count and plate reader are shown in Figures 3,4 and 6. In addition, difference in cellular morphology between the treatment groups was also observed. The most striking differences were evident between the control and high dose treatment group.

No significant difference was seen between the treatment groups in HMS 50 or HMS 50 16E6/E7. Fewer replicates of the HMS cells were performed due to the problems of over-confluency and loss of cells. Figure 4 shows the HMS 50 cell counts and fluorescence emission statistical analysis. Interestingly cellular morphology appeared to be normal from the LIVE/DEAD assay for these cells.
TTU-1 and SCC-1419 cells showed varying degree of sensitivity to Taxol. Death patterns were similar to HME cells following Taxol treatment. There appeared to be foci formation of viable cells developing in TTU-1 following Taxol treatment (Figure 5).

*Dependence of cell viability on exposure time.* For the HME cells Taxol began to show its effect between 24-48 hrs. HMS cells did not show any significant difference over the time period. Hence the exposure time was extended to 96 hrs. But no significant difference was found even after 96 hrs. The tumor cell sensitivity was associated with ER status. The ER negative tumor cell line TTU1 showed higher resistance and quicker recovery times than did the ER positive SCC 1419 cells (Figure 9).

*Cell recovery after exposure to Taxol.* HME cells never fully recovered after Taxol treatment. Though some replicates showed slight increase after 48 hours, it was not observed globally. In fact a decrease in cell count was seen over a 7 day period and after 14 days counts taken were not much different from those taken at 7 days. Control groups for all cell types showed increased cell counts over this period eliminating contact inhibition as a factor in decreasing cell number. Initial Taxol concentration did not seem to influence this loss.
HMS cells showed increased growth after exposure to Taxol for each given interval. At day 14, cells were so over-confluent that they detached as a single sheet and hence no data is reported for 14 days (Figure 9).
Tumor cells recovered almost completely with no recognizable difference between TTU-1 and SCC-1419 unlike those observed in the cell counts. Again due to over-confluence 14 days data is not reported.

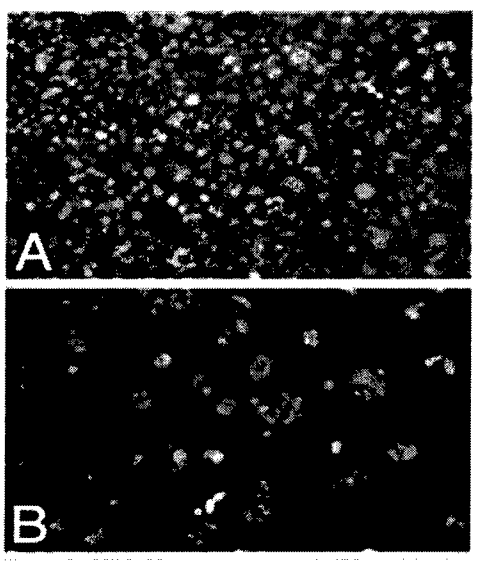


**Figure 5.** Tumor cells (TTU-1 and SCC 1419) were exposed to Taxol for 48h at the high concentration of $2.54 \times 10^{-6}$ M. Cell viability was assayed using the LIVE/DEAD cell viability kit from Molecular Probes. Green cells (calcein) were viable and red cells (ethidium homodimer) were dead. A) TTU-1 cells – Taxol; B) TTU-1 cells after Taxol exposure. Note that the overall number of cells in B is significantly less than the control group (A). The lack of ethidium stained cells is due to their detachment after the initial Taxol insult. These cells were catalogued as non-viable since collection of the supernatant and subsequent replating did not yield an attachment of cell growth after 1 week as determined by cell counts.

Mitotic index was viewed as being a possible explanation for the differences between cell types. However, the HMS cells in the treated groups showed growth curves comparable with the control cultures. In addition, the treated cultures frequently became over confluent in the culture dish after Taxol exposure. Thus, cell turn over did not to be the reason for the cells' apparent resistance to Taxol. Interestingly, the immortal cells appeared to be more affected than the mortal cells. Figure 5 is a representative photomicrograph of TTU-1 cell viability following exposure to Taxol for 48h. If cell ploidy is a determining factor for Taxol resistance, aneuploid cells would be expected to be more sensitive given the inability to correctly segregate the DNA. This does not correlate with the HME data in which the mortal, normal diploid cells were significantly more sensitive to Taxol than any of the HMS cell cultures.

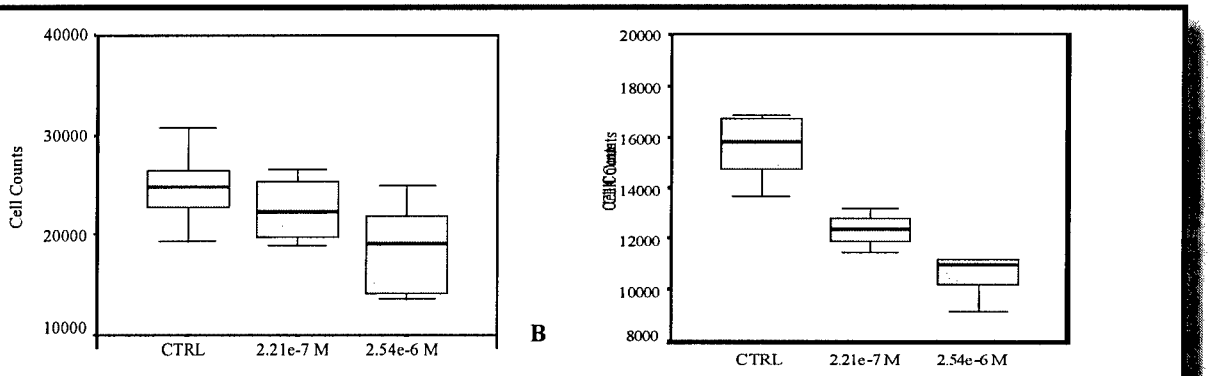


**Figure 6.** Tumor cell viability statistics are demonstrated in A and B after 48h Taxol exposure. A) Cell counts were obtained using a Coulter Counter. B) Fluorescence emissions were obtained using the LIVE/DEAD cell viability assay and measure red using a Bio-Tek fluorescence plate reader. Treatment groups: CTRL (No Taxol), Low ($2.21x10^{-7}$ M Taxol) and High ($2.54x10^{-6}$ M Taxol).

***Growth Patterns and GFP Identification.*** The goal of this set of experiments was to determine growth patterns occurred for cells in control and treated co-cultures. We had some initial setbacks. These included a delay of one month in transferring the graduate student (Sheree Case) to this project. Once the project experiments were underway, there was a problem with contamination. That took approximately 3 weeks to 1 month to isolate, clear and assess the damage to the cell lines. Several normal HMS and HME cells lines became infected. The depletion of the mortal cell stocks prompted our decision to introduce the catalytic reverse transcriptase enzyme component of telomerase (hTERT) through defective retroviral transfection. This construct was previously described in [33, 34]. This was mentioned in the initial proposal as an alternative step to maintaining normal cell lines if the mortal, primary cell cultures became a limiting factor. It has been shown in the literature that introduction of hTERT does not induce transformation nor a tumorigenic phenotype in the cells [35, 36]. To that end exogenous hTERT has been introduced into HME and HMS 73 and 87 respectively and selected with puromycin. This procedure was previously described in [35-37]. We have prior experience with such techniques, [13, 15, 38]. The only modification was the substitution of hTERT as the introduced species and selection under puromycin at concentrations between 25ng/ml to 50 ng/ml for 1 week). Upon selection of viable clones, the cells have been subcultured and frozen stocks replenished. This procedure took approximately 2 months to complete.

In order to determine whether co-culture would reveal potentially important cell specific differences to anti-tumor agents, we first investigated whether cell sensitivity would be observed in homologous populations of breast cell types treated with Taxol. The rationale for testing the effects of Taxol (paclitaxel) on the cell lineages is based upon the results observed under hyperoxic conditions where the HME cells continued to grow regardless of the 40% oxygen conditions while the HMS cells died. These data strongly suggested that different cell types might also respond differently to anti-tumor agents.

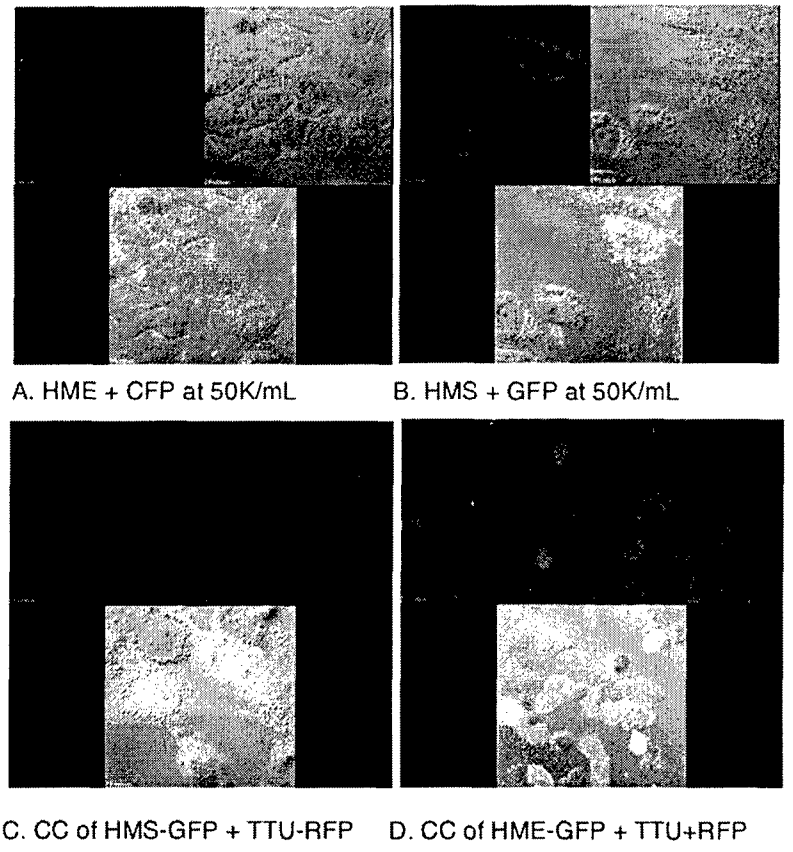


**Figure 7.** Representative HME, HMS and TTU cell cultures with transfected FPs in homogeneous cultures (A, B) and co-cultures (C,D). Although several different variants of FPs were transfected into the cells, after several months in culture, the fluorophores began to lose intensity. In addition, we began to observe unequal intensities and expression in homogeneous cell populations with FPs. Therefore, although the transfections were successful and cell identification was possible, the variability between cell populations was not consistent enough to rely fully on this technique alone to determine cell growth patters. To address the problem, we tried adding more selection antibiotic . However, we did not try different expression vectors or change promoters.
Instead, as will be shown later, we turned to the alternate solution of using cell permeant dyes from Molecular Probes. Magnification: A and D, 40x; B and C, 20X Images generated sing deconvolution microscopy.

*Exposure Time and Cell Viability.* After determining the sensitivity of the different cell types to Taxol treatment for 48h, the next step was to determine if cellular sensitivity was time dependent. Since the HME cells were significantly affected after 48h, a time course experiment was conducted to determine if shorter exposure times had any effects. Cells were counted and assayed at 0, 3, 6, 24, and 48h. For the HME cells, Taxol effects begin to take place between 24 and 48h, which was consistent with the time it takes the cells to go through the cell cycle. The tumor cells grew much more rapidly than the HME cells and quickly dominated the 24 well plates. Taxol treated HME cells number was much more than control HME cells. The number of Taxol treated TTU cells was similar to that of control TTU cells. The number of co-culture HME cells and TTU cells was much more than the number of homogenous TTU plus homogenous HME because of synergistic effect.

In contrast, HMS cells did not show significant differences between treatment groups from 0 to 48h exposure to Taxol. Therefore, an extended exposure time of 96 h was performed. Cell counts revealed no significant differences among treatment groups after the extended exposure to Taxol. This finding confirms the previous test results with HMS cells showing very little sensitivity to Taxol exposure.

Taxol is frequently used in breast cancer chemotherapy. Taxol stabilizes the dynamic microtubule environment in the cell by binding to the beta subunit of tubulin causing a blockage in mitosis. At high dosages it forms a static microtubule environment, [39-45]. At low dosages Taxol has been shown to affect the cells at metaphase by formation of multiple asters [29, 43, 46-48]. In addition, there is a relationship between Taxol, p53 and p53-associated proteins [46, 49-53]. Wahl et al., (1996) [49] showed that a reduction in normal wild type p53 levels correlated with a G2/M arrest and conferred Taxol treatment with a higher level of toxicity. Cells that survived continued through the cell cycle and accumulated in G1 where increased levels of p53 were evident. Panno et al, (2006) [46] showed evidence that low doses of Taxol enhanced the functional transactivatory properties of p53 on the p21 waf promoter in MCF-7 cells.

The toxicity in G1 arrest was not as great since the cells had already progressed through mitosis. p53 is stimulated in response to some cell stress. The most common stress condition investigated with respect to p53 is DNA damage, but other signaling conditions include hypoxia, changes in cell adhesion, and *depletion of microtubules* [54-57].

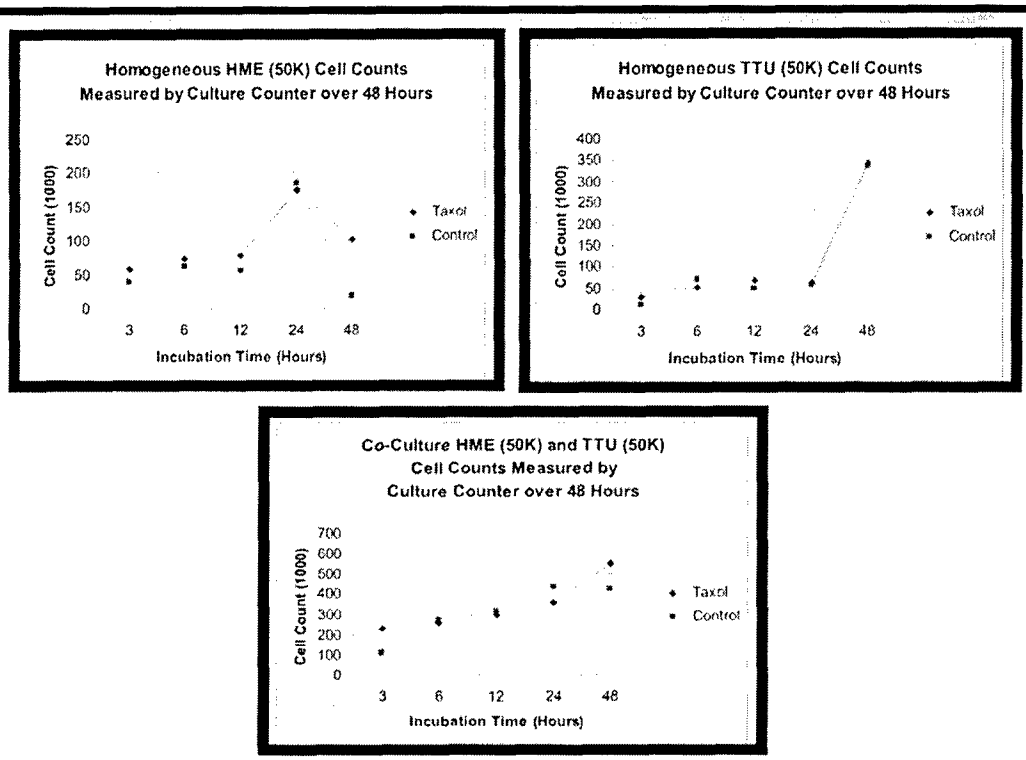


**Figure 8. Homogenous HME 50HT-GFP, homogenous TTU1-DsRedFP cells, and Co-culture of HME50HT-GFP and TTU1-DsRedFP cells Counts.** Homogeneous 50K HME50HT-GFP, homogeneous 50K TTU1-DsRedFP and Co-culture of HME50HT-GFP (50K) and TTU1-DsRedFP (50K) cells were plated in 24-well plates (Falcon). Cells were cultured for 5 days in FBM medium. Cells were treated with 2.21 x $10^{-7}$ M Taxol on the 5th day. Control plates and Taxol treated cell plates were counted after 48 hours using Coulter Z Series particle count and size analyzer.

In previous experiments, HME 50 cells were highly sensitive to Taxol and TTU-1 cells showed similar death curves with HME in Taxol. However, this data set demonstrates different death curves for HME 50HT-GFP cells and TTU1-DsRedFP cells. Interestingly, these cells were not significantly affected by Taxol when in co-culture conditions. GFP= Green Fluorescent Protein, DsRedFP=Discisoma sp Red Fluorescent Protein, HT=hTERT.

Immunocytochemistry demonstrated cell morphology changes reminiscent of the HME cells (data not shown). This is not surprising considering that these breast tumor cells are epithelial in origin. What was surprising was the fact that the tumor cells were less sensitive than the normal cells. Whether this is a function of cellular uptake and efflux or due to other factors such as ER/PR status will be addressed in this proposal. ER/PR status has been shown to be important in tumor cell response to chemotherapy and adjuvant endocrine therapy. There is also a possible connection with the cell cycle proteins bcl-2 and c-myc. [58-62]Sutherland et al. [63] showed that estrogen can bind to c-myc progressing the cell through G1. PR was postulated to bind to bcl-2 and progressing the cell through G1. The hormone receptor status may therefore play a role in cell sensitivity to Taxol through this c-myc, bcl-2 relationship. What that interaction may be has yet to be determined.

*Cellular Recovery after Exposure to Taxol.* The next series of experiments determined the amount of time different cell types required to recover after Taxol exposure. Since Taxol affects normal epithelial cells as well as tumor cells similarly, are the rates of recovery also similar? Knowledge of cellular recovery time is very important clinically. If the normal epithelial cells regain normal growth curves in a short period of time (i.e., faster than tumor cells), the clinical efficacy of the drug is much better than if the tumor cells recover from treatment very rapidly and the normal cells have

slow recovery curves. Since the Taxol did not significantly affect the HMS cells, the question becomes whether Taxol induced a permanent cell cycle exit to $G_0$, preventing them from undergoing mitosis or was reversible? Figures 9A-C demonstrates the trends in recovery for the cell types analyzed.

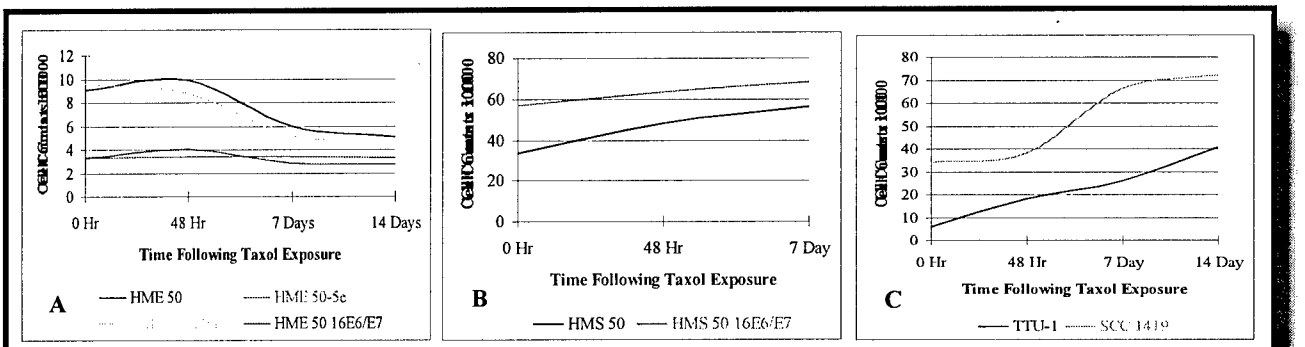


**Figure 9.** Recovery curves for the mammary cell types tested after exposure to Taxol for 48h. Cells were incubated up to 14d and harvested at intervals of 0, 2, 7 and 14 days. Collected cells were counted using a Coulter Counter. A) HME cell series: B) HMS cell series: C) Tumor cell series. All cells were exposed to high Taxol dosage ($2.54x10^{-6}$ M). Note that the HME cells never recovered after Taxol exposure regardless of immortalization status (A). The HMS cells appeared little affected and after exposure continued to grow. Limitations in counts were due to well confinement and contact inhibition in the confluent cultures (B). The tumor cells were initially affected in numbers comparable to the HME cells. However, their recovery after one week was reflective of the HMS cell growth (C).

*HME Cells.* The HME cells never fully recovered from Taxol insult. **Figure 9A** illustrates the inability of the HME cells to recover over a 14d period after exposure to Taxol. After 48h, slight increases were seen in cell counts from some of the replicates. Subsequent cell counts at 7d showed a decrease in cell counts for all cell types and replicates when compared to the controls taken immediately after the removal of the Taxol containing medium. The counts taken after 14d were similar to those taken at 7d, with no significant changes in cell counts. The control groups for all cell types continued to show increased cell counts, eliminating contact inhibition as a possible reason for the decline in cell number. The results also showed that the initial exposure concentration of Taxol was not a factor in these experiments.

*HMS Cells.* Determining the recovery curves for the HMS cells were difficult because exposure to Taxol had little effect on this cell type. However, these experiments were important in determining if Taxol had any effects on HMS cells that were not detectable due to the counting methods used in the initial tests. **Figure 9B** demonstrates the apparent lack of effect by Taxol on the HMS cells. All cells showed increased growth after exposure to Taxol for each given interval. After 14d, each replicate had grown to complete confluence, regardless of HMS cell type or the dose received. At 14d the cells were so over-confluent that they detached as a single sheet from the bottom of the well. Thus, due to this technical difficulty, no data is reported for 14d.

*Tumor Cells.* The tumor cells showed remarkably different recovery curves from those of the HME cells. It was expected that since the cells exhibited similar death curves with Taxol, the recovery curves would also be similar. However, the tumor cells recovered completely after treatment with Taxol **(Figure 9C)**. There were no recognizable differences between TTU-1 and SCC 1419 unlike those observed in cell counts due to different growth patterns. Both sets of cells reached confluence after 7d. Thus, like the HMS cells, counts at 14d were difficult to obtain so no data is reported for this interval.

Recovery curves showed that HMS cells recovered fully after 2-4 days. Tumor cells recovered after one week. HME cells had still not recovered from Taxol exposure after one month. These data and the information from the aforementioned studies suggest that active bcl-2 in HME and tumor cells may be maintained at basal levels or decreased upon exposure to Taxol. Western analysis is currently being performed to confirm these findings. Our preliminary results suggest that exposure to Taxol directly or indirectly induced a variety of signaling mechanisms that

either confer resistance or sensitivity. Other studies have shown that bcl-2 is phosphorylated in the presence of Taxol [46, 47, 64-67]. This mechanism of action has yet to be elucidated. If Taxol is affecting bcl-2 at the gene level, this supports the evidence of HMS cell resistance. In this proposed model, the HMS cells produce increased levels of bcl-2 to prevent apoptosis/necrosis. The action of Taxol is likely to be combination of both factors as well as other factors yet to be determined.

Analysis of cellular recovery from Taxol exposure provides intriguing results and shows distinct response differences among the three cell types. Levels of bcl-2 expression are also likely to play a role in determining these molecular differences between the cell types. The inability of the HME cells to recover after Taxol exposure raises some new questions. There are several mechanisms that might be permanently affected. Since Taxol causes microtubule bundling, the cell may be permanently blocked at the metaphase/anaphase transition of mitosis. The changes in cellular morphology in the HME cells after Taxol exposure might also be due to this phenomenon. Additionally, Taxol may cause the cell to terminally exit the cell cycle, preventing future replication. The morphology of the nuclei observed from immunocytochemistry is indicative of necrosis. Since the HMS cells showed very little sensitivity to Taxol, full recovery following exposure was not surprising. These results confirm that the HMS cells are resistant to the effects of Taxol, and the ability to replicate has not been lost. The tumor cells showed significant levels of sensitivity to Taxol but retained the ability to recover after exposure. This may indicate that the molecular mechanisms targeted in tumor cells versus the normal epithelial cells may be different. Alternatively, since these cells have the ability to fully recover after Taxol exposure, the ability to overcome apoptosis or recognize the cytoskeletal matrix in order to complete mitosis may be involved.

*Growth patterns in co-culture.* The cellular morphology of HMS and tumor cells in co-culture iwas expected to demonstrate HMS cells peripheral to tumor cell clusters in the ER positive and lower grade tumors that retain some of their original cell morphology This was observed but to a less marked degree than the HME and TTU cells in CC Figures 10 and 11). In the ER negative tumor TTU, there was less of a recognizable pattern than when the normal cells were in CC. Also, the more aggressive tumor cells tended to overgrow the flask, effectively pushing out the normal cells. Hence the rationale for the different plating densities. This allowed us to find the optimal plating density to observe a 1:1 ratio of cells at the end time point of the experiment.

*Cell Preparations.* To establish a novel breast cell co-culture system, we first focused on co-culture of immortal human mammary epithelial cells (HME), which still exhibit normal diploid characteristics, and invasive mammary ductal carcinoma cells (TTU). Next. HME and human mammary stromal cells (HMS) were co-cultured together. Since HMS cells and TTU cells are easily detachable when they are trypsinized, we determined that further isolation of TTU cells from HMS in co-culture would need to be accomplished using an antibody based separation system in which cell surface antigens unique to the cell type would bind to an immobilized antibody. This would result in pulling a specific subset of targeted cells out of the overall population of mixed cells. This technique was also used to purify populations of remaining HME from tumor cells after differential trypsinization.

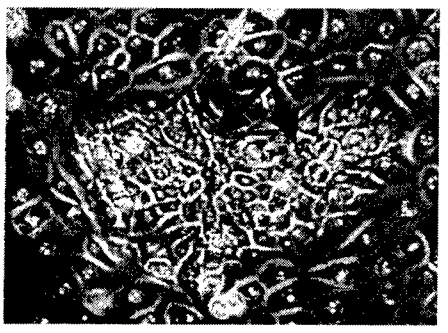

A. HME cells and TTU cells together

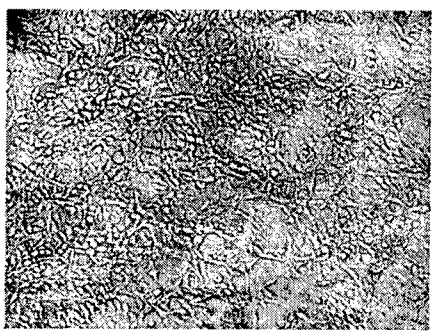

B. HMS cells and TTU cells

**Figure 10.** HME and TTU cells are co-cultured in 2D T75, HME cells formed a glandular like structure surrounded by TTU cells.The morphology of the tumor cells and the normal cells differs dramatically. As can be seen from this phase contrast micrograph, the normal epithelial cells form structures reminiscent of glands in the breast tissue (arrow). However neither the fibroblast cells nor the tumor cells demonstrate these same growth patterns. Magnification 40X.

After working with the GFP –transfected cell lines for several months, we observed that the intensity of the fluorophores was decreasing. This was particularly evident for the green and yellow variant FPs. The red FP remained relatively strong. However, the loss of signal for the GFP and YFP made critical analysis of cell growth, patterns and numbers difficult. Therefore we defaulted to the alternative scheme outlined in the proposal to utilize Cell Permeant Dyes.

2) HME cells and TTU cells together


**Figure 11.** Morphology of cells in Co-culture. A. HME and TTU cells in phase contrast. The cells forming the foci (arrow) are HME cells. B. HME cells and Tumor cells, Monochrome; DAPI only. C. HME cells (Green) and Tumor cells (Red) with CellTracker Dyes. Magnification is 20X.

Using fluorescent protein (FP) expression, different cell types were identified in co-culture. The following assays were simultaneously performed in the different cell lineages in the presence / absence of Taxol: growth pattern differences, cell counts, cell death. However, the FP signal was low. This may be due to several factors such as the length of time in culture and promoter strength. It is possible that the signal intensity has reduced because these cells have been cultured for several years. Another factor may be the promoter strength (CMV) or the fact that select pressure was decreased over time. Therefore neomycin was added to the cultures in an attempt to add selective pressure for expression of the resistance gene which would also result in expression of the FP.

An alternative strategy was to use CellTracker Dyes after isolation of tumor cells from co-culture system. Two different CellTracker Dyes (Molecular Probes) were applied to the cells; CellTracker Blue CMAC to immortal mammary cells, and CellTracker Red CMTPX to invasive mammary ductal carcinoma cells. A final concentration of 25uM/ml was used to generate a consistently strong signal.

*Types of Fluorescent Protein and CellTracker Dyes.* Originally transfected GFP cells with corresponding CellTracker colors was used. HME cells were transfected with enhanced green fluorescent protein (EGFP; Excitation maximum = 557nm, emission maximum = 579nm) using a metafectene reagent and TTU cells were transfected with Discosoma sp. Red fluorescent protein (DsRed; Excitation maximum = 488nm, emission maximum = 507 nm). Corresponding CellTracker Blue CMAC (Excitation maximum = 353nm, emission maximum = 466 nm) to EGFP transfected immortal HME cells, and CellTracker Red CMTPX (Excitation maximum = 577nm, emission maximum = 602nm) to the tumor cells. A triple band pass filter on the deconvolution microscope was used to detect the blue and red colored dyes. Figure 12 shows the cells as detected by FP emissions. As observed, the cells can be visualized. However, the intensity of the green signal is low and in some cases there appears to be overlap. Whether this is due to multiple layers of cells or problems with GFP emissions is not clear. Therefore we opted for the alternative identification strategy demonstrated in Figure 12.

Figure 13 shows the growth pattern of cells in CC detected by CellTracker dye emissions. As observed, the signal intensity is high and easily distinguishable between cell types. Figure 14 shows the stability of the CellTracker dye signal over several days in culture. Increasing exposure time compensated for any decrease in signal due to cell

division. As the exposure time indicates, it is extremely fast. Therefore increases in exposure did not affect cell viability.

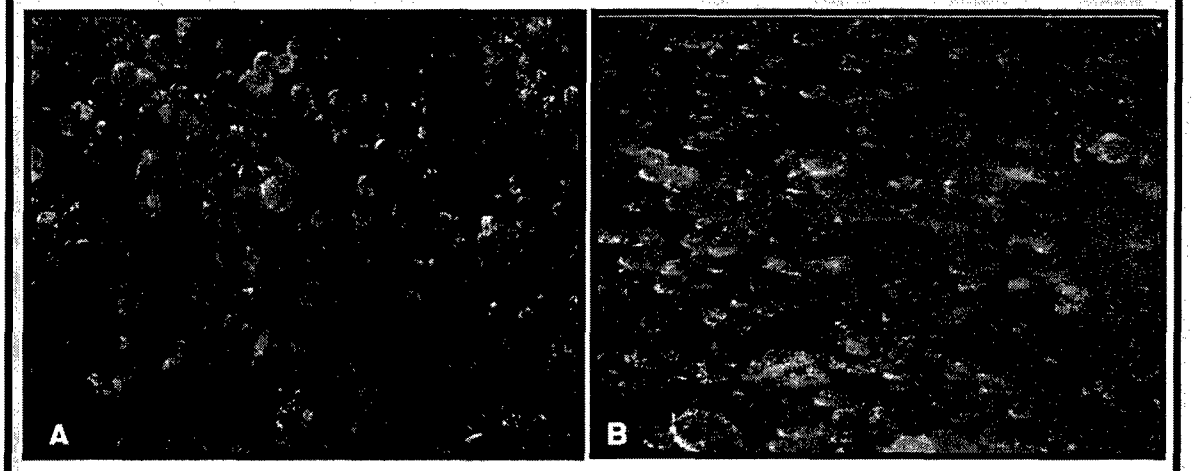


**Figure 12. Co-culture of HME50HT-GFP and TTU1-DsRedFP cells using deconvolution microscopy.** 30K HME50HT-GFP and TTU1-DsRedFP cells were plated on a 4-well chamber slide (Lab-Tek) and cultured for 5 days in DMEM-XSG medium :FBM medium = 1:1. Cells were viewed with an Olympus IX-70 deconvoultion microscope under 20X. Cells were filtered with a green color of monochrome image filter. GFP maximum excitation is 488 nm and maximum emission is 507 nm. GFP = Green Fluorescent Protein. Cells were filtered with a red color of monochrome image filter. DsRedFP maximum excitation is 558 nm and maximum emission is 583 nm. DsRedFP = Discisoma sp Red Fluorescent Protein. **B**-Another view of same

**Observations**: The previous method of co-culture showed poor growth morphology for the normal cells. In addition, given a sufficient time, the tumor cells would eventually out number the normal cells and dominate the chamber surface area. When co-cultured on a larger surface area first, the tumor cells did not show an increased growth rate over the HME and HMS cells. They appeared to grow quickly as observed in the previous platings. However, once the population sizes for the HME and HMS cells reached a certain size, they appeared to better regulate tumor cell growth and although the tumor cells did not appear to stop growing, their growth was slowed down markedly to the point that there was a much more even distribution of cells in the combined populations. This cell population has been continually cultured for 2-3 months and the tumor cells have yet to grow over the normal cells. The possibility also exists that the tumor cells are secreting a growth-enhancing compound. However, due to the fact that this phenomenon was not observed in the separate cell populations that were plated together, this hypothesis seems unlikely. When viewed under confocal microscopy, it was interesting to note that the normal cells no longer demonstrated a stressed growth phenotype. The vacuolation, blebbing and other apoptotic traits were no longer present. The HME and HMS cells looked healthier.

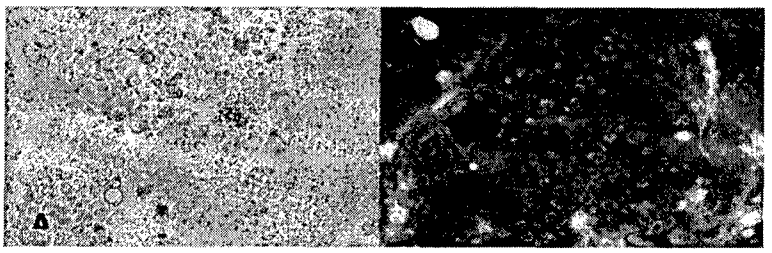


**Figure 13. Co-Culture Growth Pattern.** Co-cultured HME and Tumor cells after 5 days in culture. A. Cells visualized under phase contrast conditions. B. Cells visualized under Immunofluorescence conditions. HME cells have been dyed with CellTracker Green. TTU cells have been stained with CellTracker Dye Red. Magnification: 20X.

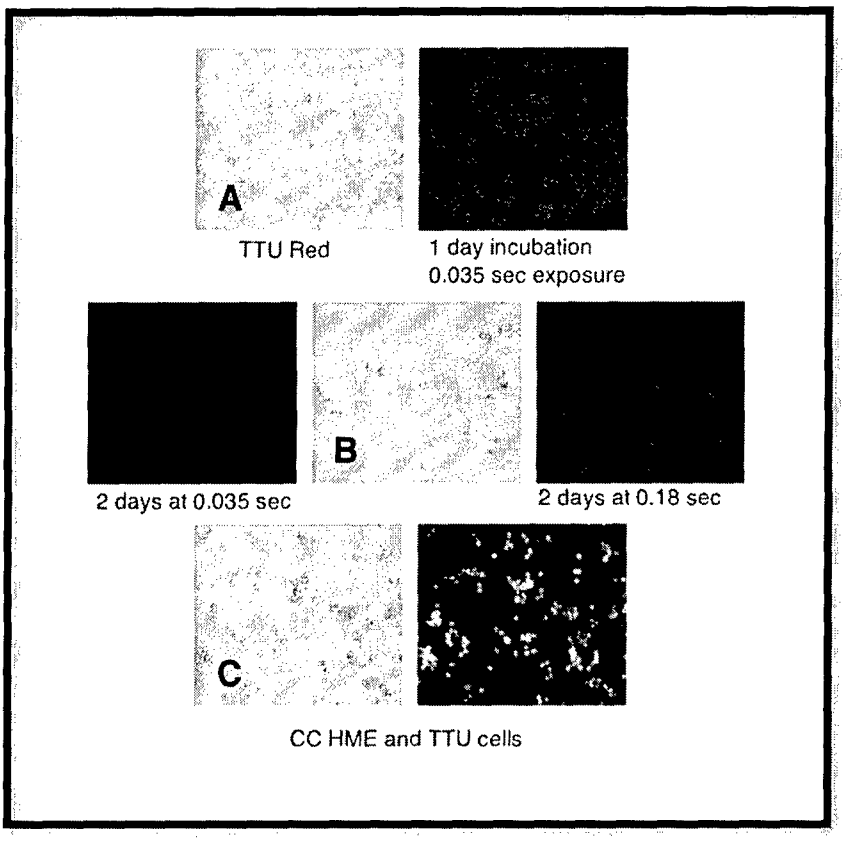


**Figure 14. CellTracker dye was used as an alternative to the weak FP signal. A.** TTU cells with 10uM Cell Tracker Red CMTPX. One day incubation. Exposure time 0.035 sec.
B. Trypsinized TTU to test dye signal intensity stabilization inside cells.
C. HME cells with 10uM Cell Tracker Green CMAC co-cultured with TTU cells with 10uM Cell Tracker Red CMTPX. One day incubation. Exposure time 0.035 sec .

As demonstrated in panel B, by increasing the exposure time slightly, we were able to obtain excellent signal. The dye signal carried through the 5 days in culture for all the experiments performed.

*Cell Counts in Taxol Exposure.* Sample preparation. Homogenous HME cells 1000K and homogenous TTU cell 500K were plated in a T75 at a ratio of 2:1, respectively because TTU cells grow faster than HME cells. After 5 days, cell distribution is observed to be close to 1:1 ratio using microscopy. Different Taxol concentrations (High Taxol; 2.54X 10-6M, Low Taxol; 2.21X10-7M) and time exposures (0, 3, 6, 12, 24, 48h) to Taxol were tried. According to cell counting and FITC conjugated Annexin V data after exposure at the listed time intervals to low Taxol and High Taxol, HME cells underwent early apoptosis after 3h of low Taxol, and TTU cells underwent late apoptosis after 24~48h of low Taxol. Interestingly, HME cells were much more sensitive to Taxol. After short time exposures to High and Low Taxol (3h), HME could not recover normal growth. However, TTU cells had similar cell numbers from 3h to 12h in High and Low Taxol, but gradually grew after 24h of High and Low Taxol. Co-culture (CC) seems to follow HME growth pattern, because TTU start to replicate after 24h of both concentrations of Taxol but CC cell numbers were not median number of homogeneous HME and TTU cells as expected. Cell numbers were reflective of homogenous HME cell counts. Low Taxol and High Taxol had a similar growth pattern to parental HME, TTU cell, and CC. In addition, HME had evident early apoptosis fluorescent signal in Low Taxol. Based on these findings, 24h in Low Taxol was chosen as the definitive time point to utilize for all future experiments, particularly for altered gene expression experiments. Figure 15 graphically illustrates these results.

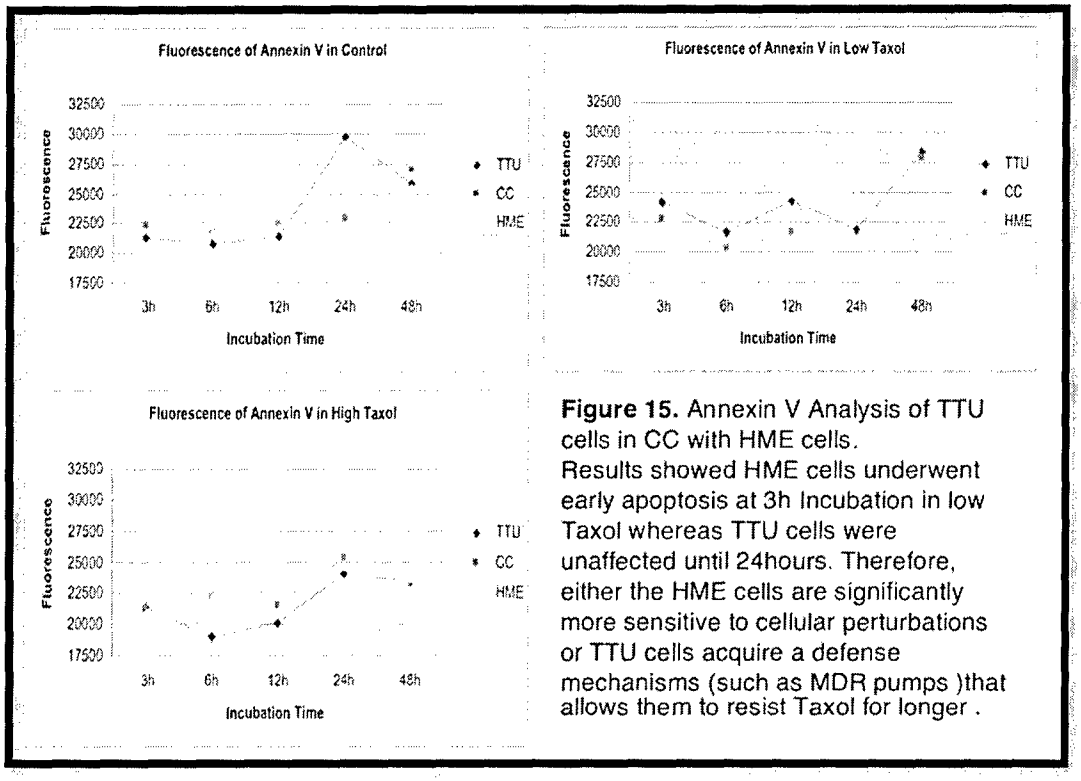


**Figure 15.** Annexin V Analysis of TTU cells in CC with HME cells. Results showed HME cells underwent early apoptosis at 3h Incubation in low Taxol whereas TTU cells were unaffected until 24hours. Therefore, either the HME cells are significantly more sensitive to cellular perturbations or TTU cells acquire a defense mechanisms (such as MDR pumps )that allows them to resist Taxol for longer .

*Cell Plating Densities.* Although there was a more even distribution of cells when plated at 50-50-3, as stated earlier, the cell morphology for the HME and HMS cells did not reflect that of normal healthy cells. There are a number of possibilities why this occurred. One reason may simply be that the normal cells do not recover and go into cell cycle as quickly as the tumor cells. As they start to recover, the tumor cells may have some factor that inhibits normal cell growth or causes a stress response may condition the medium. We are planning on investigating this possibility as a future project through a collaboration with Brian Reilly, Ph.D. in the department. He has expertise in protein isolation and identification. Another reason may simply be that the tumor cells depleted the metabolites essential to the normal cells. Whatever, the reason, we decided to try a different strategy. Since the cells were not doing well together when harvested directly from the parent cell cultures and placed in the chamber slides, we decided to allow them to grow for several population doubling levels (PDLs) as a mixed population n a T75. At this time 50k-50k-3k HME-HMS-tumor cells were plated in a T75 flask and allowed to grow for 5 days in CC medium. Several different plating densities for HME-HMS-Tumor were performed including 50k-50k-50k, 30k-30k-10k and finally 50k-50k-3k. Interestingly, the 50-50-3 also appeared optimal in the T75 for yielding a more even cell distribution.

In order to extract proteins of TTU1 and HME50HT for negative control, 30K homogenous TTU1 and 30K homogenous HME50HT were plated in 24 well plates and cultured for 5 days in DMEM-XSG or SF170 respectively. Cells were viewed using deconvolution microscopy whether these cells had fluorescent protein or not. TTU1 cells had some green fluorescence, HME50 HT cells seemed to have no green fluorescent protein on 3rd day, but they had many green fluorescent proteins on 5th day. To prohibit cross contamination between HME cells and TTU cells, made own cell split material for each cell type and plated each cells in 24 well plates. These cells were checked fluorescent protein after 1st split from cell stocks. TTU1 old stock made in 3/6/00 had no fluorescent signal. This further confirmed the need to utilize CellTracker dyes for cell identification in CC.

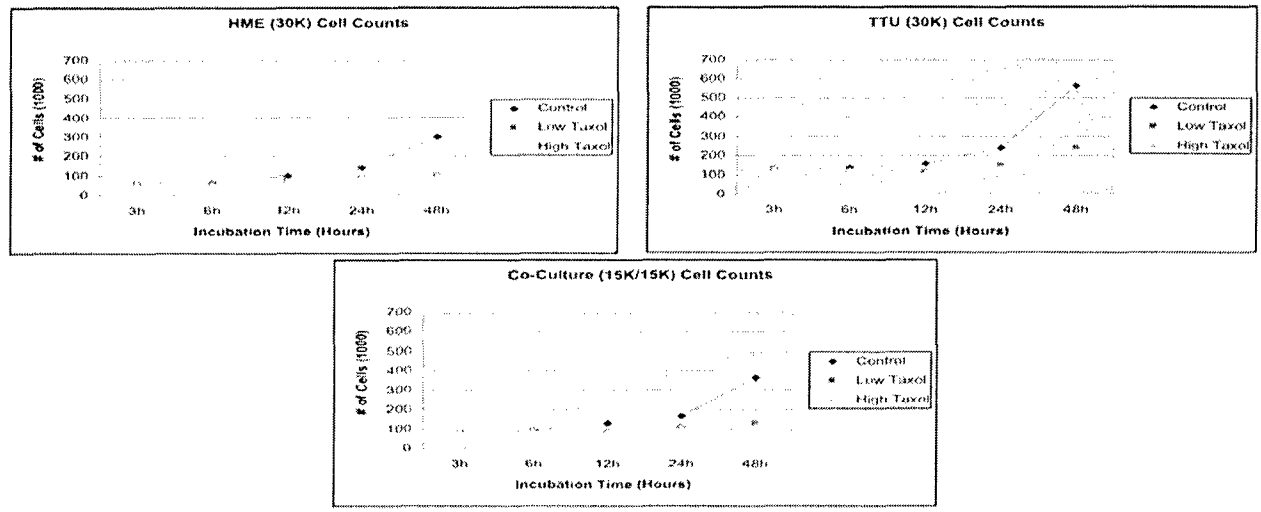


**Figure 16. Homogenous HME-GFP (30K), homogenous TC-RFP cells(30K), and Co-cultured HME-GFP(15K) and TC-RFP(15K) cells counts.**
Cells were plated in 24-well plates (Falcon). Cells were cultured for 5 days in DMEM +10% calf serum : SF170 medium = 1:1 Cells were treated with high (2.54 x 10-6 M) and low (2.21 x 10-7 M) Taxol on the 5th day. Control plates and Taxol treated cell plates were counted after 48 hours using Coulter Z Series particle counter and size analyzers. In previous experiments, homogeneous populations of HME-GFP cells were highly sensitive to Taxol and TC-RFP showed similar response curves, but recovered quickly. However, this data set demonstrates different death curves for HME-GFP cells and TC-RFP. Interestingly, these cells were *not significantly affected by Taxol when in co-culture conditions.* GFP= Green Fluorescent Protein, RFP=Discisoma sp Red Fluorescent Protein.

Summary for Tasks 1a, 2a, 3a.
Accomplishments: Baseline data for cell growth and response to different cell culture media was performed. An optimal CC medium was formulated that yielded >80% viability for each cell type. Baseline values were established for normal and tumor cells in different concentrations of Taxol equivalent to 24h blood plasma concentrations. In addition, time points for Taxol effectiveness were determined for each cell type. Cells were successfully transfected with FPs and a CC system established. Optimal plating densities were determined such that at the end of the culture time, approximate cell ratios were 1:1. Growth patterns for cells in CC were determined. Degrees of sensitivity for different cell types to Taxol was determined. CC effects on cell response to Taxol was determined.

Problems encountered: Cell line contamination, loss of several of the cell lines. Liquid nitrogen container leaked and many cell lines destroyed. As a result, we were only able to document detailed changes for 1 set of corresponding HME – HMS pair and tumor line. FP signal intensity faded in cells over several months in culture. Lifespan of normal cells limited stocks and application time for these cells.

Troubleshooting/Alternative methods to solve problems: We concentrated on 1 matched set to use with an aggressive tumor line in order to obtain results. We reintroduced several cell strains and 2 tumor lines with FPs. We introduced the normal, mortal cells with hTERT to insure availability throughout the project. CellTracker dyes were employed as an alternative to the FP and proved more effective and easier to visualize.

**TASK 1b.** Determine the ratio of cell types in controlled and treated conditions using a fluorescent plate reader (Months 1-6).
**Task 2b.** Determine the ratio of cell types in controlled and treated conditions using a fluorescent plate reader (Months 12 - 18).
**Task 3b.** Determine the ratio of cell types in controlled and treated conditions using a fluorescent plate reader (Months 24 - 30).

These three tasks were performed concurrently and will be discussed concurrently.

These Tasks focused on cells in co-culture. After the initial 48h Taxol exposure, ratios of the relative fluorescence emissions were measured using a Bio-Tek® Fluorescence Plate Reader. Fluorescence emission measurements from the plate reader should have reflected the results observed for the growth curves. We predicted that if the tumor cells have a greater mitotic activity, the ratio of red to green to should be greater. So we utilized the optimized plating densities established in Task a. In addition, the graphic area representations of fluorescent signal concentration should have exhibited intense pockets of green with an overall red fluorescent background. As the time in culture increased, it was expected that more tumor cells would become apparent versus corresponding normal cells. However, if the normal cells had an inhibitory effect on overall tumor cell growth and/or their ability to form foci effectively, then the tumor cells should not have overgrown the plate and pushed the normal cells out.. We expected that under Taxol conditions, the cell death in the epithelial cells would be greater than the tumor or stromal cells. However, the cell counts indicated that there appears to be a protective mechanism for the epithelial cells when in CC with the tumor cells. Therefore the effects were not as great as expected. This result should be manifested by differential Taxol uptake profiles as well as differential gene expression.

*Potential problems:* Within the experiments for *Strategies 2a and b,* the dsRed and ethidium homodimer presented a potential problem for clear delineation between cells and events. The dsRed has an excitation wavelength of 558 nm and emits at 583 nm. The ethidium homodimer supplied in the LIVE/DEAD viability assay is excited at 485 nm and fluorescence emission at 590 nm. There are two possible alternatives for alleviating confusing emissions signals from these dyes. First, the excitation wavelengths are very different. Thus using a conventional FITC filter, the ethidium would be visualized but not the dsRed and vice versa. With a filter specific for dsRed, the ethidium dye will not be excited. The second solution to this potential problem is based on the nature of the dyes. The ethidium homodimer only intercalates into DNA/nuclear material and only in the presence of cell membrane disruption. The dsRed is primarily expressed only in the cytoplasm. Thus if a cell is observed with nuclear staining only, it can be assumed to contain ethidium dye. Likewise, if there is red dye observed in the cytoplasm, it can only be dsRed, where red would be in expressed in the same pattern as the green FP). In the case of the two dyes occurring concurrently, the excitation wavelength should effectively distinguish between the two dyes.

During the course of these experiments, we found that the ratio of live to dead was not as accurate as first predicted. This was due to two concurrent problems. At first, we reasoned that the loss of cells after Taxol exposure was the primary cause for the inaccurate counts. Destruction of microtubules and subsequent death of the cells, caused them to lose adherence from the plate. Therefore the numbers were biased toward the live, attached cells. We tried to overcome this by aspirating the floating red, dead cells and adding them to an empty well. However, the fact that they were floating as compared to the adherent live cells coupled with the fact that we were not confident in the readings due to the planar effect of attached versus floating cells with different fluorophores prompted us to reevaluate this strategy. After closer examination of the inherent filters, we found the problem was not necessarily with the cell attachment status as much as it was with the sensitivity of the filters. Table 1 summarizes available filters and associated wavelengths.

**Table 1**: Summary of the wavelengths on the excitation and emission filters in the plate reader.

| Wavelength | Excitation filter | Emission filter |
|---|---|---|
| | 360/40 | 460/40 |
| Selected for GFP | 485/20 | 530/25 |
| Selected for DsRed | 530/25 | 590/35 |
| | 590/20 | 645/40 |

There were only 4 options of excitation and emission filters standard. Therefore, the filtered light whose range is 465~505nm to excite GFP was calculated to excite around 40% DsRed. GFP maximum excitation is 488 nm and maximum emission is 507nm. GFP= Green Fluorescent Protein. DsRedFP maximum excitation is 558 nm and maximum emission is 583 nm. DsRedFP=Discisoma sp Red Fluorescent Protein. In this case, the range of 505~555nm emission filter for GFP only could pick up a small percentage of the excited DsRed. The range of 505~555nm filtered light to excite DsRed could also excite around 20% GFP. In this case, around 80% excited DsRed and around 10% excited GFP were able to be emitted through 555~625nm emission filter for DsRed. However, in CC these excited GFP and DsRed generated considerable background. For this reason FL 600 Microplate Fluorescence Reader (Bio-Tek) was not be able to showconcurrent result with Coulter Z Series particle count and size analyzer.

In order to obtain confirmatory data of cell counts, we substitute the plate reader with another strategy. This second strategy involved the following: Cells were first dyed with cell permeant dyes as described previously and plated in a mixed population. After 5 days in culture, the cells were photomicrographed at 10 random fields of vision. These images were used to manually count the ratios of red to green cells. Then the LIVE/DEAD assay was performed. After Live/Dead staining, we pulled off the red, dead, floating cells and counted them using the coulter counter. We then photomicrographed 10 random fields of vision using the deconvolution microscope, digitized the images, and printed them out. These images were used to count red cells only. We then trypsinized the remaining attached cells and counted them. We added the red cells counted in the fields after calculating the total surface area in the well and estimating from these counts the average number of red cells left on the plate. This number was subtracted from the total attached cells counted and added to the red cells counted. A ratio was then taken for these cell counts. Table 2 summarized the results of these experiments.

| **Cell Counts** | **HME 50K** | **TTU 50K** | **CC (50/50K)** |
|---|---|---|---|
| Control 6h | 61.75 0.66 | 69.58 4.20 | 274.19 5.77 |
| Taxol 6h | 73.39 0.28 | 51.44 6.45 | 256.5 22.86 |
| **Fluorescence** | **HME-G** | **TTU-R** | **CC (50/50K)** |
| Cont 6h G (485/530) | 26916 ± 1180.2 | 28014 ± 209.30 | 23934 ± 1456.6 |
| R (530/590) | 27252 ± 761.55 | 27436 ± 86.27 | 27615 ± 1487.0 |
| Taxol 6h G (485/530) | 27515 528.66 | 25303 215.67 | 28280 1936.1 |
| R (530/590) | 28185 ± 446.89 | 27799 ± 824.49 | 28958 ± 1089.7 |

**Table 2. Cell numbers in Coulter Counter and FL 600 Microplate Fluorescence Reader (Bio-Tek).** Homogeneous 50K HME50HT-GFP, homogeneous 50K TTU1-DsRedFP and Co-culture of HME50HT-GFP (50K) and TTU1-DsRedFP (50K) cells were plated in 24-well plates (Falcon). Cells were cultured for 5 days in CC medium. Cells were treated with 2.21 x 10-7 M Taxol on day 5. Control plates and Taxol treated cell plates were analyzed after 6 hours using Coulter Counter and FL 600 Microplate Fluorescence Reader (Bio-Tek) HME50HT-GFP Cells were filtered with a range of 485 ± 25 nm excitation filter and a range of 530 ± 25 nm emission filter. GFP maximum excitation is 488 nm and maximum emission is 507 nm. GFP= Green Fluorescent Protein. TTU1-DsRedFP Cells were filtered with a range of 530 ± 25 nm excitation filter and a ranger of 590 ± 35 nm emission filter. DsRedFP maximum excitation is 558 nm and maximum emission is 583 nm. DsRedFP=Discisoma sp Red Fluorescent Protein.

From Coulter Counter counts, the co-culture cells grew faster than each homogenous cell popularion. However, readings obtained from the FL 600 Microplate Fluorescence Reader (Bio-Tek), the number of co-culture cells and each homogeneous cells was similar. After discovering the overlap in excitation and emission wavelengths, we did not continue this methodology to obtain our results. The results are incorporated in Task a along with the cell counts.

Summary for Task 1b, 2b, and 3b.
Accomplishments: Cells were counted using the methods described in the proposal. However, upon realizing the results were not valid due to overlap with filters, we felt that the results would be inaccurate and the conclusions drawn, faulty. Therefore TTU-HMS and HMS-HME results were not finished using the plate reader.

**Task 1c.** Determine differential gene expression using FACsort analysis. (Months 6-12).
**Task 2c.** Determine differential gene expression using FACsort analysis. (Months 18 - 24).
**Task 3c.** Determine differential gene expression using FACsort analysis. (Months 30 - 36).

These results were generated concurrently and will therefore be discussed concurrently.

*FACsort Analysis* (fluorescence-activated) flow cytometry (Becton Dickinson) was initally performed on these dyed cultures alone and in co-culture. This methodology separated the cells based on Fluorescence emission. Clontech® has described in detail in the manuals accompanying the GFP constructs, the excitation and emission wavelengths for each of the color variants. In addition, information about the relative half-life, photobleaching and optimal filters is included. We have successfully performed test sorts on HME cells expressing EGFP, stained with calcein green, ethidium bromide (Molecular Probes) or 2',7'-dichlorofluorescin diacetate (DCF-DA) (Sigma). However, there were several immediate problems. We Had access to a new Becton-Dickinson FACScalibur flow cytometer, under the supervision of Mr. Tom Redford and Ms. Patti Merritt, located in Covenant Health Systems less than 1 mile from our lab. However, we found it very difficult to schedule use since it is in a heavily used pathology lab. Even though Ms. Merritt and Mr. Redford made every effort to accommodate our runs and we tried to utlize their facility in less busy times, the schedules were not matching adequately for our needs. In addition, the run times were not optimal for getting enough cell numbers separated for RNA. Finally, the viability of the cells was very poor because of the fact that we had to rely on their technician as well as he fact that cells were prepared in Dr. Gollahon's lab prior to the run, then transferred to the facility (30-60 min) where they were kept at 37°C under 5% $CO_2$ until run time. The FACsort was a FACScalibur™ (Beckman) which is not an efficient cell sorter. In order to address the issue of cell viability, as the cells were sorted, populations were removed immediately and placed in medium. However, the difference between adherent cells and lymphocyes became evident as our viability dropped to <30%.

Therefore to address this particularly critical portion of the proposal, our lab developed a fast, effective and inexpensive method of cell sorting based on cell surface antigen presentation. We were fortunate to be able to utilize at least one unique, excellent, cell surface antigen for each cell type. The next section describes the initial system which was based on cell adherence properties and cell surface antigen presentation. We then refined this system to be semi-automated and obtained superior separation and viability results. The resulting papers are appended (Du, et al, 2006, Wankhede et al, 2006).

Cell Separation Techniques.
*Differential Trypsinization:* Cells were isolated from co-culture based on differential sensitivity to trypsin. Immortal human epithelial cells were observed to be more resistant to trypsin than invasive ductal breast carcinoma cells than HMS cells. Since HMS cells and TTU cells are easily detachable when they are trypsinized, we determined that further isolation of TTU cells from HMS in co-culture would need to be accomplished using an antibody based separation system in which cell surface antigens unique to the cell type would bind to an immobilized antibody. This would result in pulling a specific subset of targeted cells out of the overall population of mixed cells. This technique was also used to purify populations of remaining HME from tumor cells after differential trypsinization. Figure 17

shows cells in a mixed population before and after trypsinization. The cells populations isolated were replated to show viability and specificity.

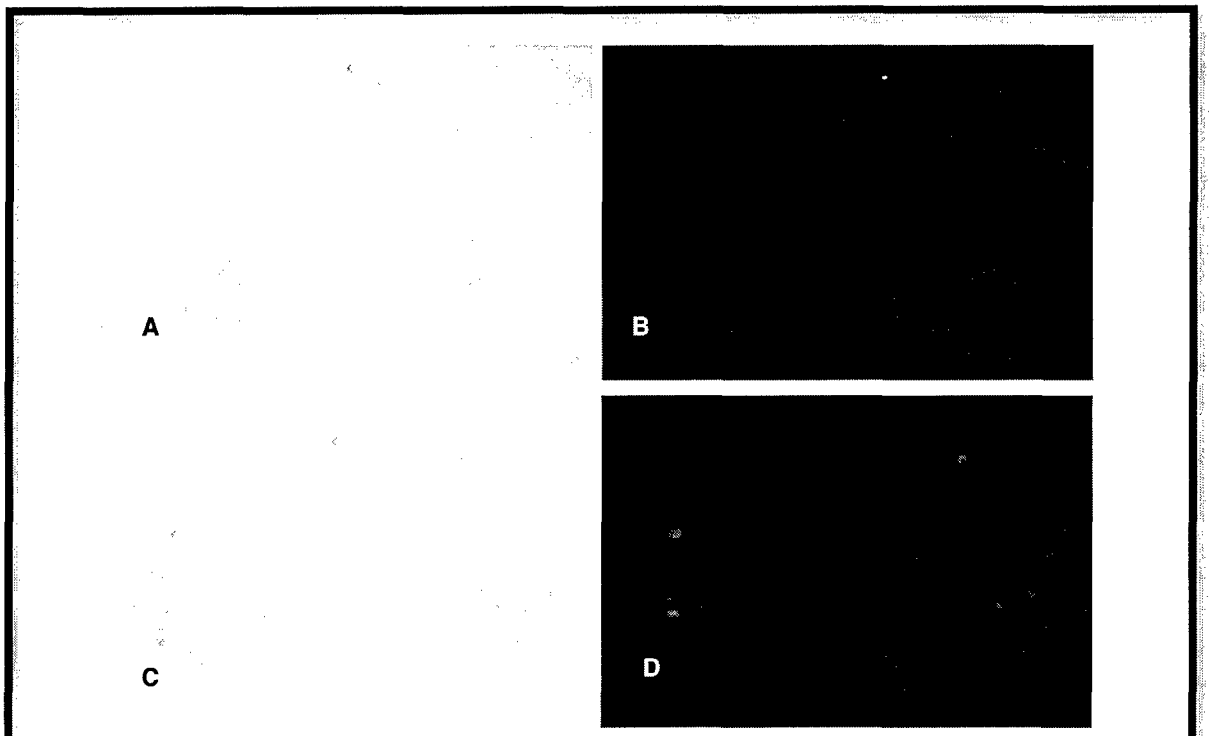


**Figure 17**. Result of separation using differential "Accutasation" to isolate TTUfrom CC with HME cells. HMEC more resistant to Accutase. Accutase ws substituted for trypsin because the harm to the cell membrne was much less. TTU cells still easily are easily detach. Two representative fields of view are shown. A. HME cells remained on the plate after isolation of TTU from CC. Cells were rinsed three times with 1X PBS. HME cells were stained Green and Tumor cells were stained Red with CellTracker Dyes. Magnification: 20X.

These different breast cells were trypsinized from co-culture system. TTU cells and HMS cells detach first then HME cells detach later using trypsin-EDTA (Gibco invitrogen corporation). TTU-DsRed cells and HME-EGFP cells together in CC, TTU-DsRed cells detach first and rinse completely T75 co-culture flask with 1X Solution A to remove mixed cells then trypsinize remained cells to get HME cells. A similar procedure is used to separate HMS cells from HMS and HME-EGFP cells in CC. We plated separated cells on the 24 well plate (Falcon) to check fluorescence to confirm purity of cell isolation. However, both TTU-Red cells and HMS cells come out easily, so we developed an antibody-based capture system to separate TTU-Red cells from the TTU-Red and HMS co-culture.

This novel, effective, inexpensive strategy was developed to separate cells in co-culture, maintained cell viability. Two runs yielded numbers of 500K+ to be used for RNA isolation. Importantly, it allowed for rapid cell capture (e.g. <20 min). The criterion to capture the cells is as followed: 1. Only expressed on cancer cells; 2. Expressed *de novo* or in very high densities on cancer cells and very low densities on normal cells; 3. Cell surface antigens. The cell surface antigens used to capture the tumor cells was Epithelial Membrane Antigen (EMA, Novocastra). The antibody used to capture the fibroblasts is Fibroblast Growth Factor Receptor (FGFR). The antibody used for the HME cells in CC to insure accurate separation and pure populations was epidermal growth factor receptor (EGFR). Figure 18 is a representative photomicrograph of TTU-1 cells incubated with mouse anti-human EMA and a goat anti-mouse secondary antibody conjugated to rhodamine. The nuclei were counterstained with DAPI. The HME cells underwent the same Immunocytochemistry conditions.

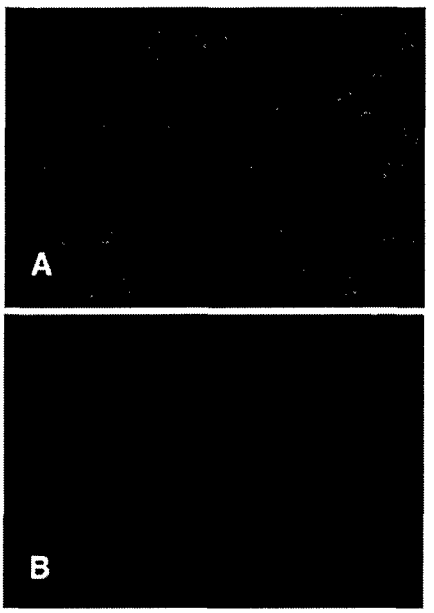


**Figure 18**. Cell Surface antigens permitted the accurate recognition and isolation of different cell types. The panel shows TTU-I cells and HME cells incubated with mouse anti-human monoclonal antibody EMA at 1:100 dilution. The secondary antibody is goat anti-mouse conjugated to rhodamine at 1:1000 dilution. Nuclei were counterstained with DAPI. A. TTU-1 cells. B. HME cells.

The system chemistry shown in Figure 19 was adapted from [68]. It consisted of 7- barrel capillaries which allowed for a larger surface area than a single capillary. These capture capillaries were soaked in 100% Methanol : Hydrochloric acid = 1:1 solution for 30min then rinsed carefully with distilled water. They were then soaked in 100% sulfuric acid for 30min then rinsed again to add hydroxyl group on the surface of capillary and sterilized in boiling water for 30min. After complete air drying, The capillaries are soaked in a cross-linker, 2% solution of 3-mercaptopropyltrimethosilane (MTS) in toluene for 30 min then soak them in heterobifunctional crosslinker 2mM N-γ-maleimidobutyryloxy succinimide ester (GMBS) solution for 30min to cross-link hydroxyl group and primary antibody.

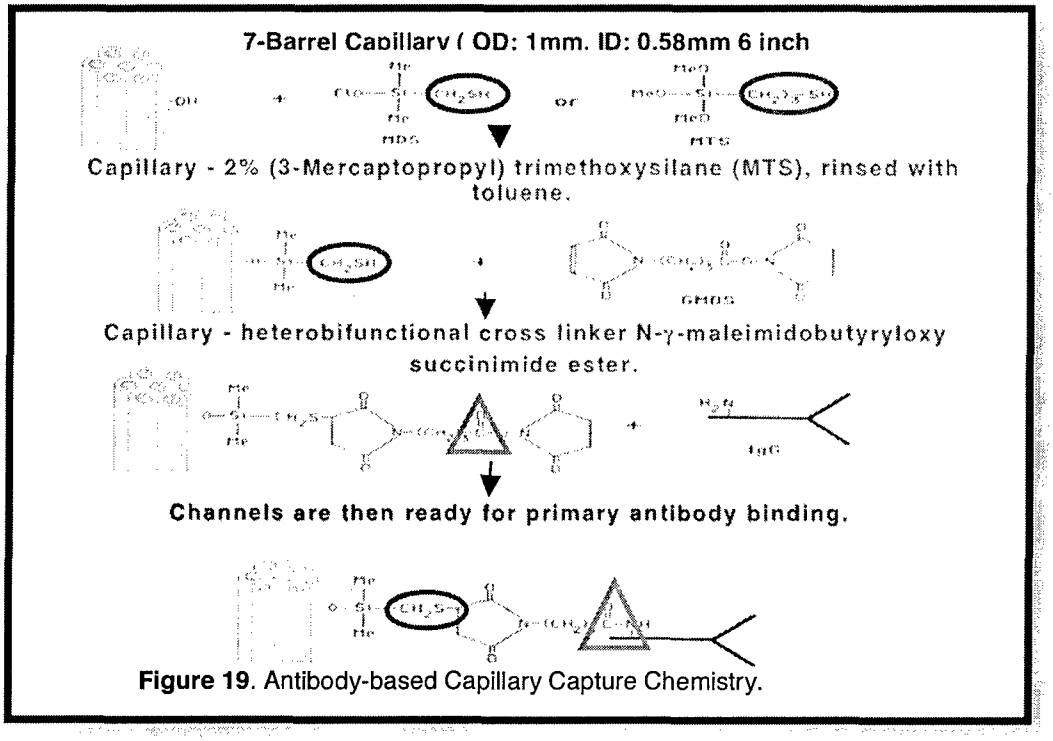


**Figure 19**. Antibody-based Capillary Capture Chemistry.

The EMA was diluted with 10% Bovine Serum Albumin (BSA) in 1x PBS at 1:50 concentration. Then the dried capillaries were plunged into EMA solution at room temperature for 1 hour. HME cells and TTU cells were flowed through these capillaries by capillary phenomenon, then gently rinsed with 1x PBS.

The cells targeted for capture were the TTU cells using EMA when in CC with HME, or the HMS cells using FGFR when in CC with the HME cells. Due to the cell surface distribution and the binding affinity, the TTU cells with EMA were also targeted when in CC with HMS cells. The cells not captured were rinsed out and collected in eppendorf tubes. After collection the cells were centrifuged, pelleted and frozen for RNA isolation. The captured cells were flushed with PBS, collected, pelleted and frozen for RNA isolation also. The overall purity of cell sorting was over 90%.

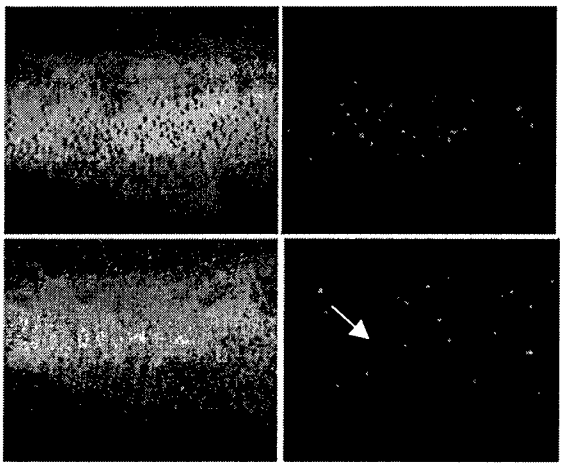

**Figure 20.** Representative section of TTU – Red cells captured in the 7-barrel capillary. The EMA was coated onto the inner lumen of the capillary. Cells were dyes with a red CellTracker dye prior to flow into the capillary. Left panel, phase contrast. Right panel, immunofluorescence. The arrow indicates 1 HME cell nonspecifically binding. Magnification – 10X.

While the capillary-based capture and separation system was being utilized, the problems of cell recognition and separation from mixed populations was discussed at length in one of our weekly lab meetings. One of my graduate students had been involved in designing a cell patterning bio-chip. He began to think about our problems and changed his research focus to designing and fabricating a microfluidics-based bio-chip that works on the same antibody-based principle as the capillaries. The goal is to recognize and enrich for cancer cells. The capture system came about as a direct result of our problems with cell separation and viability. The resulting manuscript is appended (Du et al, 2006). In addition, a second project resulted based on the idea of modeling differences between normal and tumor cell capture That article has also been appended (Wankhede et al, 2006). Below is a synopsis of his work and how that was integrated into this proposal statement of work:

Zhiqiang Du (Danny) is a Ph.D. Student in Biological Sciences under the supervision of Dr. Gollahon. In close collaboration with Dr. Kelvin Cheng (physics), Dr. Mark Vaughn (Chemical Engineering) and Dr. Jordan Berg (Mechanical Engineering), Zhiqiang has been successfully integrating the biological process of antibody recognition and capture into a MEMS-based device for enrichment of cancer cells. Cancer cell capture using an antibody-based microfluidics platform is accomplished by binding the antibodies to the surface of the polymer chip (PDMS) that contains etched microchannels. Small volumes are flowed through these channels at directed microfluidic rates. The target cells bind to the antibody. These cells can then be collected and analyzed. The ultimate goal of this research is to establish a complete device that not only recognizes and captures target cell populations for this project, but also

allows the clinician to make a diagnostic decision based upon the method of detection. This technique may therefore be useful in both the early detection of breast cancer as well as early detection of micrometastases from bone fluid aspirates.

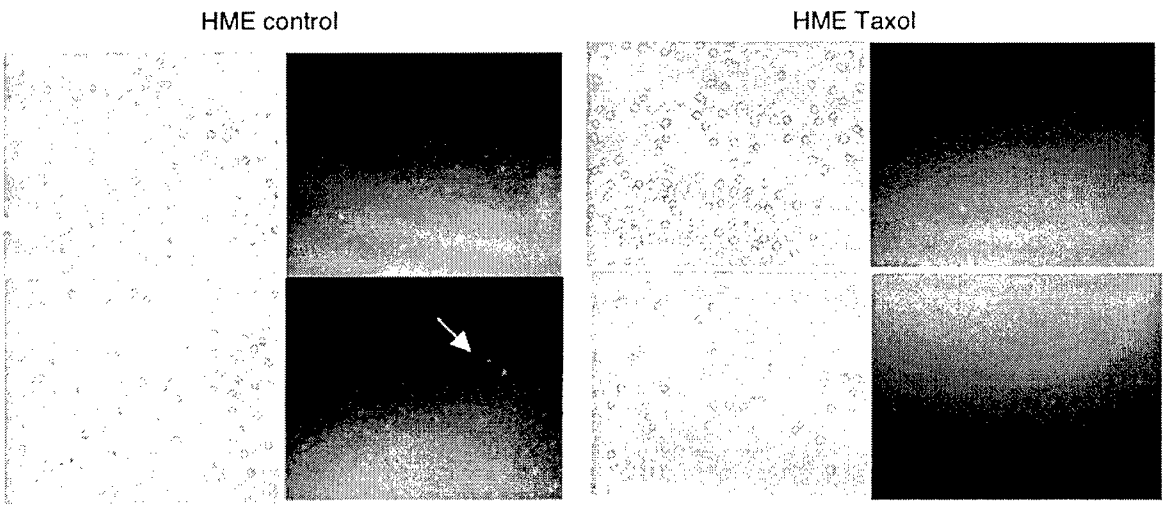


**Figure 21.** Representative capture area in the capillary showing cell capture before and after Taxol treatment for different time points. A mixed population of HME and HMS cells were treated with Taxol and flowed through the capillary after 12 h and 24h. This demonstrated the selectivity and capture before and after Taxol treatment. The arrow indicated HMS cells that bound nonspecifically. This background was calculated to be less than 10%.

The main focus of Danny's project was to develop a sensitive and accurate method for capturing and enriching cells of interest. The ability to successfully accomplish this has allowed us to apply his cell sorting system to the co-culture system. By doing this, NaYoung had the capability of separating tumor cells from normal epithelial and stromal cells in co-culture in order to perform microarray analysis. This allows a convenient method for her to prepare her cells and immediately separate them, thus avoiding long delays or accessibility issues for the FACSorter.

The resulting cells were collected and RNA extracted using Trizol® (Life Technologies). Cell viability was tested on representative samples by replating and culturing specific bumbers of collected cells, then determining the population doubling levels after 24 and 48h (Shay et al, 1995). Population numbers were obtained by visually inspecting the cell fluorescent properties using fluorescence microscopy and counting cells with a hematocytometer

*Differential gene expression*: Total RNA was isolated from cells using Trizol (Gibco/BRL). RNA was isolated from the parent cells, GFP+ cells alone, and GFP+ cells from co-culture after separation. Thus gene expression differences will be determined between: HME - HMS cells; HMS - tumor cells; and HME - tumor cells in co-culture with and without Taxol. HME50-HTcells and TTU-1 cells were CC together for 6days, then treated with Accutase; cell detachment solution, to isolate TTU cells. TTU cells detached easily and separation provided homogeneous populations. To confirm yield of cell isolation, blue and red cell permeable dyes were used for each cell. These isolated cells were plated again on the 60mm dishes for 6days, to see the effect of withdrawal of Cell-to-Cell interactions between epithelial and cancer cells. We were curious whether the cells would revert back to the parent profiles in monolayers, or if they had acquired new genotypes, reprogrammed after the physical interactions that occurred. Figure 22 shows the differential separation using Accutase and replating effectiveness after separation. The Accutase was used as a substitute for trypsin because the cells still showed the same adherence properties but with less damage to the cell membrne which proved to help retain CellTracker Dye signal intensities for longer.

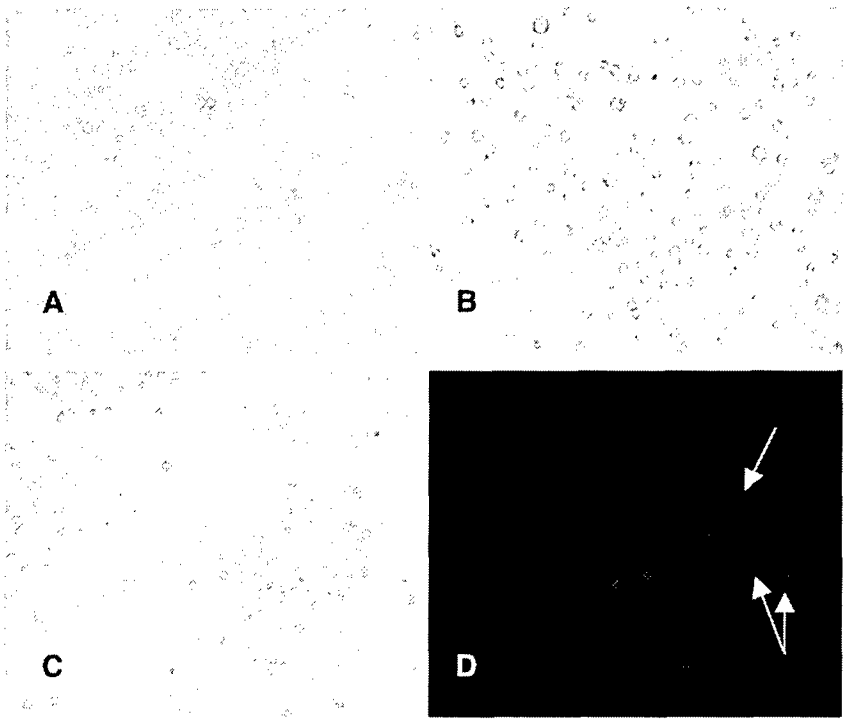


**Figure 22.** Co-cultured cells were isolated and replated for another 5 days to investigate whether the cells recapitulate the parent cell line profiles or maintained the co-cultured profiles. Co-cultures of HME and Tumor cells were replated after the initial isolation. Photos were taken 5 days later. A.HME cells. B.Tumor cells. Magnification: 20X. Co-cultures of HME and HMS cells were replated after the initial isolation. Photos were taken 5 days later. C. HME cells after separation. D. HMS cells (red) can be seen (arrows)contaminating an otherwise clean isolation. With this method we experienced <10% contamination which was viewed as acceptable for the purposes of extracting RNA and obtaining genetic profiles. Cells were visualized using deconvolution microscopy. Magnification: 20X.

The gene expression profiles were generated using ***RT Profiler PCR Array (SuperArray)***. These arrays are packaged in 96-well plate formats that have the primers already included in the wells. These plates are derived from careful research of the literature to determine genes implicated in cancer, signal transduction pathways, hormone receptor status, etc. A detailed description of each plate may be found at www.superarray.com. We decided to utilize these superarrays because as part of her research, Nayoung will be conducting loss of function assays, e.g. siRNA. Therefore we felt that a smaller, more pointed set of genes to detect and analyze would lend itself to more effectively choosing genes for knock-out RNA work while still demonstrating important differences in genetic profiles. The procedure is shown in figure 23, the plate layout and a sample plate layout is shown in Figure 24.

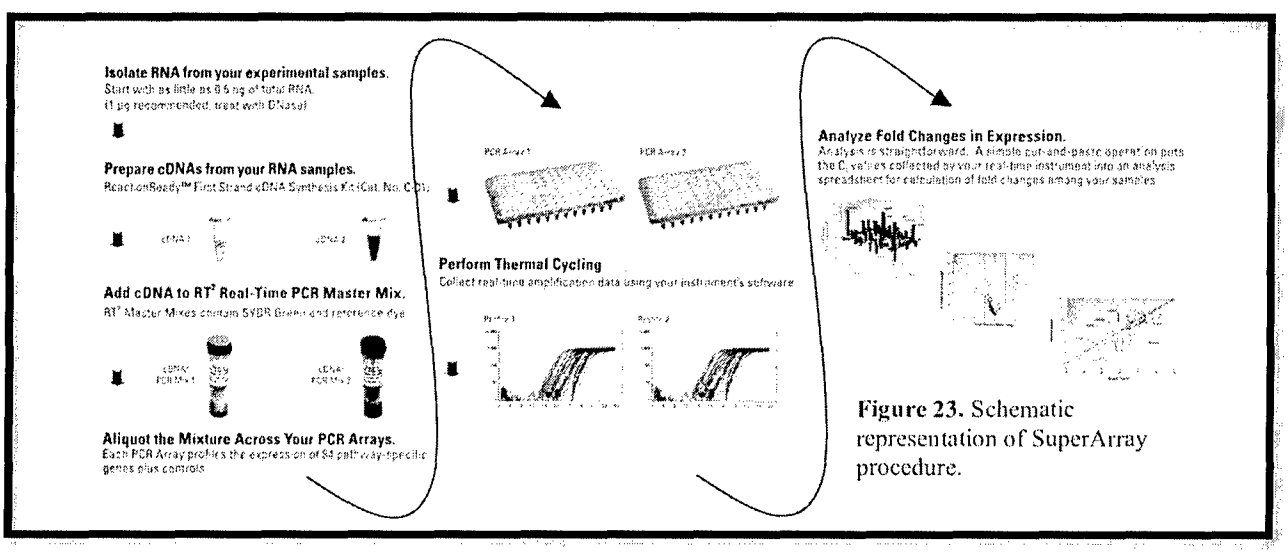


**Figure 23.** Schematic representation of SuperArray procedure.

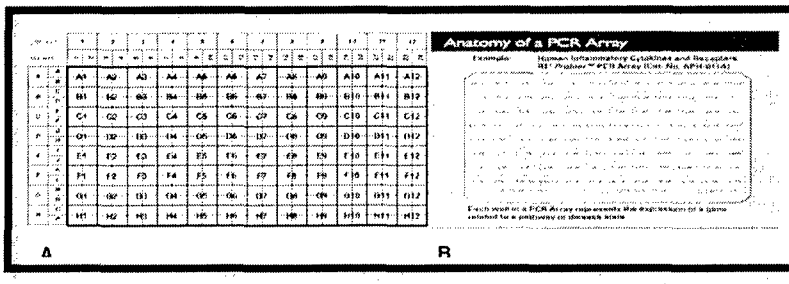


**Figure 24.** RT-PCR SuperArray layout. A. Configuration for primers within the plate. B. Configuration for the selected genes. Housekeeping and control genes are located along the bottom row.

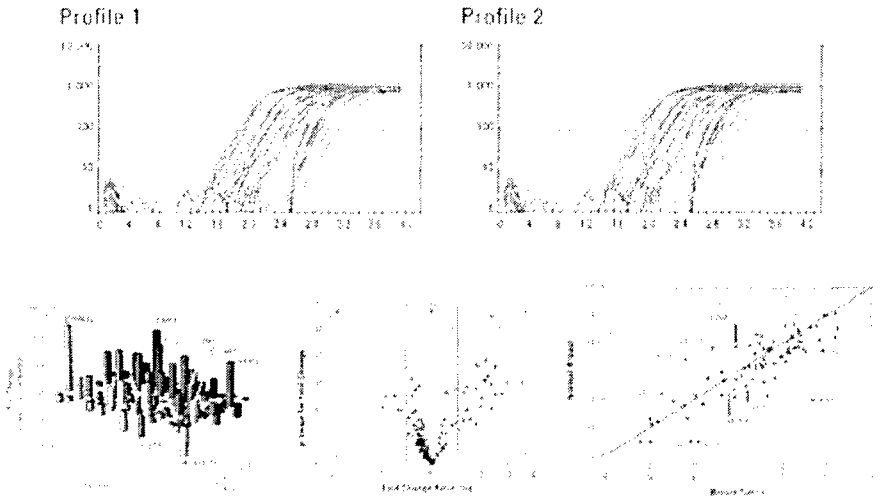


**Figure 25.** SuperArray analysis was done using Excel. Following the protocol and directions from the company (Invitrogen), the data was analyzed for over expression and unique gene expression between the sets investigated. Figures 23-25 were adapted from http://www.superarray.com .pcarraysystem.php.

The genes contained within the plate chosen for analysis included genes that were directly associated with breast cancer: CDKN1A (p21Wap1/Cip1), CLDN7 (claudin-7), CLU (clusterin), ERBB2 (Her-2), FGF1, FLRT1 (fibronectin), GABRP (GABAa), GNAS, ID2, ITGA6, ITGB4 ( 4 integrin), KLF5 (GC Box BP), KRT19 (Keratin 19), MT3 (metallothionectin-III), MUC1 (mucin), PTGS2 (COX-2), RAC2 (p21Rac2), SCGB1D2 (lipophilin B), SCGB2A1 (mammaglobin 2), SPRR1B (Spr1), THBS1, THBS2, TNFAIP2 (B94). In addition, the genes associated with the estrogen receptor signaling pathway include: AR, C3 (Complement component 3), CCND1, CTSD (cathepsin D), ESR1, ESR2, GATA3, HSPB1 (HSP28), KRT18, KRT19 (Keratin 19), PGR, SERPINA3 (a1-antichmotrypsin), SLC7A5, STC2, TFF1 (pS2). The genes associated with breast cancer prognosis are: BAD, BAG1, BCL2, CCNA1, CCNA2, CCND1, CCNE1, CDH1 (E-cadherin), CDKN1B (p27Kip1), CDKN2A (p16INK4a), COL6A1, CTNNB1 (b-catenin), CTSB (cathepsin B), EGFR, ERBB2 (Her-2), ESR1, ESR2, FAS (TNFRSF6), FASLG (TNFSF6), FOSL1 (FRA-1), GATA3, GSN (Gelsolin), IGFBP2, IL2RA, IL6, IL6R, IL6ST (glycoprotein 130), ITGA6 ( 6 integrin), JUN, KLK5, KRT19, MAP2K7, MKI67 (Ki-67), NGFB (NGF), NGFR, NME1 (NM23A), PGR, PLAU (uPA), PTEN, SERPINB5 (maspin), SERPINE1 (PAI-1), TGFA, THBS1 (thrombospondin-1), TIE1(Tie-1), TOP2A (topoisomerase Iia), TP53, VEGF. Finally, the genes associated with the response to chemotherapy are: BCL2, BCL2L2, CD44, CTSD (cathepsin D), CYP19A1, DLC1, ESR1, ESR2, HMGB1, KIT, NFYB, PAPPA, PGR, RPL27, VEGF.

The cells analyzed include parent, homogeneous strains of HME, HMS and TTU; HME and TTU isolated from CC; HME and HMS isolated from CC; TTU and HMS isolated from CC; HME and TTU isolated from CC and replated to determine whether the physical contact incurred newly programmed expressions or if the cells reverted back to the homogeneous parent profiles; HME and HMS isolated from CC and replated to determine whether the physical contact incurred newly programmed expressions or if the cells reverted back to the homogeneous parent profiles; HMS and TTU isolated from CC and replated to determine whether the physical contact incurred newly programmed expressions or if the cells reverted back to the homogeneous parent profiles. The SuperArray Data analysis was based on the ΔΔCt method with normalization of the raw data to either housekeeping genes or an external RNA control.

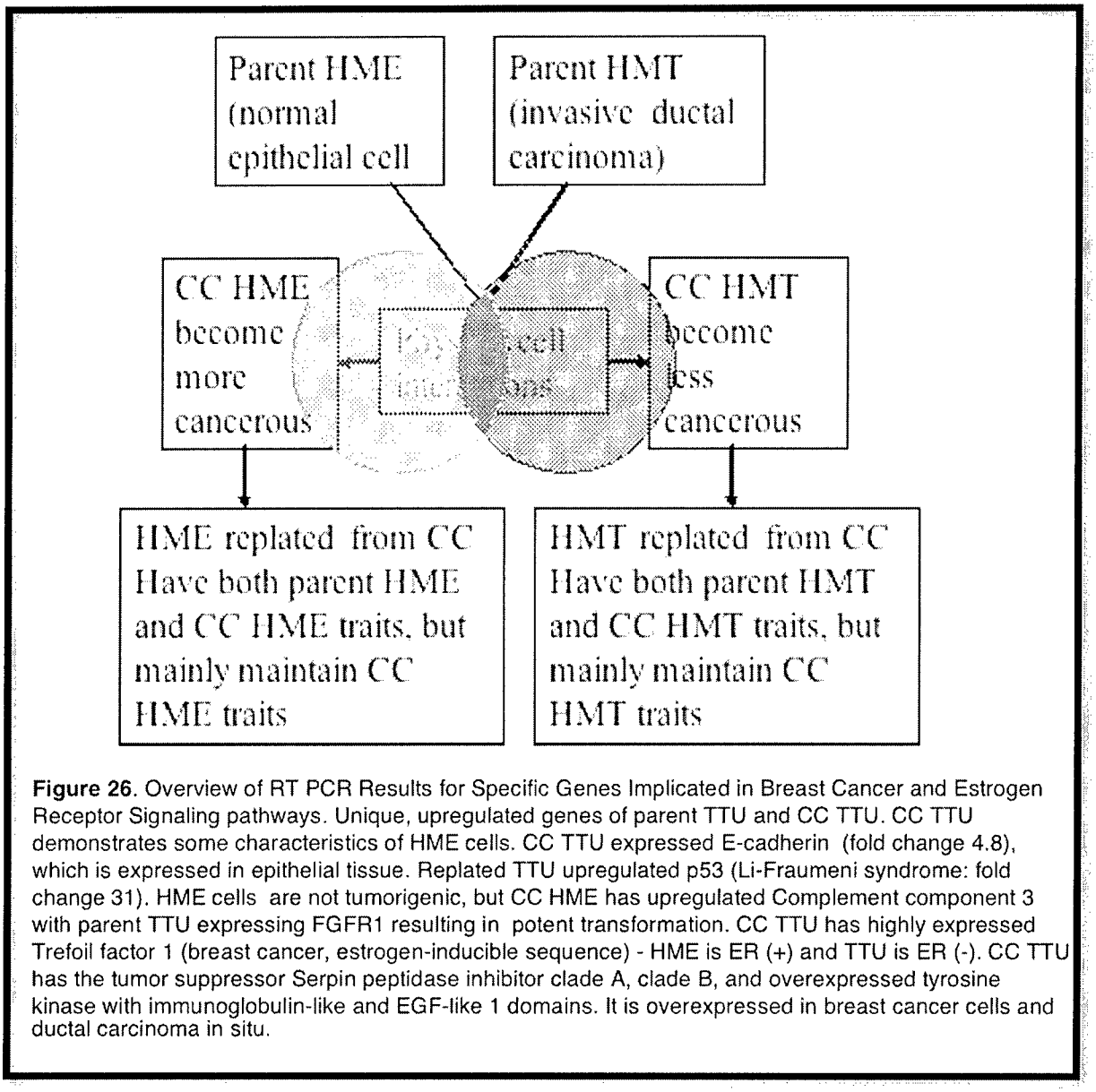


**Figure 26.** Overview of RT PCR Results for Specific Genes Implicated in Breast Cancer and Estrogen Receptor Signaling pathways. Unique, upregulated genes of parent TTU and CC TTU. CC TTU demonstrates some characteristics of HME cells. CC TTU expressed E-cadherin (fold change 4.8), which is expressed in epithelial tissue. Replated TTU upregulated p53 (Li-Fraumeni syndrome: fold change 31). HME cells are not tumorigenic, but CC HME has upregulated Complement component 3 with parent TTU expressing FGFR1 resulting in potent transformation. CC TTU has highly expressed Trefoil factor 1 (breast cancer, estrogen-inducible sequence) - HME is ER (+) and TTU is ER (-). CC TTU has the tumor suppressor Serpin peptidase inhibitor clade A, clade B, and overexpressed tyrosine kinase with immunoglobulin-like and EGF-like 1 domains. It is overexpressed in breast cancer cells and ductal carcinoma in situ.

The procedure involves mixing the cDNA template with the appropriate ready-to-use PCR master mix, aliquoting equal volumes to each well of the same plate, and then running the real-time PCR cycling program. The samples were then run in an ABI Prism 7000. We felt that the PCR Arrays were the best way to analyze the expression of a focused panel of genes. Each 96-well plate includes SYBR Green-optimized primer sets for a thoroughly researched panel of relevant, pathway- or disease-focused genes. The primer design and master mix formulation enable the PCR Array to amplify 96 different gene-specific products simultaneously under uniform cycling conditions. In addition, the specificity of the system, imparted by the combination of SYBR Green primers and PCR master mixes, produces a single product of the predicted size from every reaction without generating primer dimers. The RT² PCR Array is sensitive enough that as little as 5 ng up to 5 $\mu$g of total RNA per array plate would yield greater than 85 percent present call rates. Replicate correlation coefficients of $> 0.99$ allows experimental samples to be reliably compared across plates and runs.

**TTUCombinations.** Results of upregulated genes in homogeneous TTU parent cell populations; CC TTU and replated CC TTU cells is shown in figure 27.

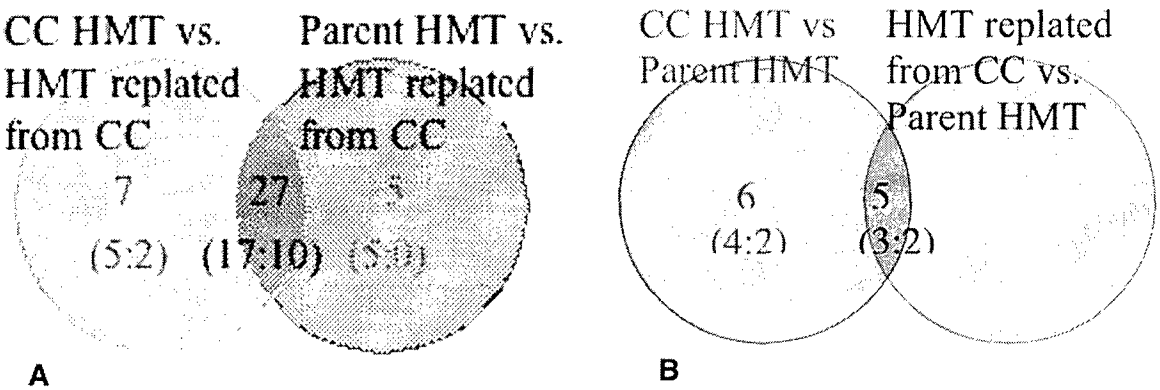


**Figure 27.** A) Determination of differences in expressed genes between TTU parent cell strains and TTU in co-culture. B) Determination of differences in expressed genes between co-cultured TTU cells and TTU cells isolated from co-culture and replated

(number of anti-apoptotic genes: number of pro-apoptotic genes)

Figure 27A shows 7 unique genes of CC TTU that are upregulated. They are divided into to groups: Anti-apoptotic genes and Pro-apoptotoc genes. The anti-apoptotic genes include Cyclin A2, Cyclin D, E-cadherin, IL6 receptor1 Intergrin beta 4. The pro-apoptotic genes include P21(tumor suppressor), Serpin peptidase inhibitor, clade A (tumor suppressor).

There are 5 unique genes upregulated in the Parent TTU. They include: Anti-apoptotic genes; BAG-1,High mobility group box, Trombospondin 1 and Pro-apoptotic genes: IGF BP2 ;biomarker for ER(-) breast cancer, Nuclear transcription factor Y, beta; a marker of tumor aggressiveness .

CC TTU demonstrated many of the same traits as Parent TTU cells as well as some HME traits. The overlapping genes (27 genes and 5 genes) are unique for both sets and are not repeated. These are graphically illustrated in Figure 28. TTU replated from CC were shown to be more similar to CC TTU, than the parent TTU cells. The tumorigenicity of CC TTU may have been mediated since it appears that tumor suppressor genes were expressed.

Figure 27B shows 6 unique genes of CC HMT upregulated. The Anti-apoptotic genes are Complement component 3, Kallikrein 5, Trefoil factor 1; estrogen inducible gene in ER (+) breast cancer, E-cadherin, Serpin peptidase inhibitor, clade A : tumor suppressor Serpin peptidase inhibitor, clade B .

The 5 Overlapping genes include: Anti-apoptotic genes: Androgen receptor, IL2 receptor alpha, TIE1 and Pro-apoptotic genes: Cornifin; important to terminal differentiation of human epidermis and Tumor protein p53(Li-Fraumeni syndrome).

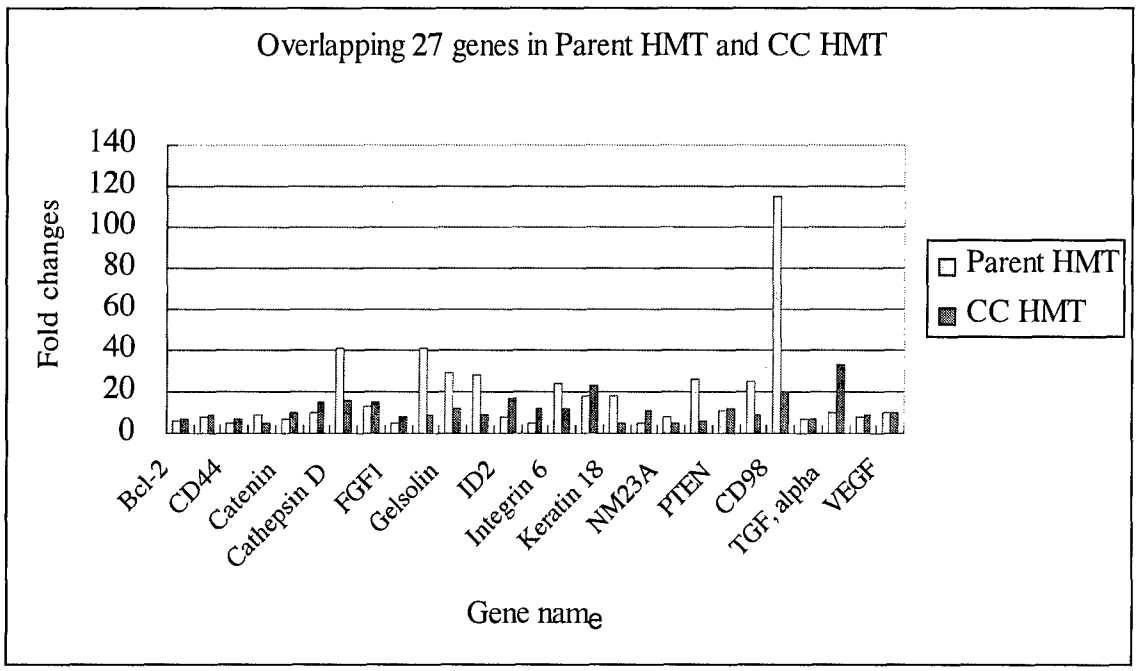


**Figure 28.** Fold changes for overlapping genes sets. Among them, 8 genes, Cathepsin D, Fra-1, Gelsolin, Hsp 27, Urokinase plasminogen activator, Inhibitor of uPA, Solute carrier family 7, and IL2 receptor alpha denote significant fold changes (>15 fold changes) between CC TTU and Parent TTU.

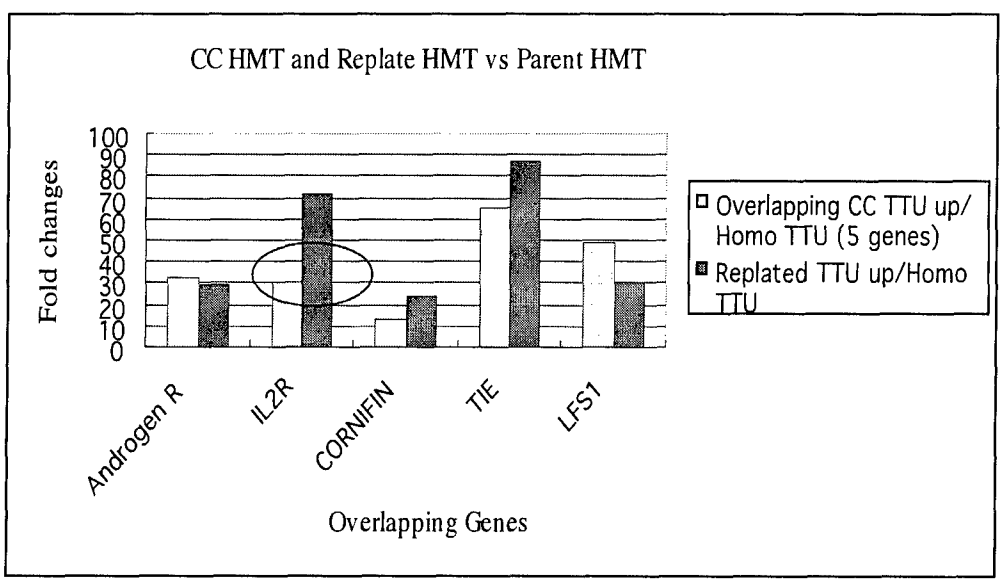


**Figure 29.** CC TTU and replated TTU cells have 4 genes similarly upregulated except IL2 receptor expression. IL2 is a marker of tumor progression, and stimulates cell proliferation in breast cancer.

**HME Combinations.** Result of upregulated genes in homogeneous HME parent cell populations and in CC HME compared to replated CC HME cells. Our experiments showed that the 9 overlapping genes have differences in the fold changes between Parent HME and CC HME cells. Several anti-apoptotic genes are highly expressed in Parent HME. Parent HME is precancerous and demonstrated some gene expression associated with cancer progression. RT-PCR on the Parent HME plate needs to be repeated to validate results these. These results are illustrated in Figure 30.

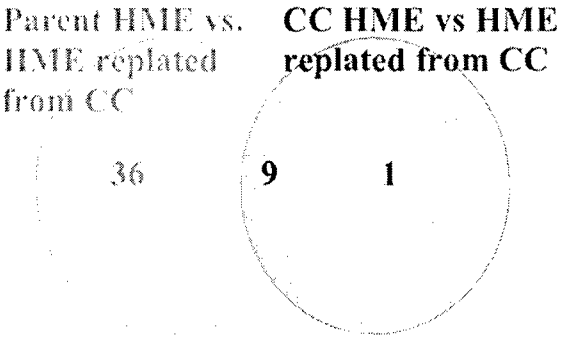


**Figure 30.** Determination of differences in expressed genes between HME parent cell strains and HME in co-culture. i) Unique upregulated gene of CC HME is GABA A receptor; tumor suppressor. ii) Among Common 9 genes, CC HME more tumorigenic compare to Parent HME except cathepsin D, IGF binding protein, AP1. This data is further graphically represented in Figure 31.

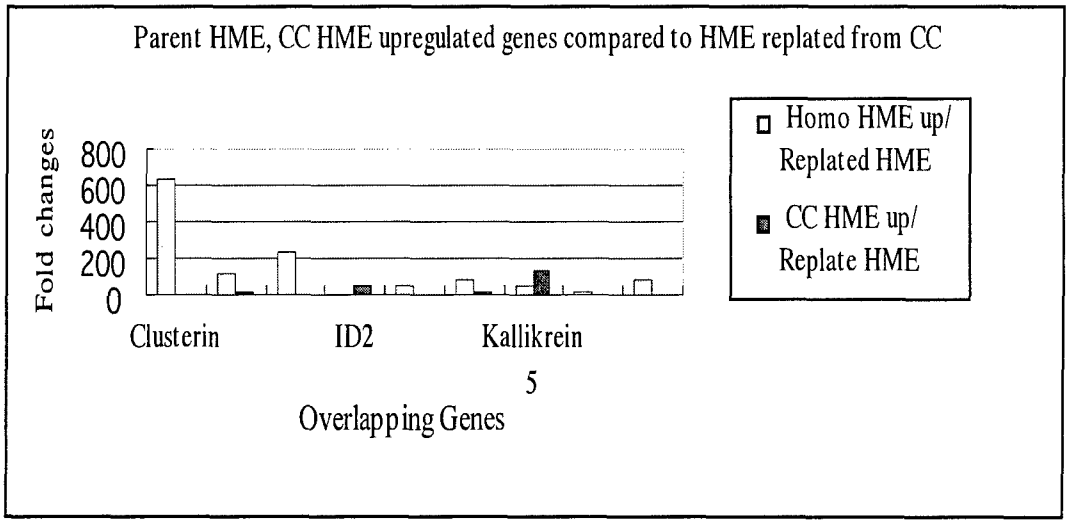


**Figure 31.** Genes upregulated in parent and CC HME that differ from replated HME after CC.

The next analysis was to determine differences in expressed genes between co-cultured HME cells and HME cells isolated from co-culture and replated. Figure 32 shows the results obtained from analysis of fold changes in gene expression between sample sets.

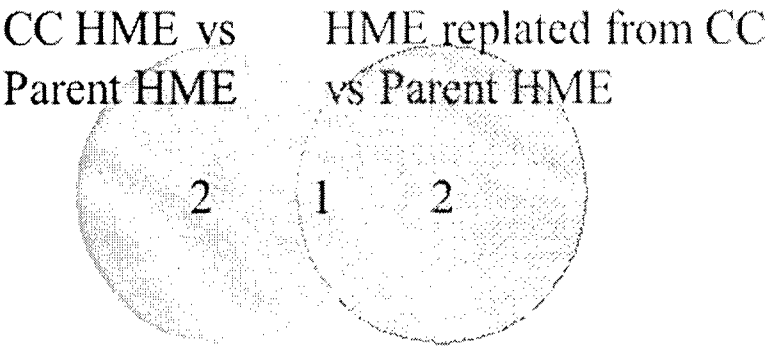


Figure 32. Representation of differences in the genetic profiles of CC HME compared to parent HME and the replated HME from CC compared to parent HME. The uniquely upregulated genes of CC HME not observed in parent HME were: IL2R (develop breast cancer) and IL6 ( proliferation and metastasis of cancer). There were two uniquely upregulated genes of HME replated from CC: GABA, A receptor (tumor suppressor) and ID2A (inhibitor of DNA binding 2 ; promote differentiation and inhibit proliferation. Overlapping gene: TIE (Tyrosine kinase with immunoglobulin-like and EGF-like domains 1) is overexpressed in epithelial breast cancer cells and ductal carcinoma *in situ*. This evidence suggests that due to the physical interactions, CC and Replated HME have similarly upregulated TIE.

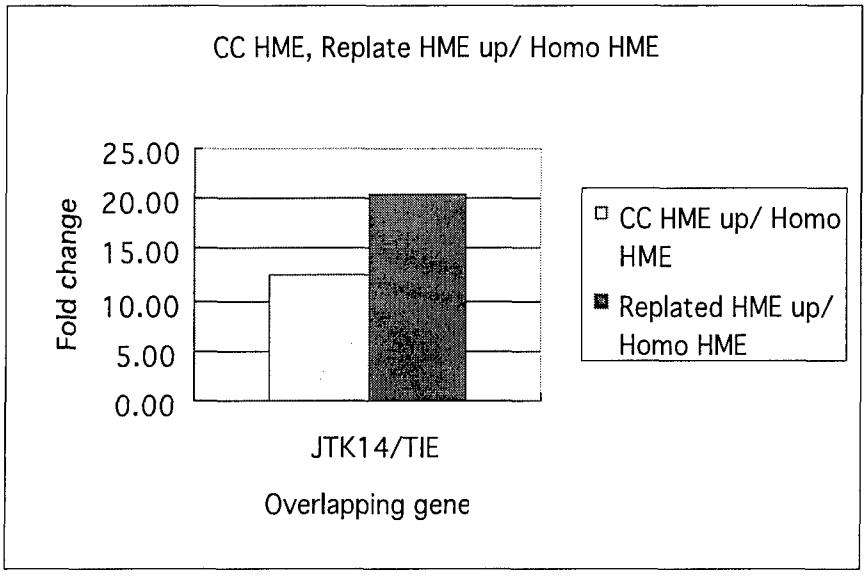


**Figure 33.** Graphic representation of the gene uniquely regulated between the CC HME and the replated HME (after CC). This gene was not observed to be uregulated in the Parent HME, This suggests that the physical interactions which occurred during CC caused the upregulation of this tyrosine kinase that not only remained expressed, but appeared to increase slightly in expression.

This next series of analyses involved comparing fold changes in gene expression between HME cells replated after separation from CC and the CC HME, and the parent HME compared to the CC HME. Figure 34 shows these results.

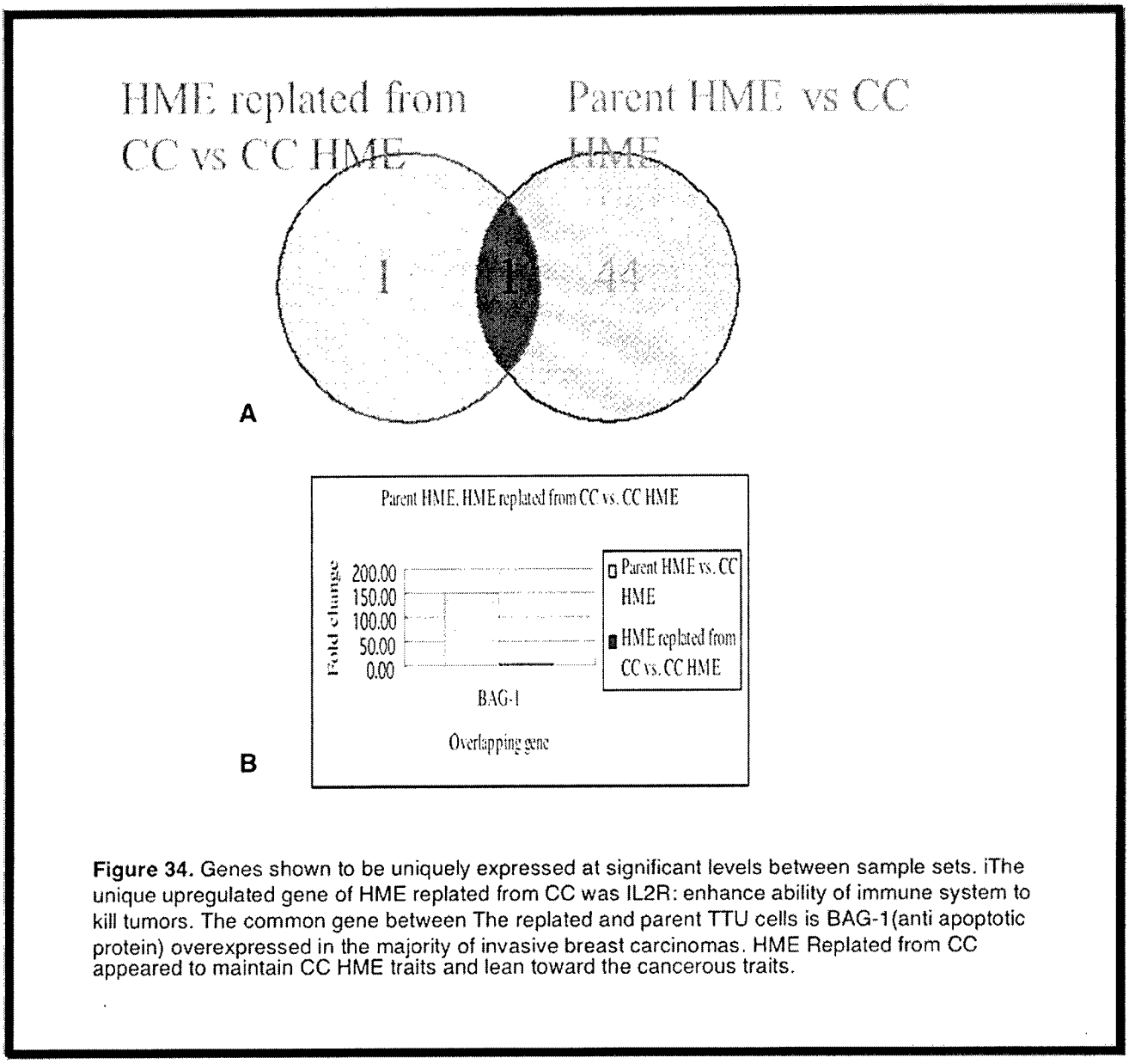


**Figure 34.** Genes shown to be uniquely expressed at significant levels between sample sets. iThe unique upregulated gene of HME replated from CC was IL2R: enhance ability of immune system to kill tumors. The common gene between The replated and parent TTU cells is BAG-1(anti apoptotic protein) overexpressed in the majority of invasive breast carcinomas. HME Replated from CC appeared to maintain CC HME traits and lean toward the cancerous traits.

**TTU and HME Combinations**. In this series of analyses, the genetic profiles for combinations of TTU and HME cultures were cross-references. The cultures compared included parent TTU cells and parent HME cells; CC TTU and CC HME; Replated TTU and replated HME cells after CC and separation. Figure 35 shows these results.

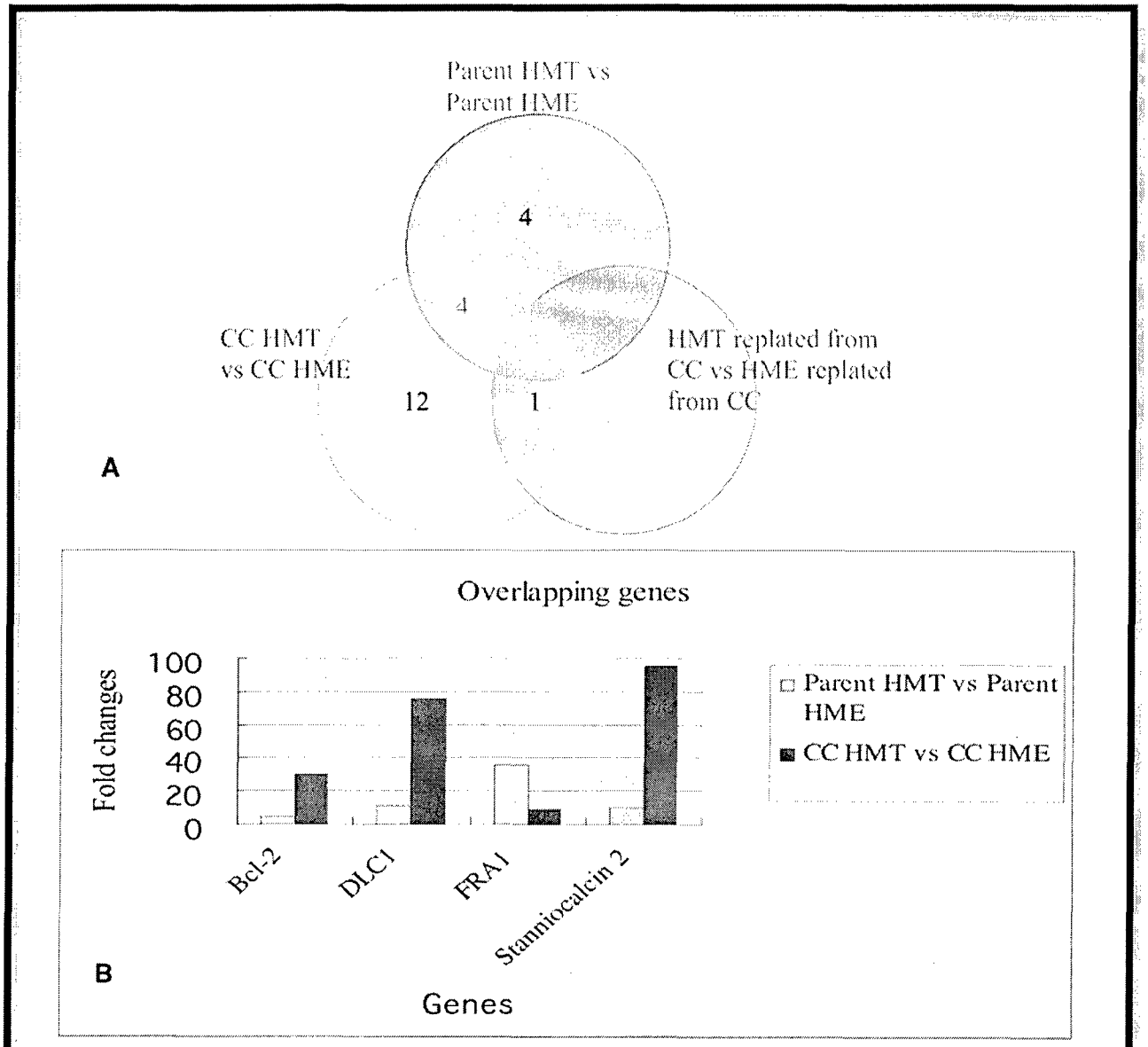


**Figure 35.** A. Determination of differences in expressed genes between homogeneous TTU parent, CC TTU and TTU replated from CC cells compared to corresponding same set of HME cells.
i) Overlapping upregulated 4 genes of Parent TTU and CC HMT: CC TTU tumorigenicity may be inhibited in CC due to direct cell contact with HME. CC TTU showed a significant upregulation of "Deleted in liver cancer 1 (tumor suppressor), Stanniocalcin 2 (an estrogen-responsive gene co-expressed with the estrogen receptor in human breast cancer)" and less regulated Bcl-2. Fra-1(highly expressed in ER(-) breast cancer) was downregulated due to cell direct contact. ii) Overlapping upregulated genes of CC TTU and TTU replated from CC: CC TTU has upregulated clusterin, which promotes oncogenic transformation and tumor progression by interfering with Bax pro-apoptotic activities. Replated TTU show this weakly. iii) Parent TTU unique upregulated 4 genes: Cyclin E, Inhibitor of DNA binding 2, Keratin 18, Non-metastatic cells 1(oncogene)

The final set of analyses presented in this report is the determination of differences in expressed genes between homogeneous HME parent, CC HME and HME replated from CC cells compared to the corresponding same set of TTU cells. Figure 36 Presents these results.

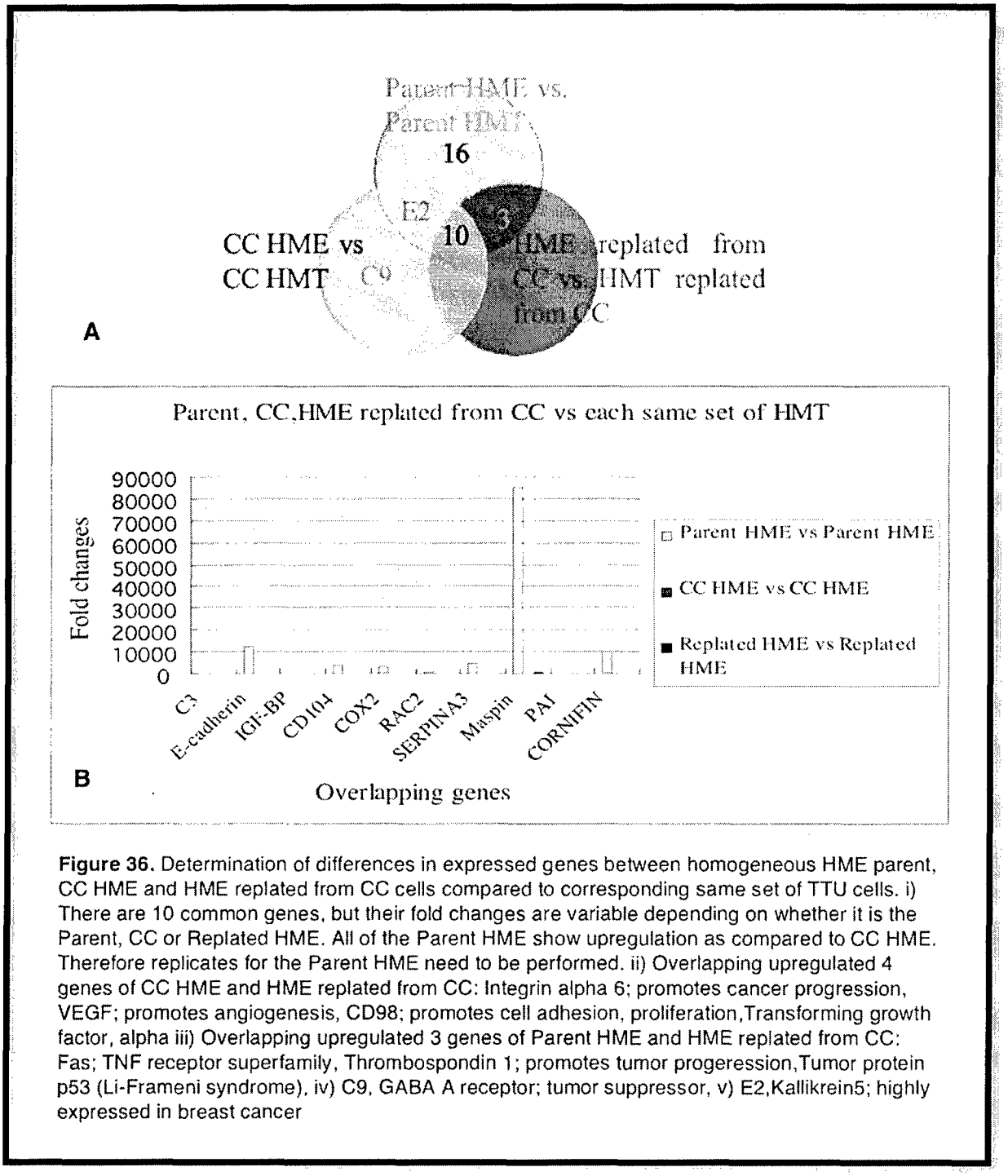


**Figure 36.** Determination of differences in expressed genes between homogeneous HME parent, CC HME and HME replated from CC cells compared to corresponding same set of TTU cells. i) There are 10 common genes, but their fold changes are variable depending on whether it is the Parent, CC or Replated HME. All of the Parent HME show upregulation as compared to CC HME. Therefore replicates for the Parent HME need to be performed. ii) Overlapping upregulated 4 genes of CC HME and HME replated from CC: Integrin alpha 6; promotes cancer progression, VEGF; promotes angiogenesis, CD98; promotes cell adhesion, proliferation,Transforming growth factor, alpha iii) Overlapping upregulated 3 genes of Parent HME and HME replated from CC: Fas; TNF receptor superfamily, Thrombospondin 1; promotes tumor progeression,Tumor protein p53 (Li-Frameni syndrome), iv) C9, GABA A receptor; tumor suppressor, v) E2,Kallikrein5; highly expressed in breast cancer

***Ongoing Experiments.*** Since this project is the dissertation topic for one of my students, we will continue through all the tasks until the project is completed. In addition, we will be incorporating functional assays such as siRNA work on selected genes shown to be expressed at significantly higher levels between analyzed cell sets. We are currently Repeating the RT-PCR Parent HME for data consistency, to validate the fold observed after analysis. Nayoung is currently finishing up the RT-PCR based analysis for the Parent HMS and HME50, Co-cultured HMS and HME, Replated HMS and HME. Once she completes the genetic profile analysis for these, she will repeat the same series of experiments in the presence of Taxol at physiologic concentrations. After clustering and/or comparative data analysis, we will have detailed gene expression information of isolated cells compared to homogeneous cells. Several key genes such as MMP, EMMPRIN, HTERT, VEGF etc., will be selected for functional assay such as RT-PCR, si-RNA and Western Blotting.

*Discussion of Conclusions may be found in the conclusions section of the fina report format sheet.*

Summary of Accomplishments for Tasks 1c, 2c, 3c.

Task 1C controls completed.

Task 2C controls completed.

Task3C control completed.

In cells treated with Taxol, we expect that bcl-2 and telomerase will be downregulated in HME and tumor cells while p53 and p21 will be upregulated. This is based on the relative decrease in telomerase activity for the HME and tumor cells. In considering the effects of Taxol on the HME and tumor cells, and the lack of effect on the HMS cells, the relationship between bcl-2 with the mitochondria and endoplasmic reticulum, leads us to suspect that genes associated with the caspase initiated apoptosis pathways would also be differentially expressed. Thus caspase-9, APAF-1, caspase-3 would be expected to be upregulated as well as BID, BAX and BIM after translocation to the mitochondria. Caspase-12 activity has been associated with the endoplasmic reticulum. If necrosis is the actual mechanism of cell death, then expression of NF-κB would be interesting to note. In contrast, bcl-2 is expected to be highly expressed in the HMS cells as well as other anti-apoptotic genes such as bcl-XL, mcl1 and bfl1. Other genes with significant differences in expression include pRb,p53, p21, c-myc and the endoplasmic reticulum and mitochondrial membrane associated proteins involved in stress response such as calreticulin and the family of heat shock proteins. Differential expression of these genes named (as a few examples) would correlate with the effects of Taxol on the HME/tumor cells vs. the HMS cells.

While comparing the sensitivities of different cell types to Taxol it is interesting that the HME and tumor cells were greatly affected, whereas the HMS cells appear to be resistant to treatment. The HMS cells may be resistant due to the expression of the mdr gene(p-170-mdr) which acts to remove lipophilic compounds like Taxol out of the cell [69, 70]5). Over-expression of this gene has been shown to cause drug-resistance in many cell lines [71-74]. Another gene implicated is c-erb2 which has similarities to epidermal growth factor receptor (EGFR). Resistance of HMS cells could be due to the increased expression of either or both of these genes. This also suggests that the HME and tumor cells are not expressing those genes and hence are sensitive to Taxol treatment. Cellular apoptosis must also be considered while looking at cellular sensitivity. Bcl-2 levels are likely to influence this differential response to Taxol. Our results suggest that active bcl-2 is maintained at basal levels or decreased in HME and tumor cells. The HMS cells by producing increased levels of bcl-2 prevent apoptosis. This would be true if Taxol influenced bcl-2 expression, either directly or indirectly in addition to causing its phosphorylation.

The analysis of cellular recovery provides intriguing results. The inability of HME cells to recover and their change in morphology could be due to permanent blockade of cells in metaphase-anaphase transition of mitosis. Additionally, Taxol may cause the cells to terminally exit the cell cycle, preventing further replication. Since the HMS cells showed little sensitivity, their full recovery following the exposure was not surprising. This confirms the resistance of these cells to Taxol and that their ability to replicate has not been lost. The tumor cells TTU-1 and SCC-1419 show high sensitivity to Taxol with the ability to recover after the exposure. This suggests different molecular targets of Taxol in epithelial versus the tumor cells. Also it indicates an ability to overcome apoptosis or recognize the cytoskeletal matrix

in order to complete mitosis. Previous studies showed no influence of Taxol on telomerase activity [75-77]. Results from our study showed that HME and tumor cells had decreased telomerase activity following exposure to Taxol. HMS cells showed increased telomerase activity following the exposure. Bcl-2 has been implicated in telomerase activity enhancement [78]. If HMS cells expressed high levels of bcl-2 as previously proposed, telomerase activity would increase accordingly. With low levels or inactive bcl-2, the HME cells and tumor cells would either have constant or decreased telomerase activity.

Only two possible mechanisms have been proposed here to explain the differential response to Taxol seen between the HME and HMS cells. Many other factors could play a role. For example, the HMS cells could have a mechanism to metabolize the drug, unlike the HME cells and thereby be able to prevent the action of Taxol. Additional studies need to be done to further confirm this cell-lineage specific response to Taxol using more replicates and over a longer time period.

This study has however underlined the need to realize the significance of considering lineage derived characteristics of cells while using cell-lines for study. Also complete recovery of tumor cells following removal of Taxol sets an alarm.

**Other methods attempted for generating genetic profiles:** In this proposal, several options were discussed for microarray analysis to generate gene expression profiles. We looked at several options and initially decided to apply Serial Analysis of Gene Expression (SAGE). Although the sequencing can be very expensive, we had discussed a considerable discount with the Biotech facility on campus. Figure 37 summarizes this technique. The most attractive aspect to the SAGE is there is no normalization run necessary. SAGE is an open system for gene expression profiling analysis. The advantage is its inclusiveness and the ability to detect relatively rare transcripts. It can potentially reveal expression levels of all genes. It is "unbiased" and "comprehensive" compared to microarray, because microarrays are closed, since they only allow you to investigate the genes spotted on the array. However, the procedure is rather tedious and involves multiple steps and extensive sequencing (normally, close to 50,000-100,000 clones will be sequenced per library and the data analyzed). Therefore, all the products would be considered *de novo*.

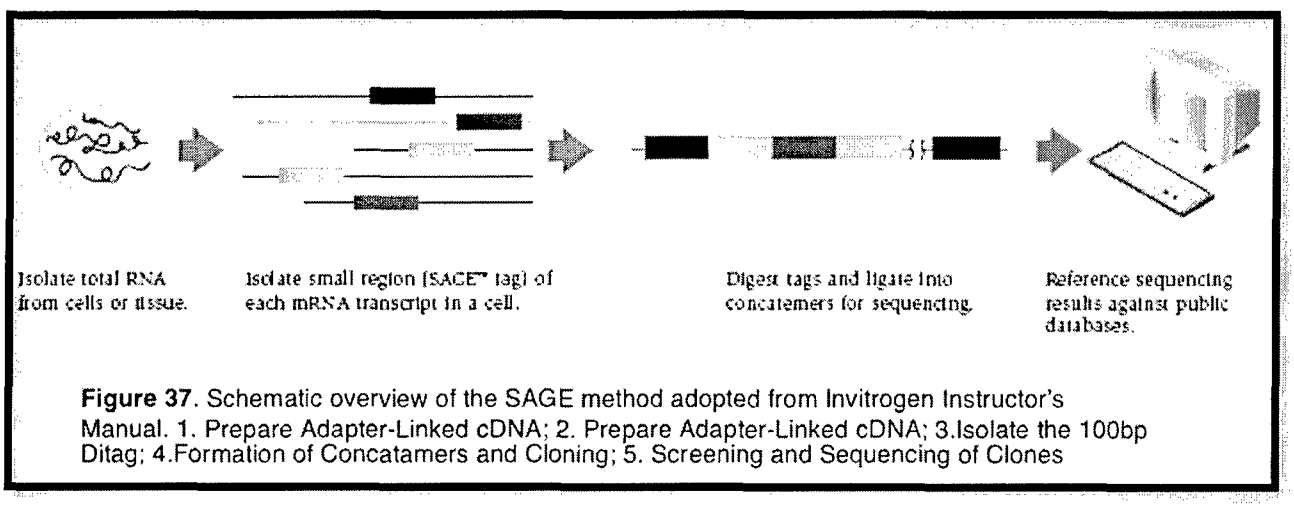


**Figure 37**. Schematic overview of the SAGE method adopted from Invitrogen Instructor's Manual. 1. Prepare Adapter-Linked cDNA; 2. Prepare Adapter-Linked cDNA; 3.Isolate the 100bp Ditag; 4.Formation of Concatamers and Cloning; 5. Screening and Sequencing of Clones

*SAGE (Serial Analysis of Gene Expression)* is a method to construct SAGE libraries for quantitative analysis of gene expression in samples of cells. The procedure is as follows (referring invitrogen I-SAGE kit):

1. Isolate total RNA from cell lysate
2. Checking the total RNA Quality using a regular 1% agarose gel. We should see the 28S and 18S rRNA bands. The 28S band should be twice intensity of the 18S band.
3. Prepare oligo (dT) beads and bind my RNA sample to oligo (dT) magnetic beads. The beads capture poly A+ RNA (mRNA) directly from my total RNA
4. Synthesize double stranded cDNA on the beads containing my mRNA using SuperScript II reverse transcriptase and E.coli DNA polymerase.

5. Digest the double stranded cDNA with a sequence specific restriction enzyme (an anchoring enzyme) that cleaves most transcripts at least once. Nla III is used as an anchoring enzyme since Nla III sites are known to occur approximately every 250bp.
6. Verifying cDNA synthesis and Nla III digestion by PCR
7. Divide the cDNA into two fractions and ligate with two adapters (A and B,~40bp each). The adapters contain cohesive 4bp overhangs (CATG) complementary to the Nla III digested cDNA, a Type IIS restriction enzyme (tagging enzyme; BsmF I) recognition site at the 3' end, and priming sites for PCR amplification at 5' end.
8. Cleave with Type IIS restriction enzyme (tagging enzyme), BsmF I. The tagging enzyme binds to the recognition sequence in the adapter and cleaves the cDNA 10~14bp downstream from the recognition site releasing a ~50bp tag with a 4bp overhang at the 5' end. The tag consists of ~40bp of adapter sequence and 10~14bp of unique sequence from a single transcript.
9. Perform a Klenow reaction to fill-in the 5' overhangs created by BsmF I digestion and ligate the two fractions of tags to form ~100bp ditags.
10. Amplify the ~100bp ditags using primers specific for the primer binding sites in the adapters to produce sufficient ditags for subsequent generation of concatamers. However, Ditag Primer (DTP) -1 and -2 provided by invitrogen have low yield. Specially, a large percent of the DTP-2 oligonucleotide is self-complementary. The majority of original primer DTP-2 formed dimmers, thus reducing the PCR efficiency. I found another paper mentioning modified ditag primers, and sequenced oligonucleotides based on their modified ditag primers. They designed a new primer pair located at the 3' ends of each linker.
11. Cleave the ~100bp ditags with the anchoring enzyme that was used to cleave the original cDNA (Nla III) to release a 26bp ditag. These ditags are comprised entirely of sequences derived from transcript cDNAs. Each ditag is punctuated by Nla III recognition sequence. The 26bp ditags are purified away from the adapters by 20% polyacrylamide gel electrophoresis.
12. Ligate the 26bp ditags to form concatemers. Gel purify fraction containing 20~50 tags (usually 520bp~1300bp)/concatemer
13. Clone the concatemers into the pZErO-1 vector to obtain a SAGE library. Sequence selected clones. Each transcript is identified by its unique 10~14bp sequence tag and is quantified by the number of times the tag occurs within a given population of clones. We sequenced 14 transcripts then did BLAST search in NCBI web, but most of them have not characterized yet.

Figure 38 demonstrates the concatamers generated and the relative success from the method. The problem became the cost, labor and time intensive experiments. In addition, in discussions with the student responsible for this project, for her dissertation, we decided to add functional assays as well to key genes that were reported as upregulated. Therefore we compared traditional spotted microarray (~35K probes) , illumina beadchip. "Human illumine 6 BeadChip (~47K probes) and the Superscript RT-PCR based Arrays.

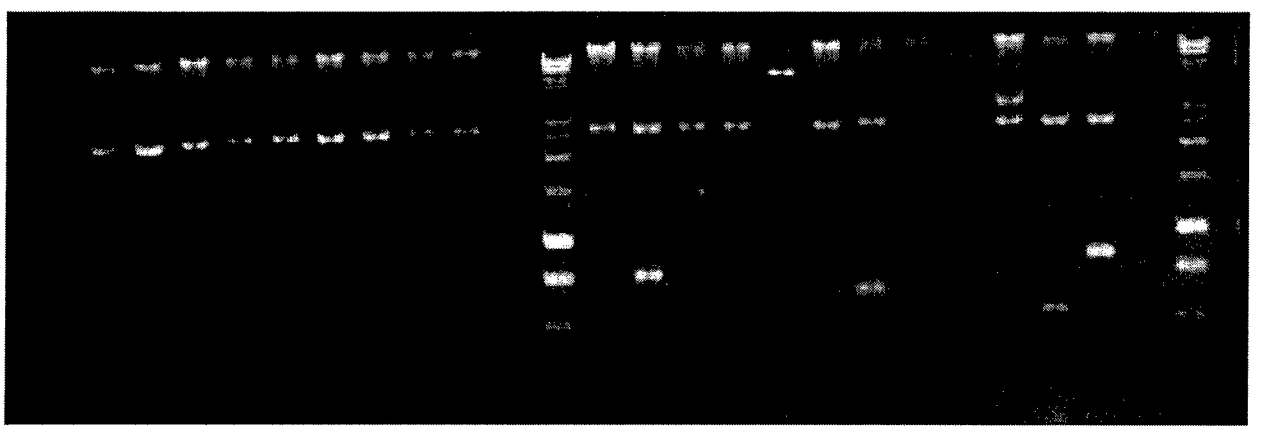

**Figure 38.** SAGE results. BamHI and Xbal digestion results for concatamers generated s result of the ditags. Several of the relatively big inserts (>600bp) were selected in order to reduce the overall sequencing price. Approximately 15 transcripts were sequenced. However, this did not yield any useable results because generally 100,000 are needed to form a genetic profile. For this reason, SAGE was replaced in lieu of SuperScript RT-PCR Arrays.

**Task 1d.** Determine the differences between HME and HMS cells in the uptake and efflux transport characteristics for Taxol (Months 6-12).

The goal of these experiments was to study the contribution of drug accumulation to Taxol resistance. The ability of tumor cells to efflux cytotoxic drugs like Taxol is a major cause of multidrug resistance in chemotherapy [79, 80] Krishna and Mayer, 2000). Typically, multidrug resistance results from the expression of ATP-dependent drug efflux transporters ("pumps") in the plasma membrane [3, 81]. For example, meta-analysis of some 31 reports (from 1989-1996) found that 41 % of breast tumors expressed one such pump, known as multidrug resistance protein 1 (MDR1) [9]. MDR1 and several other transporters are capable of extruding Taxol (and a broad array of other anti-tumor drugs) from the cell, reducing its ability to kill the cancer cell [7, 82, 83].

To measure Taxol accumulation in normal human mammary cells, we first carefully validated several critical transport and cell culture characteristics. These included 1) cell culture substrate, 2) shaking speed during the transport assay, 3) initial seeding density, 4) duration of cell growth prior to transport measurements, and 5) influence of growth factors on transport. These validation studies were extensive and time-consuming, but absolutely necessary. All subsequent transport measurements employed an optimal combination of experimental conditions based on these findings.

For the validation studies, we chose normal human mammary epithelial cells (HME 50) over equivalent cell lines because our stock of these cells was the most plentiful. Given that extensive experiments require large numbers of cells and our normal mammary cell lines can undergo only a limited number of population doublings, this choice was advantageous. In addition, because of numerous validation experiments, we chose to study glucose transport as a surrogate solute for Taxol uptake, for several reasons. First, the validation experiments were aimed at selecting cell culture conditions that optimized speed of cell growth, tolerance to the high shaking speeds used in the transport experiments, and expression of membrane transporters. Glucose uptake is a faithful reporter of cell viability, membrane integrity, and transporter differentiation, particularly when the transport assay measures influx mediated by glucose transporters (i.e., GLUT1), as our technique does [84]. Second, breast tumor cells show increased expression of GLUT1 compared to normal cells [85] so that changes in glucose uptake may parallel the upregulation of other transporters (e.g., MDR1). Finally, the cost of radiolabeled glucose is only one-fifth that of labeled Taxol. Hence, it was prudent to reserve the more costly Taxol transport experiments for post-validation experiments.

To validate our transport assay for later measurements of Taxol uptake, it was essential to establish cell growth conditions that would enable the cells to withstand significant shaking speeds encountered in the transport assay. Why not simply eliminate shaking during the assay, preventing any chance of cells becoming detached or damaged? The absence of shaking produces unstirred layer effects, causing the solute concentrations in the bulk solution to differ significantly from that adjacent to the plasma membrane, owing to diffusional resistance. This results in a serious underestimation of solute uptake by several fold. For hydrophobic solutes like Taxol, the effect of unstirred layers is disproportionately large (i.e., unstirred-layer resistance becomes rate-limiting for highly permeant solutes). Unfortunately, previous studies of Taxol transport have typically failed to measure transport under conditions where unstirred layer effects were minimized [see 83, 86, 87, 88]. We aimed to avoid this error by analyzing the effects of stirring rates on solute uptake.

HME 50 cells were seeded at 50,000 cells/well in 24-well plates, grown to a confluent monolayer for 5 days directly on plastic substrate, with a low epidermal growth factor (EGF) concentration (10 ng/ml) in the medium. For the transport assay, the culture medium was replaced with transport buffer (37 EC) containing 50 mM D-glucose in the apical (milk) compartment, together with trace amounts of $^{14}$C-D-glucose as probe and $^{3}$H-L-glucose as marker. The cells were incubated for 15-min, then rinsed to reduce adherent fluid before lysis in NaOH. An aliquot of the lysate was reserved for protein determination and the remainder counted in a liquid scintillation spectrometer. Under these conditions, the resulting transport calculations represents initial rate influx through membrane glucose transporters (e.g., GLUT 1), having been corrected for both extracellular adherent fluid and simple diffusion of glucose.

Figure 39 shows the results for measuring glucose uptake at different shaking speeds. As shaking speed increases up to 900 rpm, there is a linear increase in nutrient uptake, as unstirred layer effects are proportionately reduced.

However, at the maximum speed tested (1200 rpm), membrane integrity or cell viability is dramatically reduced, as evidenced by the 80 % fall in glucose uptake.

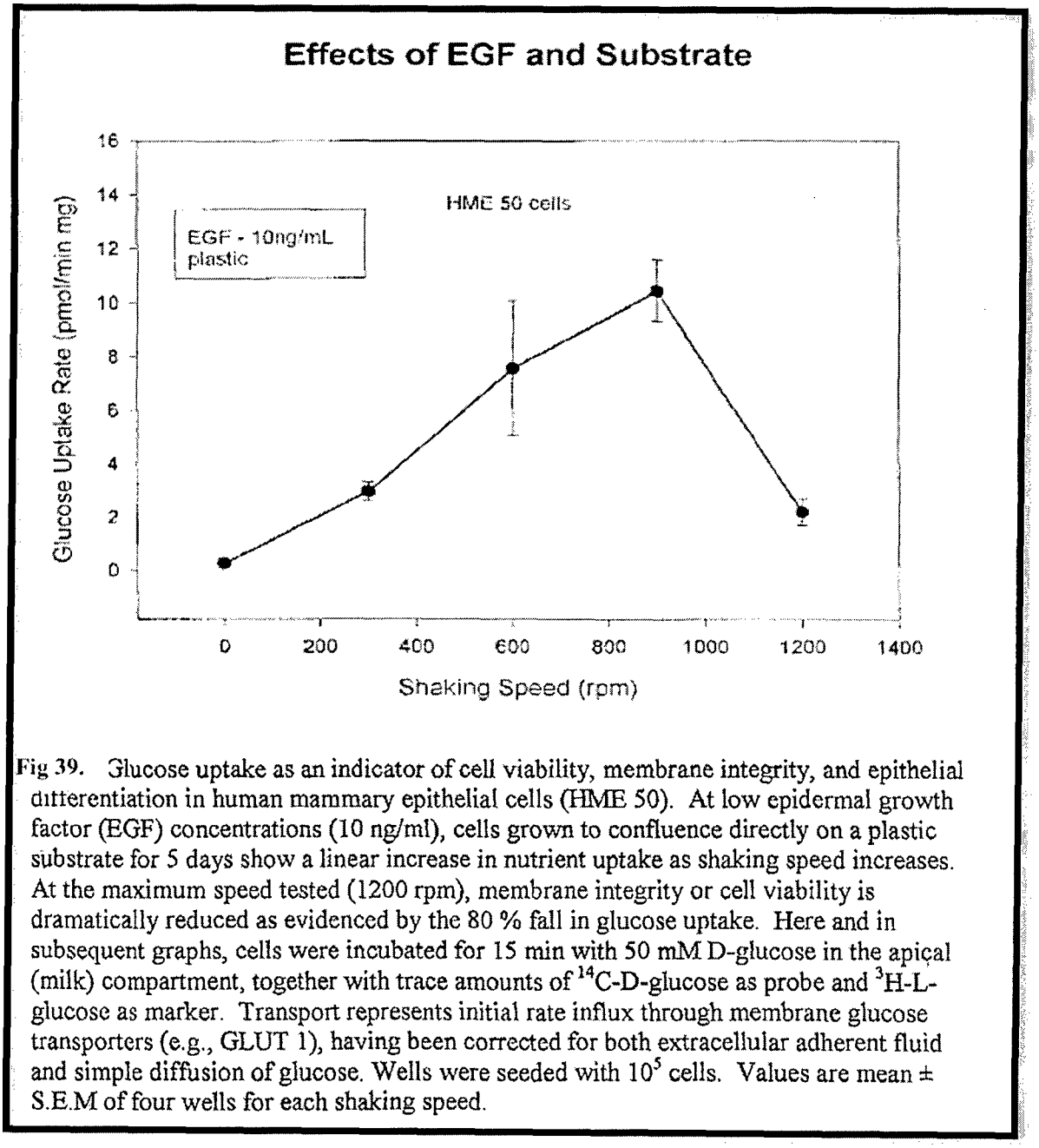


Fig 39. Glucose uptake as an indicator of cell viability, membrane integrity, and epithelial differentiation in human mammary epithelial cells (HME 50). At low epidermal growth factor (EGF) concentrations (10 ng/ml), cells grown to confluence directly on a plastic substrate for 5 days show a linear increase in nutrient uptake as shaking speed increases. At the maximum speed tested (1200 rpm), membrane integrity or cell viability is dramatically reduced as evidenced by the 80 % fall in glucose uptake. Here and in subsequent graphs, cells were incubated for 15 min with 50 mM D-glucose in the apical (milk) compartment, together with trace amounts of $^{14}$C-D-glucose as probe and $^{3}$H-L-glucose as marker. Transport represents initial rate influx through membrane glucose transporters (e.g., GLUT 1), having been corrected for both extracellular adherent fluid and simple diffusion of glucose. Wells were seeded with $10^5$ cells. Values are mean ± S.E.M of four wells for each shaking speed.

Next, we examined how glucose uptake changed under different seeding densities, duration of cell culture post-seeding, and with shaking during cell growth. The last of these variables–shaking during cell growth– was included because in multi-well plates, some cells on a single plate may be assayed on different days and thus, subjected to shaking before the actual transport assay. We wish to know how this might affect transport, and the results are shown in Figure 40. With one exception (cells seeded at the lower density and shaken during culture), glucose uptake generally increases with time in culture after seeding. Higher seeding densities (which uses up more cells) produced greater uptake rates only in cells shaken during culture and only at the longest duration in culture (14 days). Accordingly, there was no significant advantage to using the higher seeding density. Although all cells were shaken

during the transport assay, those that were subjected to a shaking episode during growth in culture clearly exhibited a glucose uptake pattern that was different and not desirable compared to those not shaken. Hence, growing cells for 7 - 10 days at the lower seeding density (5 x $10^4$) and not shaking them during culture appears the best compromise among the multiple conditions tested.

**Effects of Seeding Density and Shaking During Growth**

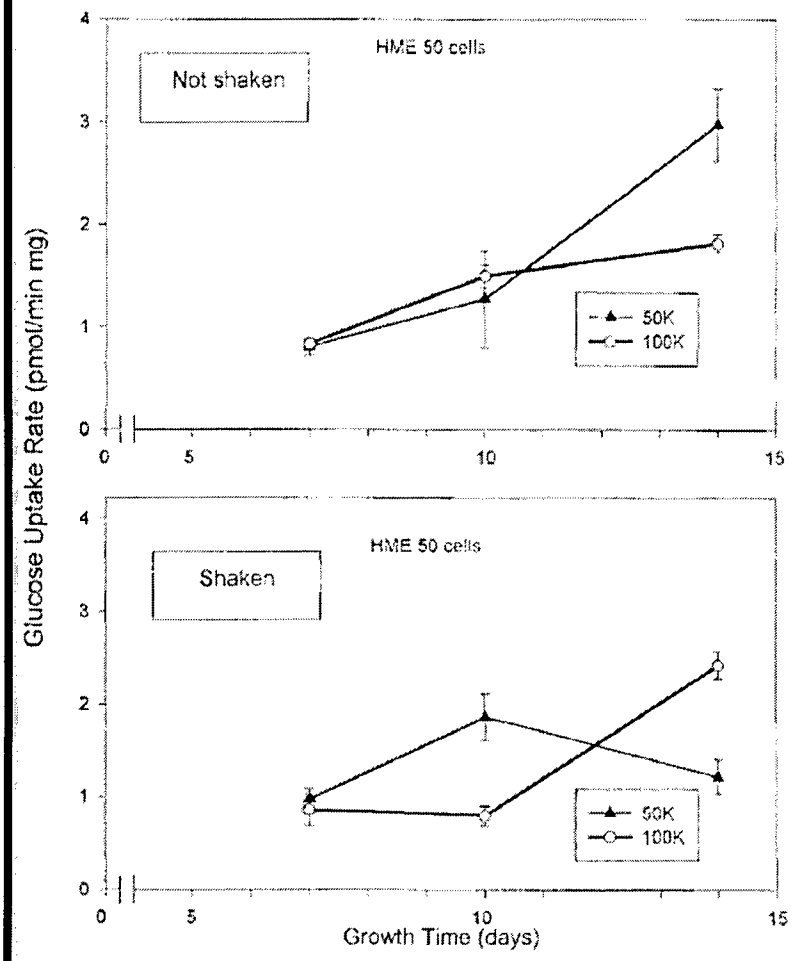


Fig 40. Effects on glucose uptake of seeding density (50K vs. 100K), duration of cell culture after seeding, and shaking during cell growth. Overall, glucose uptake increases with time in culture after seeding, with one exception (cells seeded at the lower density and shaken during culture). Seeding cells at higher densities produced greater uptake rates only in cells shaken during culture and only after 14 days post-seeding. Cells that were shaken during growth (as opposed to during the uptake measurement) showed a pattern of glucose uptake with time in culture that was clearly different, though not superior to those not shaken. Thus, growing cells for 7 - 10 days at the lower seeding density (5 x $10^4$) and not shaking them during culture appears the best compromise among the multiple conditions tested. Other conditions were identical to those listed in Figure 39 legend.

Optimal growth rates that rapidly produce differentiated cells with high transporter expression was another aim of these experiments. We tested the effects of adding at higher concentration EGF to achieve that result. For HME 50 cells grown on plastic wells for 7 days post-seeding, the higher EGF concentration gave unexpected results, as shown in Figure 41. Although the cells reached confluence faster, glucose uptake rates were depressed and essentially independent of stirring speeds, except at the highest speed tested (600 rpm). A possible explanation is that cells grown on plastic divide rapidly at the higher EGF concentration, but fail to differentiate and to express GLUT1 transporters at high levels. Alternatively, at higher cell division rates, a different substrate may be required to support adequate cell adhesion and transporter differentiation.

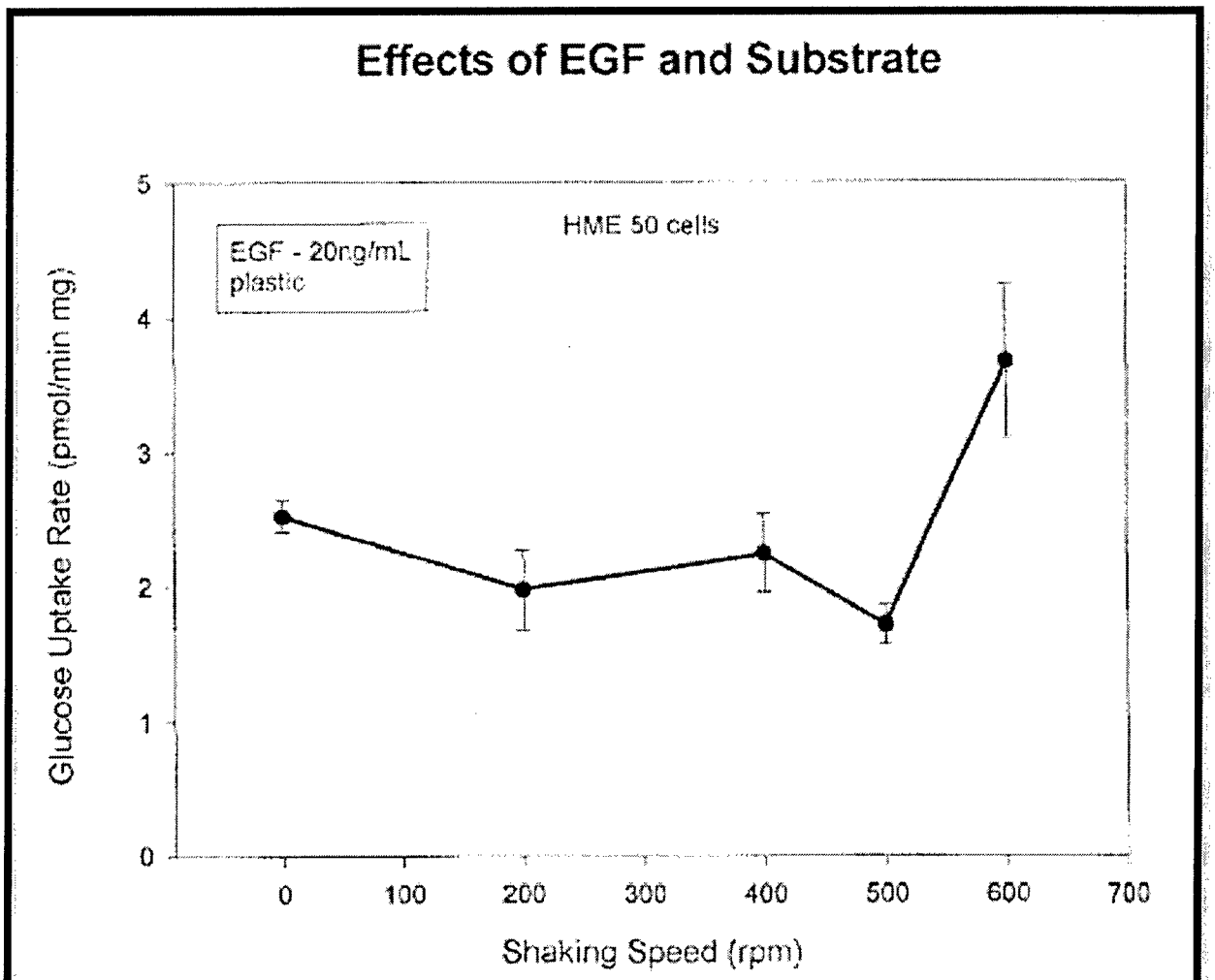


**Fig 41.** Glucose uptake as a function of shaking speed in cells grown at a high EGF concentrations to accelerate growth. Although the mammary cells became confluent faster, glucose uptake rates were depressed and increased slightly only at high shaking speeds (600 rpm). Other conditions were identical to those listed in **Fig. 39 legend.**

We tested how coating the wells with two different extracellular matrix proteins (ECMs) might influence transporter expression. Both fibronectin and laminin are ECMs found underlying mammary epithelial cell in normal breast tissue. When cells exposed to the higher EGF concentration were grown on fibronectin-coated wells, glucose uptake was significantly enhanced at all stirring speeds, compared to those grown on plastic at the same EGF concentration (Fig. 42. In contrast, growing cells on fibronectin, but adding a lower EGF concentration, resulted in depressed glucose

uptake rates (Fig. 43, appendix). Moreover, the transport rates no longer increased as a function of shaking speed. Thus, growing cells on fibronectin at high EGF concentrations produced the best combination of rapid cell growth and transporter expression.

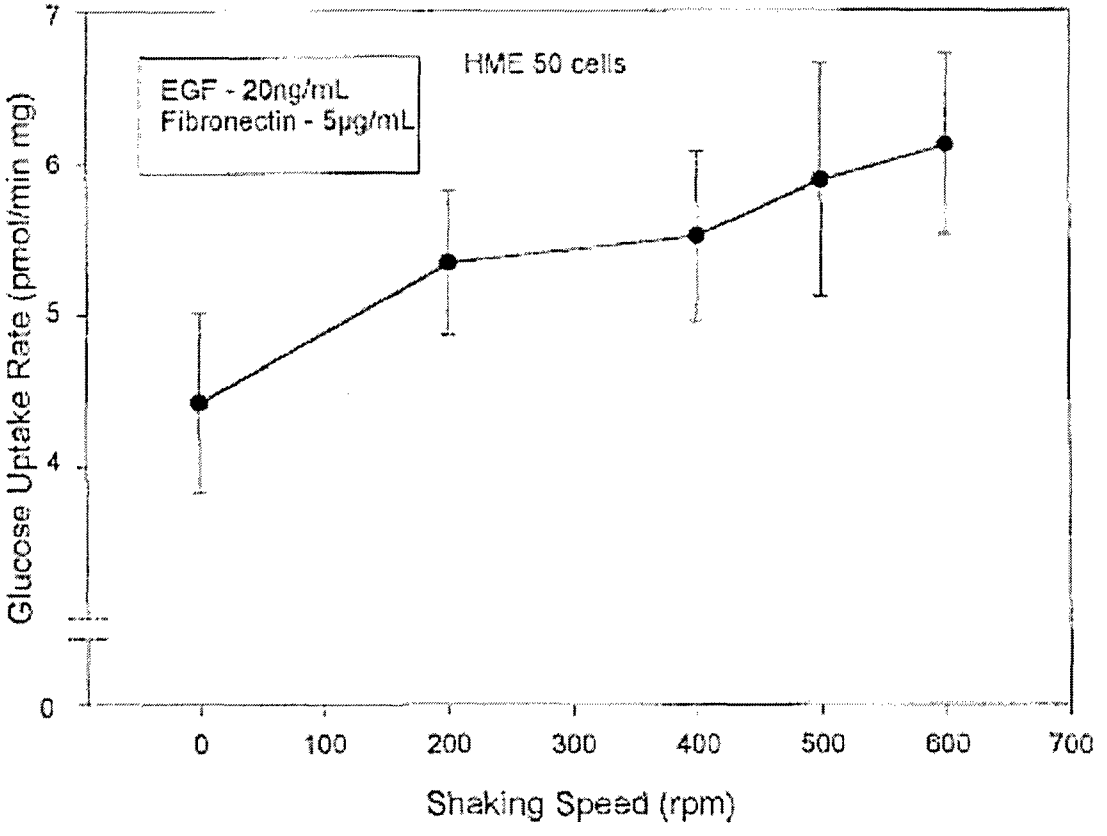


**Fig. 42** Effects on glucose uptake of growing cells on a substrate coated with the extracellular matrix protein fibronectin. In contrast to mammary cells grown on plastic, those grown on fibronectin at high EGF concentrations show a linear increase in glucose uptake as shaking speed was raised to 600 rpm. See **Fig. 39 legend** for other conditions.

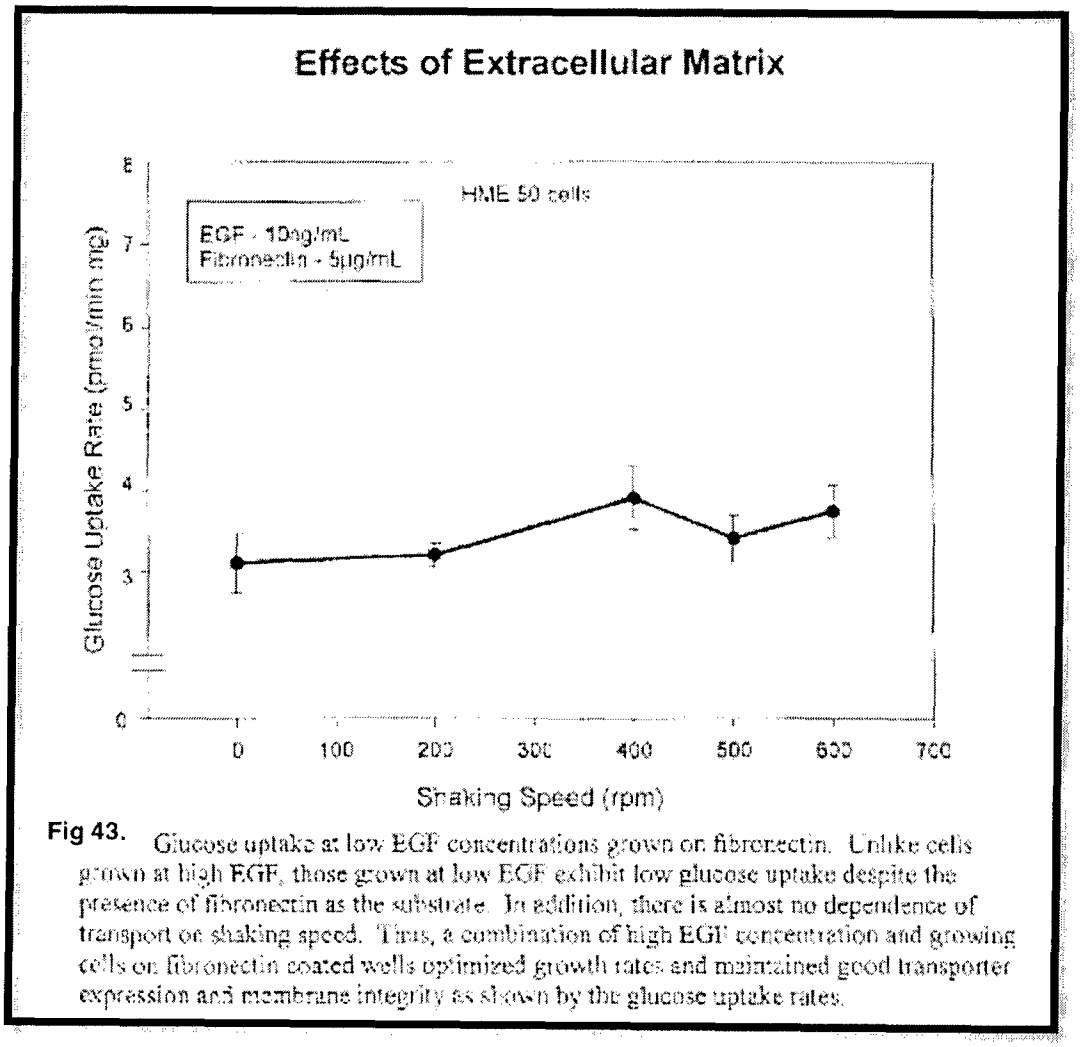


**Fig 43.** Glucose uptake at low EGF concentrations grown on fibronectin. Unlike cells grown at high EGF, those grown at low EGF exhibit low glucose uptake despite the presence of fibronectin as the substrate. In addition, there is almost no dependence of transport on shaking speed. Thus, a combination of high EGF concentration and growing cells on fibronectin coated wells optimized growth rates and maintained good transporter expression and membrane integrity as shown by the glucose uptake rates.

We also examined whether growing cells on laminin might enhance glucose uptake rates. At the lower EGF concentration, cells grown on laminin did exhibit higher glucose uptake rates than those grown on fibronectin (Fig. 44). Nevertheless, when shaking speeds were raised moderately above 200 rpm, glucose uptake dropped precipitously. This indicates that the cells, although well differentiated, were adhering less tightly to their underlying substrate.

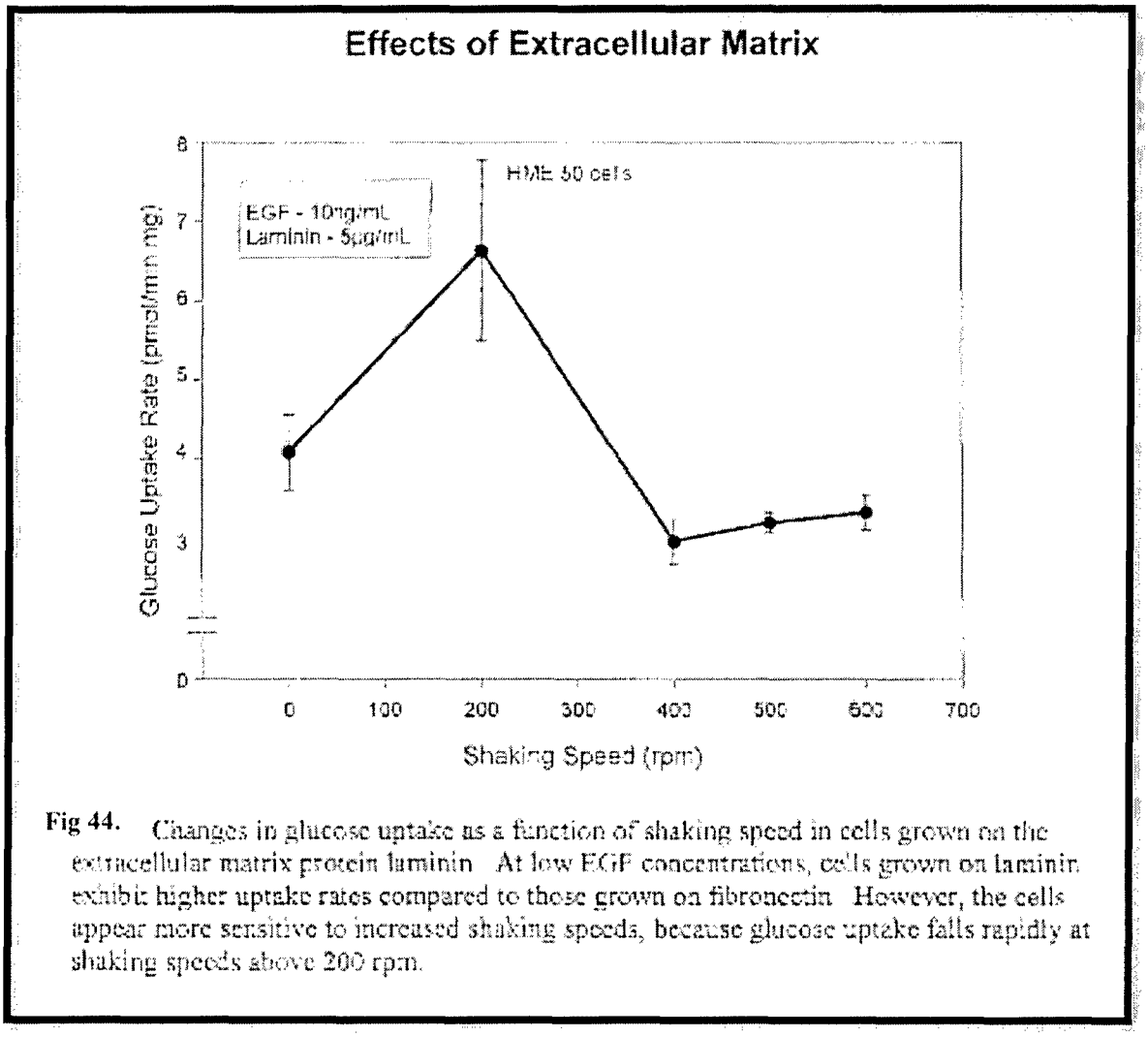


**Fig 44.** Changes in glucose uptake as a function of shaking speed in cells grown on the extracellular matrix protein laminin. At low EGF concentrations, cells grown on laminin exhibit higher uptake rates compared to those grown on fibronectin. However, the cells appear more sensitive to increased shaking speeds, because glucose uptake falls rapidly at shaking speeds above 200 rpm.

With the completion of these initial validation studies, three problems remained. First, the growth of cells in culture was variable, sometimes requiring up to two weeks to achieve confluent monolayers that could be used for the transport experiments. Second, the protein determinations used to normalize the transport uptake per well were inherently variable. Third, the transport measurements conducted at different shaking speeds were unpredictable. We addressed these problems in the following way.

Normal human mammary epithelial cells (HME-50) cells were initially seeded at 50,000 cells/well in 24-well plates, grown to a confluent monolayer for 5 days directly on plastic substrate, with a low epidermal growth factor (EGF) concentration (10 ng/ml) in the medium. To speed up the time to confluence, reduce variation, increase replications, and improve assay flexibility, we changed to a multichannel pipetter/96-well plate format (seeding at 100,000 cells/well). This allowed for more consistent cell numbers in each well and confluent monolayers at 3-4 days, depending on the cell type studied.

For the transport assay, the culture medium was replaced with transport buffer (37°C) containing 50 mM D-glucose or 1 $\mu$M Taxol in the apical (milk) compartment. The 50-mM D-glucose included trace amounts of $^{14}$C-D-glucose as probe and $^{3}$H-L-glucose as marker. For 1$\mu$M Taxol, $^{3}$H-Taxol was used as probe and $^{14}$C-inulin as marker. The cells were incubated for various time periods, then rinsed to reduce adherent fluid before lysis in NaOH. Initially in our tests, an aliquot of the lysate was reserved for protein determination and the remainder counted in a liquid scintillation

spectrometer. However, we discovered that NaOH interfered with the protein determination due to interactions with the kit reagents, changing their colormetric response. To circumvent this serious problem, we switched from protein determination to cell enumeration via measuring a fluorescent probe (carboxyfluorescein diacetate succinimidyl ester (CFSE) from Molecular Probes) in black-wall/clear-bottom 96-well plates. Since many fluorescent dyes are excellent solutes for MDR pumps, we specifically selected the CFSE dye because it is inaccessible to the pump, owing to the dye's conjugation to intracellular amine groups and retention inside the cell [89-91].

Through extensive testing, 10 $\mu$M CFSE in transport buffer was determined to be optimal for cell enumeration in 96-well plates for HME, HMS and tumor cell types (see Fig. 45). It was important to carefully rinse off excess extracellular CFSE without losing cells as this affected the fluorescence measurement for both adherent and suspended cells (for the standard curve). As Figure 46 shows, pairing CFSE measurements with Coulter cell counts has shown that fluorescence measurements accurately reflect cell number per sample well.

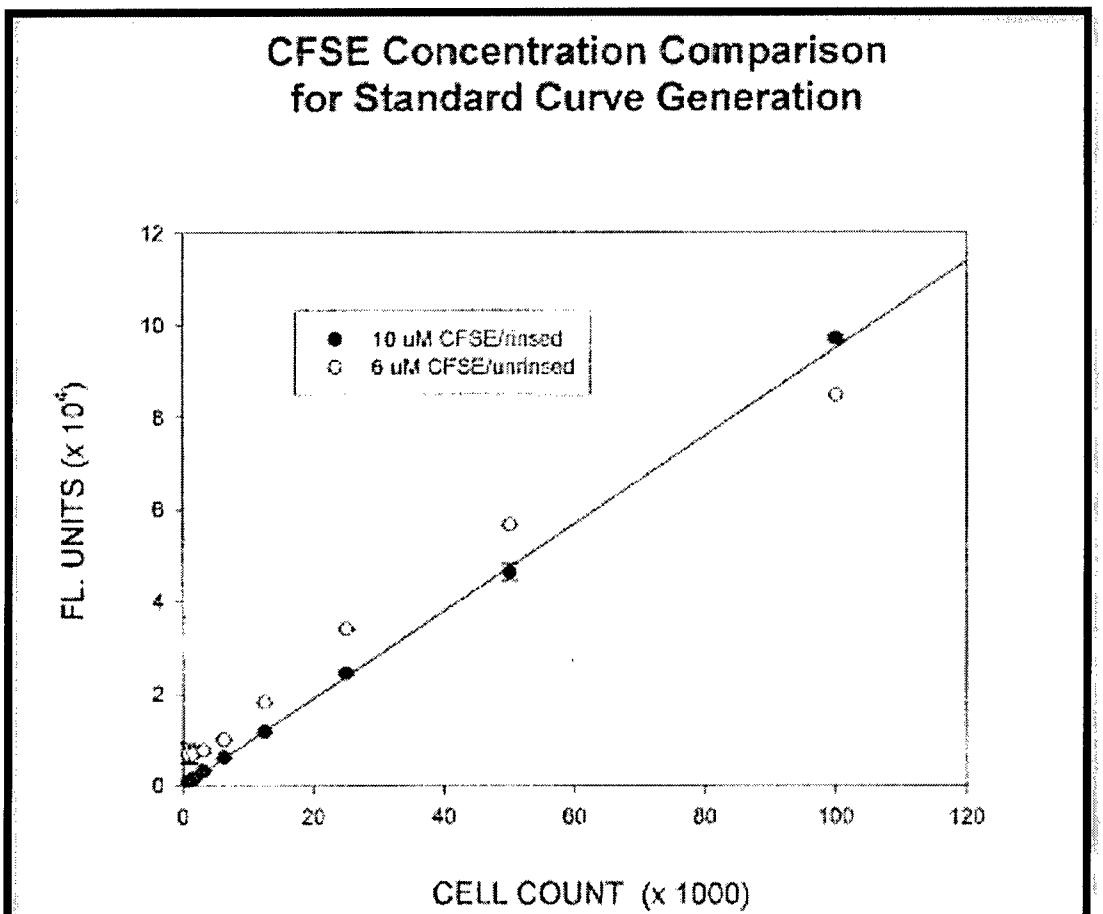


Fig 45 Generation of standard curve using 10 um (rinsed) and 6 uM (unrinsed) CFSE in transport buffer for human mammary epithelial cells (HME-50) cells. Standard curves wells were established by Coulter counts, normalizing fluorescence counts. Note nonlinearity of the 6 uM (unrinsed) curve.

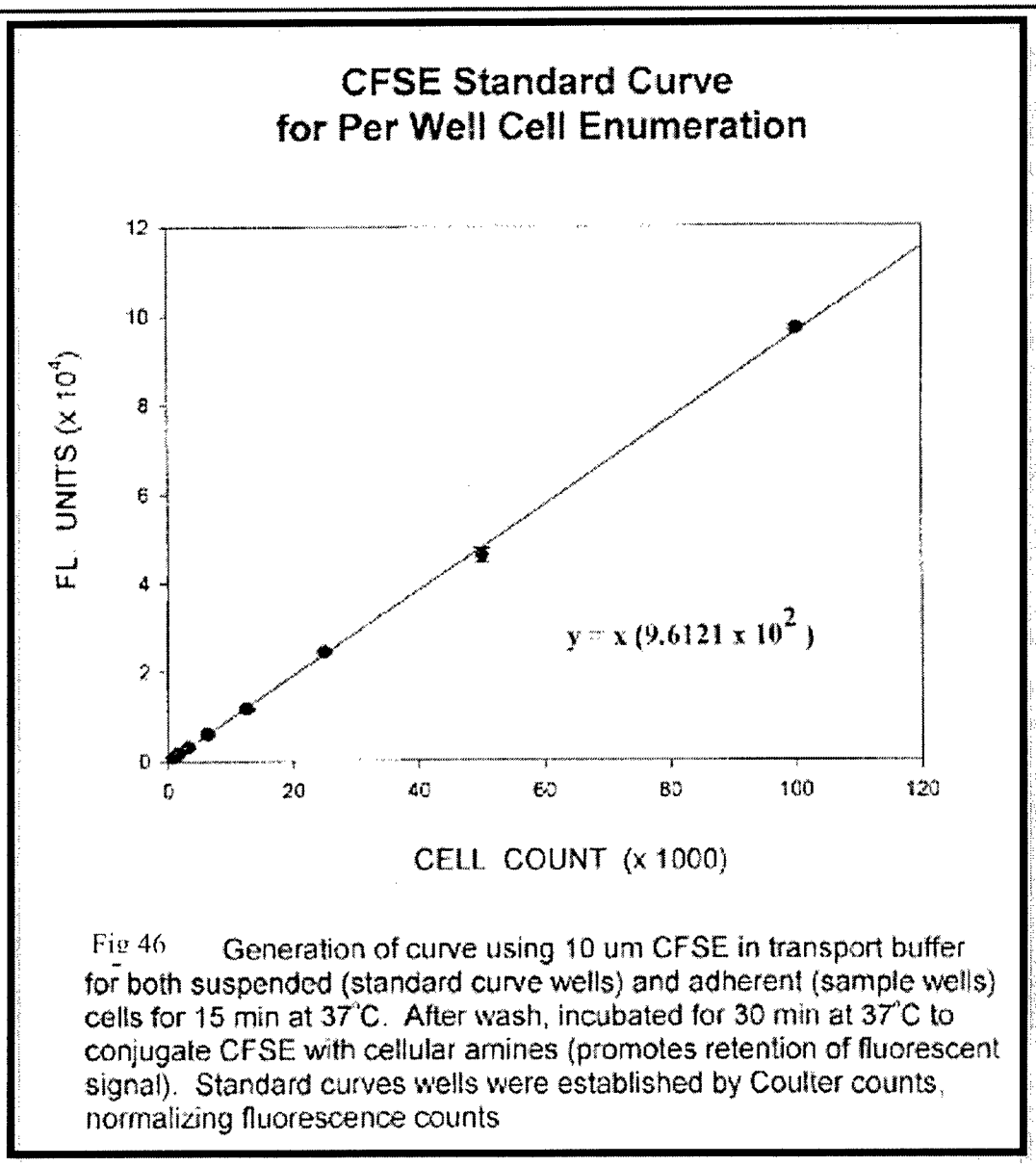


Fig 46 Generation of curve using 10 um CFSE in transport buffer for both suspended (standard curve wells) and adherent (sample wells) cells for 15 min at 37°C. After wash, incubated for 30 min at 37°C to conjugate CFSE with cellular amines (promotes retention of fluorescent signal). Standard curves wells were established by Coulter counts, normalizing fluorescence counts

Thus, for the first time we were able to normalize our transport measurements based explicitly on cell number, rather than using an indirect indicator, such as cell protein. Using this normalization mode significantly reduced sample-to-sample variation in the transport assay. This switch to a fluorescence method of cell counting allowed for all the lysate to be counted via scintillation spectroscopy, which contributed to the increased precision in the transport assay. Since the CFSE procedure was done prior to scintillation counting, the fluorescence assay was tested and proven to not interfere with the determination of radioactive solute transport. The greater number of wells in a 96-well plate allowed for a standard curve to be generated on each individual plate, in addition to the blanking and sample wells. Once we were able to generate an accurate standard curve for fluorescence, we then established the cell numbers in each sample well of the plate. Combining the fluorescence measurements with scintillation counts gives glucose or Taxol transport rates normalized by cell number.

Figure 47 shows the results for measuring glucose uptake at minimum and moderate shaking speeds in the new 96-well plate format. When the shaking speed was increased from 200 to 400 rpm, there was a large decrease in nutrient uptake for HME-50 cells, suggesting that membrane integrity or cell viability is dramatically reduced for this

cell type grown on plastic. However, the HME-50 cells appeared to hold firmly to the plastic plate at low shaking speeds, helping reduce variation due to cells lost during rinsing. Our experience with human mammary stromal (HMS) and tumor cell types suggests that they are less adherent than HME cells on plastic.

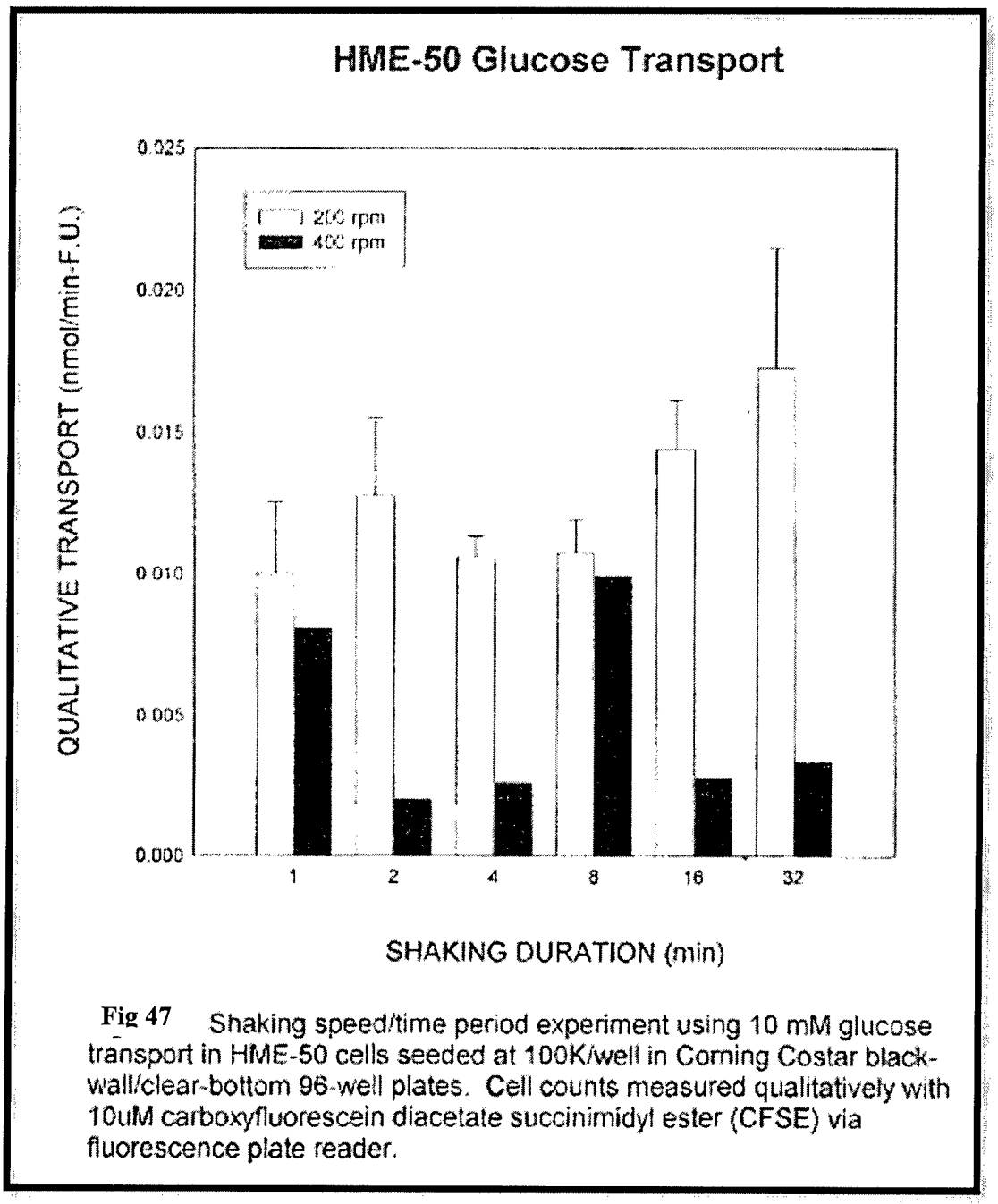


**Fig 47** Shaking speed/time period experiment using 10 mM glucose transport in HME-50 cells seeded at 100K/well in Corning Costar black-wall/clear-bottom 96-well plates. Cell counts measured qualitatively with 10uM carboxyfluorescein diacetate succinimidyl ester (CFSE) via fluorescence plate reader.

Resolution of the three problems enabled us to grow cells faster and more consistently, increase the precision of transport measurements, and reduce unstirred layer effects at an appropriate shaking speed.

Next, we examined how glucose uptake changed through a time course in our new transport format. Our procedural changes did result in lower variation in both cell enumeration and nutrient transport (see Fig. 47). In Figure 48, use of CFSE generated an exceptional standard curve to establish cell numbers in the sample wells. Glucose uptake

increases as a square hyperbola , with time as the variant, reaching maximum uptake at steady-state ($J_{ss}$) and establishing a $t_{1/2}$ value (half-time to $J_{ss}$). These values were critical in comparing HME, HMS and tumor cells in their Taxol transport profiles, as discussed below.

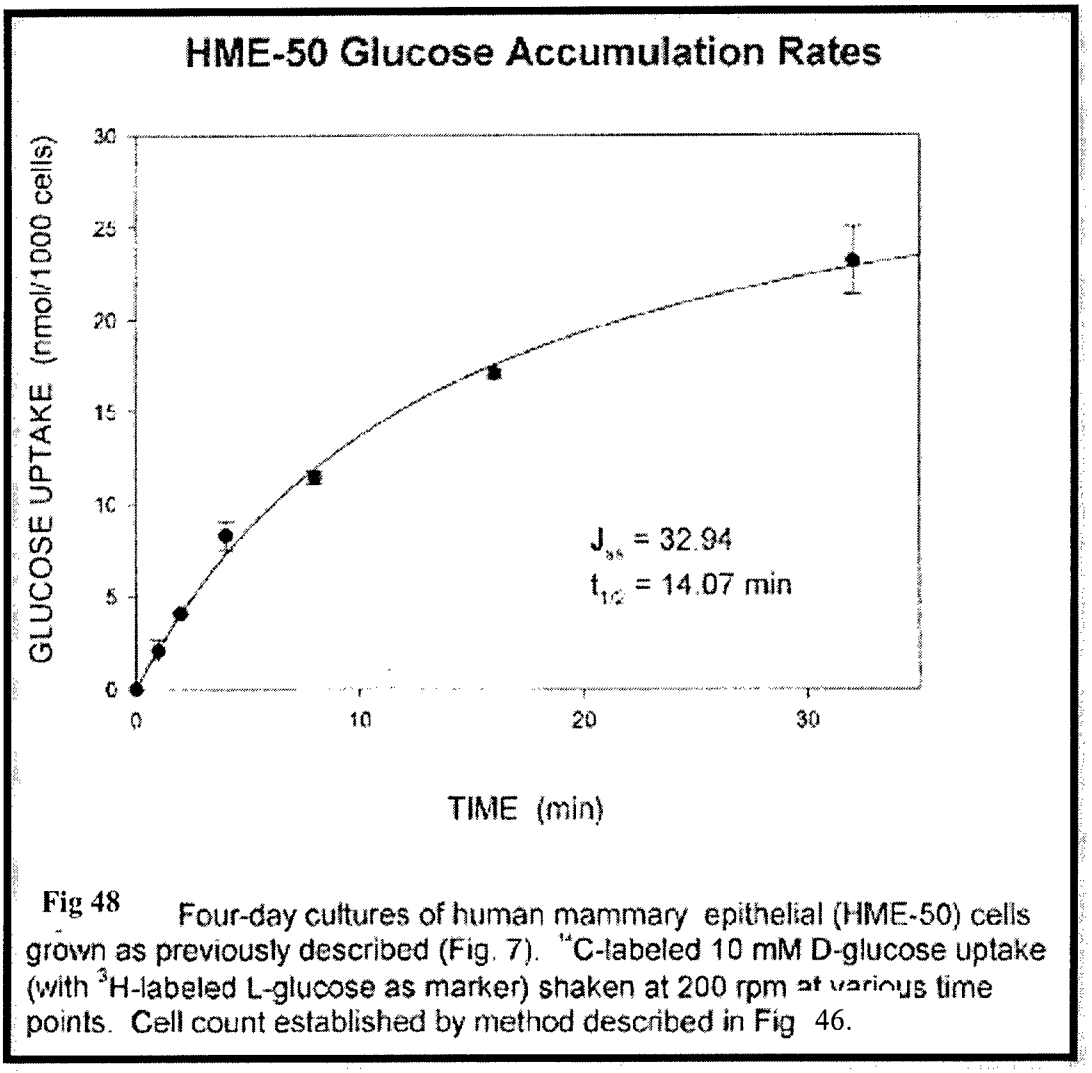


**Fig 48** Four-day cultures of human mammary epithelial (HME-50) cells grown as previously described (Fig. 7). $^{14}$C-labeled 10 mM D-glucose uptake (with $^{3}$H-labeled L-glucose as marker) shaken at 200 rpm at various time points. Cell count established by method described in Fig 46.

In our time-course experiments with 1 uM Taxol uptake in HME-50 cells, we also saw a hyperbolic increase in intracellular Taxol to steady-state levels (Fig. 49). The calculated $J_{ss}$ value represents the maximal accumulation of Taxol inside the cell. This parameter is particularly useful because it is a composite value of Taxol influx and its efflux from the cell. Cells that overexpress MDR1 exhibit lower $J_{ss}$ values (accumulation rates) for Taxol because drug efflux is enhanced. A second useful parameter is also derived from the curve, the $t_{1/2}$ value. Cells that are resistant to Taxol because they overexpress MDR1 should have lower $t_{1/2}$ values than those that have modest MDR1 expression. Cells with low (short) $t_{1/2}$ values rapidly reach steady-state levels of Taxol inside the cell due in part to rapid efflux of drug out of the cell. It should be noted that both parameters are most informative about the drug efflux status of cells if the size, shape, and number of cells being compared are similar.

The $J_{ss}$ and $t_{1/2}$ of Taxol transport were quite different from those of D-glucose, as would be expected for two such different solutes. $J_{ss}$ was almost 6-fold higher and $t_{1/2}$ , 3-fold lower for D-glucose compared to Taxol. The entry of glucose into breast cells is facilitated by an isoform of the GLUT transporter family, the solute being unable to cross the plasma membrane by simple diffusion at significant rates. In contrast, Taxol is lipophilic and diffuses through the

membrane slowly, unaided by transporters. The exit of glucose from the cell is carried out by the same GLUT transporter that mediates influx. For Taxol, however, efflux pumps (e.g., MDR1) actively transport Taxol out of the cell in addition to a slow, simple diffusion component. So the accumulation rate is determined by the combination of diffusive influx and MDR-driven efflux of Taxol.

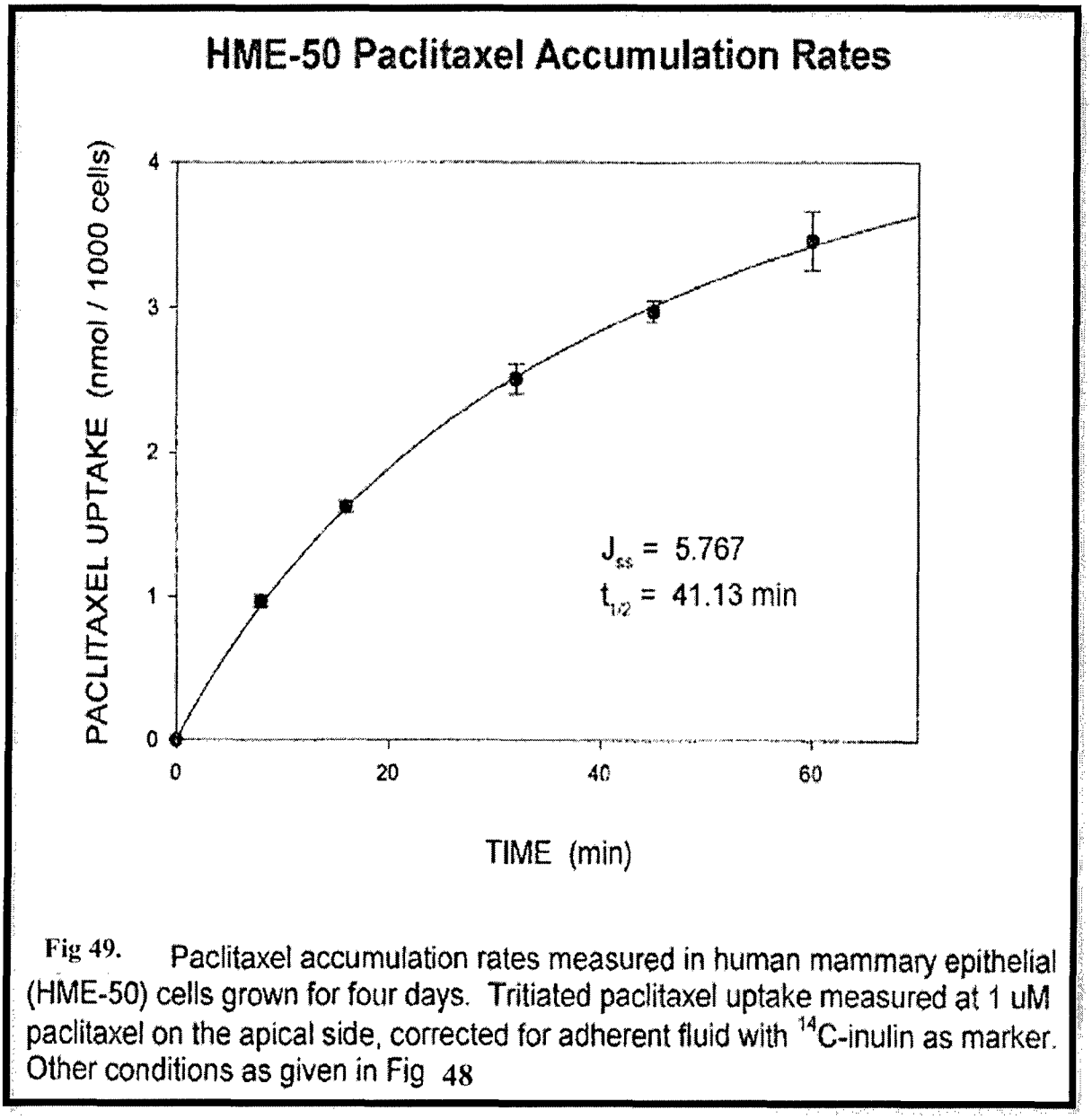


**Fig 49.** Paclitaxel accumulation rates measured in human mammary epithelial (HME-50) cells grown for four days. Tritiated paclitaxel uptake measured at 1 uM paclitaxel on the apical side, corrected for adherent fluid with $^{14}$C-inulin as marker. Other conditions as given in Fig 48

HMS cells grew quickly in the new cell culture format, reaching confluence faster than HME cells in the 96-well plates. However, they were less adherent and prone to loss during rinsing steps. This propensity probably increases the variation through loss of cells during transport measurements. Figure 50 shows Taxol accumulation rates for HMS-50 cells. The breast stromal cells had Jss values that were slightly higher (32 %), but comparable to those for breast epithelial cells. This suggests that the two different cell types should accumulate similar concentrations of Taxol when exposed to high drug levels (i.e., 1 μM) over a sufficiently long time interval. Interestingly, compared to breast epithelial cells, the stromal cells reach steady-state levels of Taxol much faster, as evidenced by a 3.7-fold lower $t_{1/2}$ value (Fig. 12, appendix). One explanation for this difference may be that higher levels of MDR1 are expressed in stromal compared to epithelial cells. However, other contributing factors must be ruled out, such as differences in cell surface area and volume. Nevertheless, the results do suggest that further characterization of Taxol transport is worth pursuing and may contribute to our understanding of how stromal and epithelial cells differ in their resistance to Taxol.

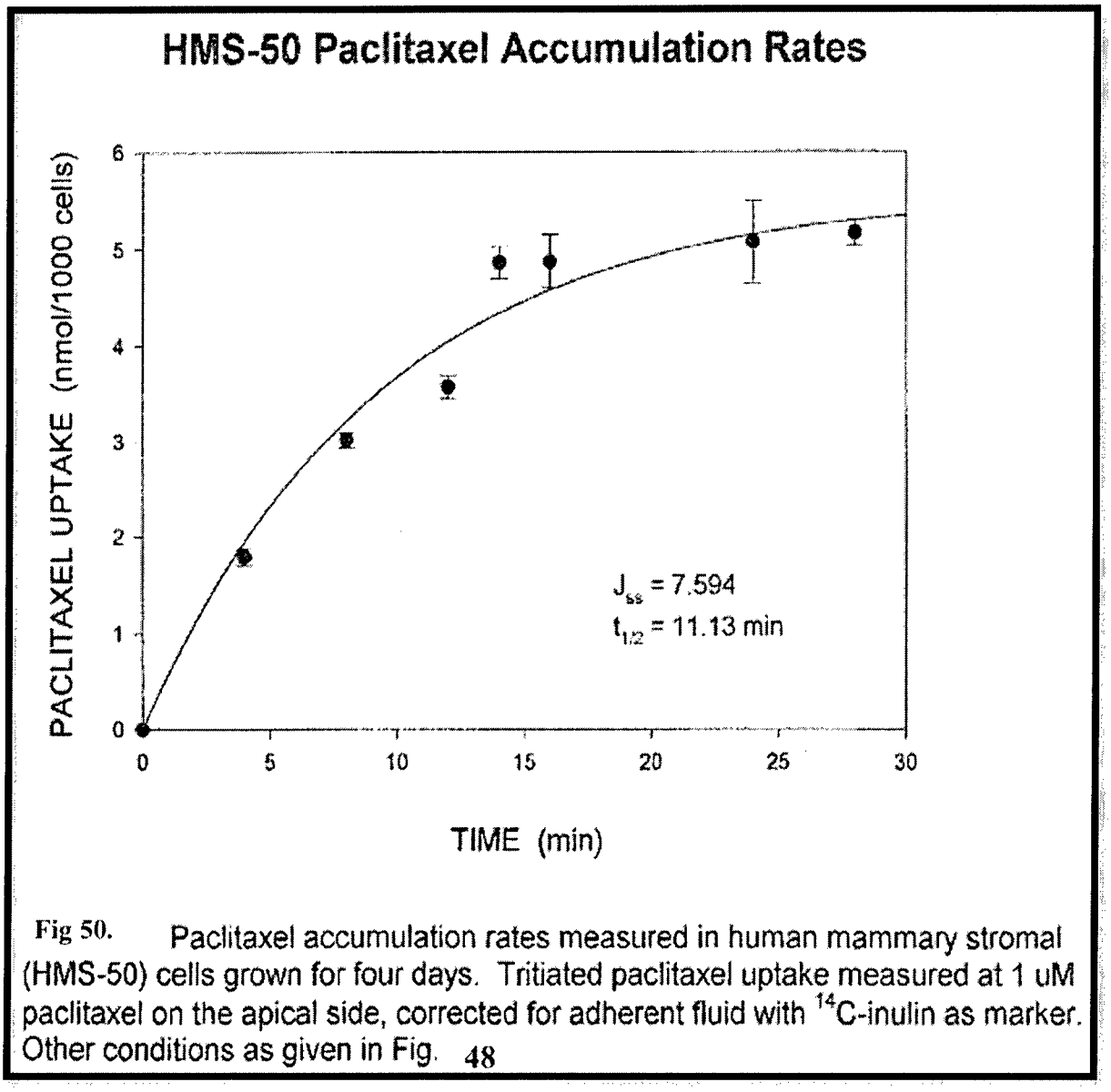


**Fig 50.** Paclitaxel accumulation rates measured in human mammary stromal (HMS-50) cells grown for four days. Tritiated paclitaxel uptake measured at 1 uM paclitaxel on the apical side, corrected for adherent fluid with $^{14}$C-inulin as marker. Other conditions as given in Fig. 48

***Task 2. Co-culture normal HMS cells with corresponding tumor cells under control conditions and in the presence of Taxol: (Year 2):***

**Task 2d.** Determine differences between HMS and tumor cells in the uptake and efflux transport characteristics of Taxol. (Months 18 - 24).

**Task 3d.** Determine the differences between HME and tumor cells in the uptake and efflux transport characteristics for Taxol (Months 30-36).

**Note:** We were able to simultaneously accomplish both Task 2d and Task 3d by determining the Taxol transport characteristics for breast epithelial-derived tumor cells and comparing their characteristics with those of HMS (Task 2d) and HME cells (Task 3d) determined under Task 1d, as reported above.

The tumor cell line (TTU-1) grew very aggressively in the new transport assay format, reaching confluence earlier than the HME cell line. TTU-1 cells appeared to adhere better than HMS cells, but not as well as HME cells. As shown in Figure 51, when Taxol uptake was measured in TTU-1 cells as a function of time, the tumor cells exhibited a $J_{ss}$ value essentially identical to normal epithelial cells, but slightly lower than stromal cells. Interestingly, the tumor cells showed the shortest $t_{1/2}$ value (4 min) compared to either normal breast epithelial (41 min) or stromal cells (11 min). The combination of lower accumulation rates and rapid approach to steady-state values strongly suggests that higher drug efflux rates may be present in the tumor cells. If so, this would directly contribute to greater Taxol resistance. This hypothesis can be confirmed by 1) characterizing Taxol transport rates over a range of drug concentrations, 2) measuring drug efflux directly, and 3) quantifying the expression of MDR1 in these cells versus HME and HMS cells.

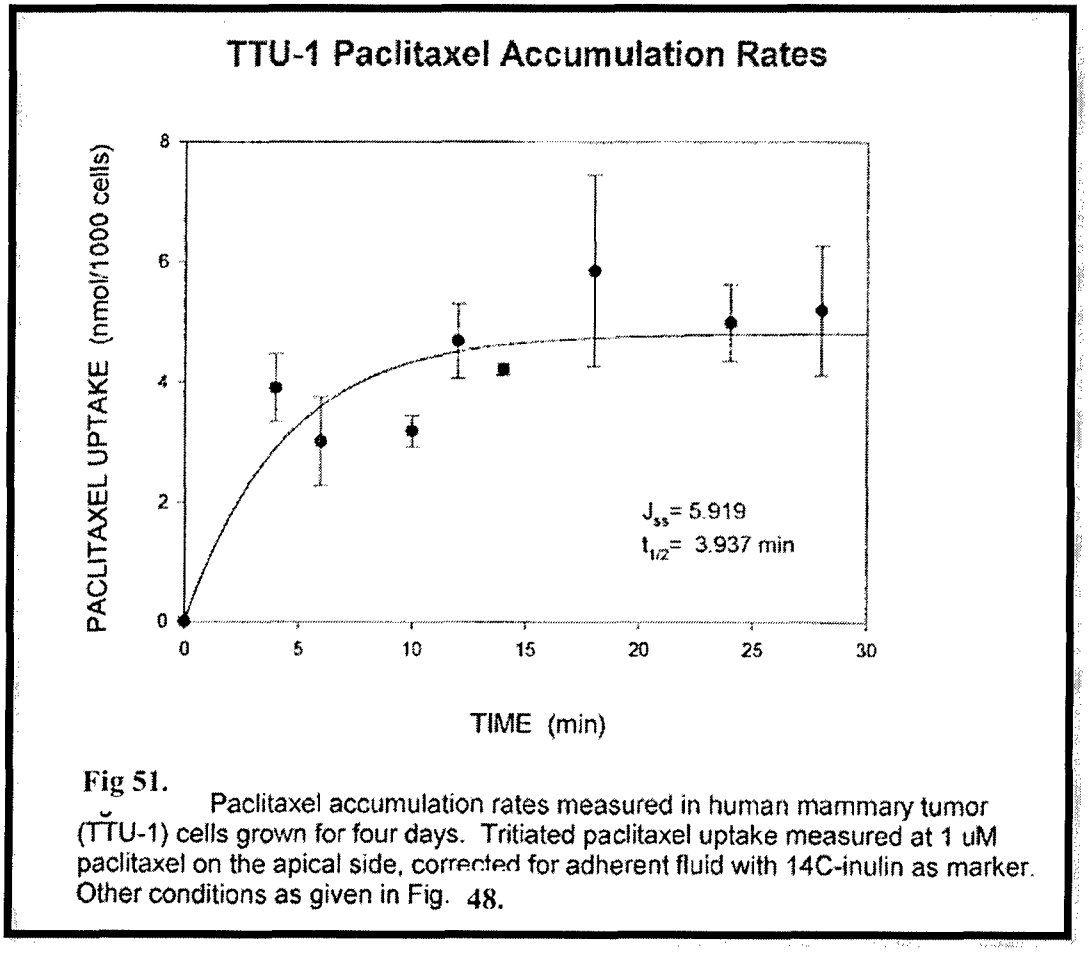


**Fig 51.** Paclitaxel accumulation rates measured in human mammary tumor (TTU-1) cells grown for four days. Tritiated paclitaxel uptake measured at 1 uM paclitaxel on the apical side, corrected for adherent fluid with 14C-inulin as marker. Other conditions as given in Fig. 48.

We have begun developing a new way to measure Taxol efflux (and that of other drugs) directly that has several advantages over previously reported methods. Briefly, it relies on measuring fluorescently-labeled Taxol as it pumped out of single cells grown in continuous flow cell culture chambers. The change in cytoplasmic Taxol concentration over time allows us to calculate the efflux kinetics for the MDR pumps expressed by any of the cell types grown in the chamber. The Taxol efflux is measured directly by confocal microscopy in individual cells. A list of the advantages of this method includes:

- In a multi-well cell culture plate, efflux measurements are extremely labor intensive because the individual wells must be washed numerous times and the drug activity in the washes measured and summed over time. As a result, the drug activity outside the cell is never maintained at a true zero-trans concentration, as required for an ideal drug efflux condition. Our single-cell fluorescence flow (SCFF) assay avoids these complications because drug efflux is continuously measured, which greatly improves the time resolution and, hence, the accuracy of the flux measurement.

- The drug concentration outside the cell is continuously washed away in the flow cell. Hence, a true zero-trans drug condition is achieved, meaning the drug efflux kinetics will accurately report the transporter activity expressed on the cell membrane.

- With the new assay, there is no need to normalize the efflux measurements to a proxy for cell number, such as total protein concentration or cell counts. The efflux data are collected from a single cell. Thus, the efflux kinetics are already normalized for single cells.

- It will now be possible to co-culture more than one cell type together (e.g., human mammary epithelial cells and breast tumor cells) and determine the drug transport kinetics for each cell type ***in situ***. Previous methods required that the different cell types grown in co-culture be trypsinized (to separate them) and then sorted into individual populations by fluorescence-activated cell sorting. By avoiding the latter manipulations, cell-to-cell contacts are preserved in our assay, permitting the MDR pump activity to be recorded under relatively undisturbed conditions.

The relationship between p53 and bcl-2 has been mentioned previously. Bcl-2 in cooperation with c-myc can sequester p53 in the cytoplasm during G1 and G2/M (coinciding with the findings by Wahl et al., (1996) [92] and Taxol cytotoxicity), disrupting normal DNA-protein interactions. Thus, it will be interesting to analyze cell-specific responses between the cell types in co-culture given the known differences in p53 and pRb expression between HME and HMS cells [18, 93] and these prior observations. In conjunction with those results, we are also interested in investigating how the tumor cells are affected by Taxol [32].

In addition to the aforementioned rationale for choosing Taxol, several other reasons made Taxol the ideal anti-tumor agent to study lineage-specific cellular perturbations. Hyperphosphorylation of bcl-2 has been observed in cells exposed to Taxol, causing the protein to lose its ability to bind to bax, a pro-apoptotic protein [66, 67, 94, 95]. The bcl-2 protooncogene encodes an intracellular membrane-associated protein localized to the nuclear membrane, endoplasmic reticulum (ER) [96-99], and mitochondrial membranes [25, 67, 96, 100, 101]. However, it is unknown whether this phosphorylation is the direct result of Taxol exposure or through other signaling mechanisms triggered by microtubule disruption [102]. Other arguments suggest that the resultant phosphorylation of bcl-2 is dependent on the upstream kinase, raf-1 [103, 104]. It has also been suggested that bcl-2 is hyperphosphorylated through p21 signaling. Studies have also shown that bcl-2 and c-myc cooperate to completely overcome the growth inhibitory and cytotoxic effects of p53 [92]. There is also evidence that telomerase activity is modulated by bcl-2 [78]. Taken together, the mechanism of Taxol action and its apparent relationship with bcl-2 and the functional role of bcl-2 in the cell made cell lineage responses to Taxol a pertinent topic for investigation.

Cell-to-cell interactions will be investigated in the development of a co-culture system more closely simulating *in vivo*. Shennan [105] comprehensively reviewed the known mechanisms of mammary gland transport systems with respect to milk contents and production. Within this review, it was apparent that the studies to date have focused solely on the epithelial cells. Little is known about stromal cell transport systems in the breast. Furthermore, the polarity of the

membrane transport systems makes in vivo study difficult and there are no in vitro systems that are able to reproduce the complete range of mammary functions. The system we propose studying is also lacking with respect to mimicking natural mammary gland function. However, it is an important and necessary first step in developing a fully functional in vitro mammary gland. In addition, results from this study will yield important information concerning cell-to-cell interactions in this dynamic environment. Investigation of this proposed system would then evolve to systems containing a 3-dimensional matrix, endothelial cells, vascular smooth muscle cells, and become more complete as our knowledge and technology grow. Within the scope of this proposed research, the effects of Taxol treatment on different mammary cell types will be studied. There are very few studies showing mammary cell response to Taxol and most of the cellular uptake studies done were performed on the colon carcinoma line CaCo2 or HeLa cells. Consider that an important determinant of anti-tumor effectiveness is drug transport into and out of the cell. However, there are no studies to date of Taxol accumulation rates in breast cells. Yet, Taxol sensitivity of specific cell types has been shown to correlate with drug accumulation rates. For example, Taxol-resistant rodent tumor cell lines exhibit Taxol uptake rates that are several fold lower than do Taxol-sensitive cells. Conversely, drug efflux rates are elevated in resistant compared with sensitive human tumor cells [106-108]. Transfection of cells with the multidrug-resistance protein-1 (MDR1), an active efflux pump, confers Taxol-resistance [109, 110]. Thus, the membrane permeability of diverse cell types and their expression of efflux pump proteins may contribute to Taxol sensitivity. Ultimately, it is the combination of drug transport and intracellular drug-resistance mechanisms (e.g., elevated bcl-2) that determine anti-tumor agent effectiveness. Thus it is imperative that mammary cell types be utilized to address investigations focusing on uptake and effects of Taxol considering the high frequency of use in treating breast cancer patients.

KEY RESEARCH ACCOMPLISHMENTS:

- Optimized cell co-culture conditions for HME-HMS, HME-TTU, HMS-TTU.
- Optimized transfection and visualization with FPs in cell types.
- Optimized Taxol concentrations, time points and treatment strategies to obtain both a high number of cells and analyze effects on cells.
- Optimized cell separation technique that allows for accurate cell separation, high population purity (>90%), high viability (>90%).
- Optimized assays for generating genetic profiles to be compared between sample sets as well as identifying key genes for siRNA or RNAi assays.
- Determination of kill curves and effects of Taxol on parent, CC and CC-replated cells showing cell sensitivity. The HME cells were most sensitive with tumor cell sensitivity dependent upon ER status. HMS cells were least sensitive. In CC of HME-TTU, the TTU appeared to confer some resistance to the HME. Recovery times showed tumor cells recovered quickly, HME cells did not recover inparet lines, recovery was greater in CC. HMS showed very little effects fromTaxil, therefore their growth appeared unaffected.
- Genetic profile analysis determined for HME and TTU subsets showing direct effects of inhibition on carcinogenicity of TTU as well as upregulation of premalignant oncogenes in HME CC with TTU.
- Replating of CC HME and TTU showed that once they have interacted, there is a re-programming of certain traits, which appeared to endure in homogeneous culture.
- Optimized cell culture conditions and transport assay procedures to permit accurate measurements of Taxol transport in human mammary epithelial cells.
- Determined accurate measurements of Taxol transport in human mammary epithelial cells, human mammary stromal cells, and human mammary tumor cells. Specifically, Taxol transport *per cell* can now be precisely quantified.

- All three cell types exhibit unique patterns of Taxol accumulation, which may reflect differences in several transport properties. In particular, the human mammary tumor cells achieved steady-state levels of drug the fastest. This finding is consistent with the higher efflux rates of Taxol described in resistant tumor cells, and warrants further investigation.

- Initiated development of a new drug efflux assay, the single-cell fluorescence flow assay, which we allow us to examine in monoculture or in co-culture how drug efflux in the above-mentioned cell types—measured in situ—contributes to differences in Taxol accumulation rates.

- Assays developed
  - Multi-well assay for Taxol accumulation rates (Collie)
  - Antibody-based Microfluidics Recognition and Capture Assay
  - Antibody-based capillary separation system

- Research Training

Gollahon:
This project supported two graduate students (Sheree Case – Currently a High School Biology Teacher in N.C. and Nayoung Kim, currently finishing up the last portions of Task 2c and 3c. Will graduate in Dec 2007).

Howard Hughes Medical Institute Science Education Program Undergraduate Research Fellows trained through this project:
Joshua Balch, graduated 2004. Currently working as a laboratory Research Associate at TCU in Fort Worth, TX.
Minesh Patel, graduated 2005. Currently applying to medical schools while working for his family.

McNair's Scholar trained through this program.
Uriyah Robinson, gradated 2005, currently working for Biotech industry in Dallas, Texas.

Undergraduate Research Fellows trained through this program
Nadia Bakdash, graduated 2002, just completed a Ph.D. at George Washington University in Cancer Biology, specializing in Breast Cancer. Currently applying for postdoctoral fellowships.
Brad Gholston, graduated 2003. Currently in grad school in Biology at Kansas State.
Katie Leonard, currently working in the lab.
Marc Macaluso, graduated 2006, currently working in the lab as a research associate support - Receptor Logic Inc.
Rebecca Brousseau, graduated 2004, currently in graduate school at UT Southwestern Medical Center, Dallas, TX.

Collie:
This project supported two Ph.D. students (Dustyn Webb, left program due to health issues)
Arup Chakraborty (in progress) (Collie)

David Keelen, graduated May 2004, currently a medical student at University of Texas Medical Branch at Galveston;
Christina Eaton (in progress).

REPORTABLE OUTCOMES:

**Manuscripts**

Martinez, G.M., L.S. Gollahon, K. Shafer, S.K. Oomman, C. Busch and R. Martinez-Zaguilan. (2001). Fluorescent pH probes, Fluorescent Proteins, and Intrinsic Cellular Fluorochromes are Tools to Study Cytosolic pH (pH cyt) in Mammalian Cells. Proc. Soc. Int. Opt. Engin. SPIE. 4259: 144-156, 2001 (This was a study that helped define the use of GFPs in co-culture).

Elmore, L.W., K.C.Turner, L.S.Gollahon, M.R.Landon, A.Akalin, C.K.Jackson-Cook, and S.E.Holt. 2002. Telomerase protects cancer-prone cells from chromosomal instability and spontaneous immortalization. Cancer Biology and Therapy, 1:4, 391-397. (This study was done using the cell lines established for the DOD work).

Wankhede S.P., Z. Du, J.M. Berg, M.W. Vaughn, T. Dallas, K.H. Cheng, and L.S. Gollahon, "Cell Detachment Model for an Antibody-Based Microfluidic Cancer Screening System," Biotechnol. Prog.; 2006; ASAP Web Release Date: 09-Aug-2006; (Article) DOI: 10.1021/bp060127d (This study was done in conjunction with designing a mathematical model for effective captire and isolation of target cells. This was done based on the capture technique to separate cells in mixed populations while retaining cell viability).

Du Z., K.H. Cheng, M.W. Vaughn, N.L. Collie and L.S. Gollahon. Recognition and capture of breast cancer cells using an antibody-based platform in a microelectromechanical systems device. Biomedical microdevices, In Press. (This paper was a result of our work in developing an effective separation technique for the breast cell types in co-culture that would allow us to retain cell viability and process them expediently).

**Manuscripts in Preparation**

Zhang, Z., S. Case, and L.S. Gollahon. Establishment of a novel co-culture system for human breast cells utilizing green fluorescent protein technology. (This was the initial preliminary work that led to the GFP transfections in the proposal).

Herring, C.B., N. Bakdash, M. Patel, N. Collie and L.S. Gollahon. Differential breast cell-lineage sensitivity to Taxol. (This work laid the groundwork for our hypothesis). For Submission to Molecular Carcinogenesis.

Kim, N., S. Case, N. Collie and L.S. Gollahon. Normal Mammary Epithelial Cells, Normal Mammary Stromal Cells and Breast Tumor Cells Show Differential Gene Expression in Co-culture Conditions as Compared to Homogeneous Parent Cell Cultures. For Submission to Molecular Cell Biology.

Kim, N., S. Case, N. Colls, Z. Du and L.S. Gollahon. An Antibody-Based Separation Technique Using Glass Capillaries Effectively Separates Target Cells from Mixed Populations and Retains High Viability.

Kim, N., S, Case, B. Herring, N. Collie and L.S. Gollahon. Normal Mammary Epithelial Cells, Normal Mammary Stromal Cells and Breast Tumor Cells Show Differential Gene Expression in Co-culture Conditions as Compared to Homogeneous Parent Cell Cultures after Exposure to Taxol. For Submission to Clinical Cancer Research.

Chakraborty, A.R., Eaton, C.A., Webb, D.K., Gollahon, L.S., and Collie, N.L. Expression patterns and characterization of multidrug resistance transporters in normal breast stromal and epithelial cell lines compared to those in ductal carcinoma cells. For submission to: J. Pharmacol. Exp. Ther.

Chakraborty, A.R., Kim, Nayoung, Eaton, C.A., Bozarth, W.A., Gollahon, L.S., and Collie, N.L. Single-cell paclitaxel efflux kinetics in co-cultures of normal breast cell types and tumor cell lines. For submission to: Cancer Res.

**Presentations**

L.S. Gollahon, N. Bakdash, G. Li, and C.B. Herring. Differential breast cell-lineage sensitivity to Taxol. Proceedings from the 92nd Annual AACR Meeting. New Orleans, LA. 2001.

Patel, N., Z. Du, D.J. Bornhop, and L.S. Gollahon. Hydrodynamic focusing for cell patterning. 18th Annual Women's All – University Conference. Women in Science: Bridges Women Build. Texas Tech University. April 12, 2002.

Manor, R., Yun, J., Datta, A., Dhar, A., Holtz, M., Berg, J., Gangopadhyay, S., Dasgupta, P., Temkin, H., Gollahon, L., Shao, H., Yu, T., Veeraraghavan, V., Vijayaraghavan and T. Dallas. Microfabricated liquid core waveguides for micro TAS (Total Analysis Systems). 18th Annual Women's All – University Conference, Women in Science: Bridges Women Build. Texas Tech University. April 12, 2002.

Balch, J, Du, Z, and LS Gollahon. Investigation of three key components of cellular immortalization and a

possible correlation with telomere lengths. Texas Tech University – HHMI Research Days, March 26 – 28, 2003.

Patel, M, Herring, B, Bakdash, N, and LS Gollahon. Effect of Taxol on Telomerase Activity and Expression of Key Cell Regulating Proteins in Normal and Cancerous Breast Cells. Texas Tech University – HHMI Research Days, March 26 – 28, 2003.

Zhigiang, D., K. Cheng, M. Vaughn and L.S. Gollahon. Recognition and Capture of cervical and Breast Cancer Cells Using an Antibody-Based Platform in a Microelectromechanical Systems Device. TexMEMS VI, Sept 9, 2004, Texas A&M University, College Station, Texas. Abstract.

L.S. Gollahon. Merging Biomedical Research and Engineering For Development of Drug Delivery Systems And Cancer Cell Study Platforms. Department of Chemical Engineering, Texas Tech University, Lubbock, Tx. October 29, 2004.

L.S. Gollahon, S. Case, Z. Du, D. Webb, N. Kim and N. Collie. Department of Biological Sciences, Texas Tech University. DAMD-17-02-1-0581. Title: Analysis of Breast Cell-Lineage Response Differences to Taxol Using a Novel Co-culture System. DOD Breast Cancer Research Program – Era of Hope Meeting (April 2005, Washington, D.C.) This was both Poster and Talk.

N. Kim, S. Case, Z. Du, N.L. Collie and L.S. Gollahon. Analysis of breast-cell lineage response differences to Taxol using a novel co-culture system. American Society for Biochemistry and Molecular Biology (ASBMB) Meeting and Centennial Celebration. San Francisco, April 1-5, 2006.

N. Kim, S. Case, and L.S. Gollahon. Analysis of breast-cell lineage response differences to Taxol using a novel co-culture system. 29th Annual San Antonio Breast Cancer Symposium. Henry B Gonzalez Convention Center, San Antonio, Texas. December 14-17, 2006.

patents and licenses applied for and/or issued;

None

degrees obtained that are supported by this award;

1. Noel Colls (M.S.) 1998 – August 2002. Topic: Establishment of a multipurpose, biologically-based fiber-optic immunosensor for breast cancer.

2. Sheree Case (M.S.) 2001 – 2004. Topic: Characterization of a novel breast cell co-culture system utilizing green fluorescent protein technology.

3. Zhiqiang (Danny) Du (Ph.D.) 2001 – 2005. Topic: Detection of human breast cancer cells and cervical cancer cells utilizing an on-chip hydrodynamic focusing system.

4. Vinaya Bhandarkar (Ph.D.) 2001 – present. Graduates May 2007, ABD. Topic: Investigating cell-lineage differences in telomere-binding protein regulation.

5. Nayoung Kim (Ph.D.) 2003-present. Graduates December 2007. Topic: Analysis of breast-cell lineage response differences to Taxol using a novel co-culture system.

development of cell lines, tissue or serum repositories;

Human mammary epithelial cell lines transduced with hTERT (human telomerase enzyme reverse transcriptase). Cell lines: HME 50hTERT, 73hTERT, 87hTERT; HMS 50hTERT, 73hTERT, 87hTERT

Human mammary epithelial cell lines transfected with fluorescent proteins(FP). Colors transfected: green(GFP), red(RFP), yellow(YFP), cyan(CFP). Cell lines: HME 50 GFP, YFP and CFP, 73 GFP and RFP, 87 GFP; HMS 50 GFP and RFP, 73 GFP, RFP, 87 GFP, RFP

Breast tumor cells transfected with FP. Cell lines: TTU1-RFP, YFP; SCC1419 RFP, GFP;

infomatics such as databases and animal models, etc.;

None

funding applied for based on work supported by this award;

1. A Tumor Microvascular Chip for Drug Delivery Study. Program:
APPLICATION OF EMERGING TECHNOLOGIES FOR CANCER RESEARCH
RFA Number: RFA-CA-05-003,
Amount Requested: $250,000

2. Source of Support: NSF – REU supplement.
Total Award Amount: $12,000
Project Duration: 6/1/2003 – 5/31/2004
PI: Tim Dallas, Co-PI: Lauren Gollahon, Jordan Berg, Mark Holtz.
Project Title: Curriculum Development for the Design Fabrication and Utilization of Chip-based Microanalytical Systems

3. Source of Support: DOD Breast Cancer Research Program Idea Award
Amount Requested: $ 415,009
Project Duration: Sept 2004- August 2007
PI: Lauren S. Gollahon
Co-PIs: Kelvin Cheng, Nathan Collie, Mark Vaughn, Jordan Berg
Project Title: Recognition and Capture of Breast Cancer Cells Using a Novel Antibody-Based Platform in a Microelectromechanical Systems Device

4. Source of Support: DOD Breast Cancer Research Program BC03-CA Concept Award
Total Award Amount: $75,000
Project Duration: Sept 2004- August 2005
PI: Lauren S. Gollahon; Co-PI's: Kelvin Cheng, Jordan Berg, Mark Vaughn
Project Title: Detection of metastatic breast cancer cells using hydrodynamic focusing

5. Source of Support: NIH Exploratory/Developmental Bioengineering Research Grant (EBRG)
Amount Requested: $393,701
Project Duration: Sept 2004 – August 2006
PI – Kelvin Cheng; Co-PI's: Lauren S. Gollahon. Shaorong Liu, Mark Vaughn
Project Title: Creation of a Microvascular Biochip for Chemotherapy Study

6. Source of Support: DOD Breast Cancer Research Program BC03-CA Concept Award
Amount Requested: $109,875
Project Duration: Sept 2004- August 2005
PI: Lauren S. Gollahon; Co-PI's: Kelvin Cheng, Shaorong Liu, Mark Vaughn
Project Title: Development of a Novel Screening System for Breast Cancer Cells Incorporating Antibody-Based MEMS Technology

7. Source of Support: DOD Breast Cancer Research Program Predoctoral Award
Amount Requested: $
Project Duration: Sept 2004- August 2005
PI/Mentee: Zhiqiang Du
PI/Mentor: Lauren S. Gollahon

Co-Mentors: Kelvin Cheng, Nathan Collie, Mark Vaughn, Jordan Berg
Project Title: Recognition and Capture of Breast Cancer Cells Using a Novel Antibody-Based Platform in a Microelectromechanical Systems Device

8. Source of Support: DOD Breast Cancer Research Program Multidisciplinary Postdoctoral Award BC050748
Amount Requested: $ 448,624
Project Duration: Sept 2005- August 2007
PI: Zhiqiang Du
Mentor: Lauren S. Gollahon
Co-Mentors: Kelvin Cheng, Nathan Collie, Mark Vaughn, Jordan Berg
Project Title: AN ANTIBODY-BASED MEMS DETECTION SYSTEM FOR METASTATIC BREAST CANCER CELLS

9. Source of Support: DOD Breast Cancer Research Program Predoctoral Award
Amount Requested: $63,617
Project Duration: Sept 2005 - August 2007
PI/Mentee: Zhi Pan
PI/Mentor: Lauren S. Gollahon
Co-Mentors: Nathan Collie, Brian Reilly, Lou Densmore
Project Title: The Role of Calcium in Taxol-induced apoptosis of Breast Cancer Cells

10. Source of Support: DOD Breast Cancer Research Program Idea Award BC051110
Amount Requested: $ 439,500
Project Duration: Sept 2005- August 2008
PI: Lauren S. Gollahon
Co-PIs: Kelvin Cheng, Nathan Collie, Mark Vaughn, Jordan Berg
Project Title: Development of a Breast Tumor Microvascular Bio-Chip for Drug Delivery Studies

11. Source of Support: TTU VPR – Research Development Funding
Amount Requested: $600,701
Project Duration: Sept 2005 – August 2006
PI – Kelvin Cheng; Co-PI's: Lauren S. Gollahon, Nathan Collie, Mark Vaughn
Project Title: Creation of a Microvascular Biochip for Chemotherapy Study

12. Source of Support: NIH RFA-CA-05-003 Applications of Emerging Technologies for Cancer Research. R21/R33 Program.
Total Amount Requested: $1,002,635
Project Duration: 7/01/05-6/30/09
PI. Kelvin Cheng. Co-PIs: Lauren Gollahon, Nathan Collie, Mark Vaughn, Shaorong Liu.
Project Title: A Tumor Microvascular Bio-Chip for Drug Delivery Studies.

*13. NSF – IGERT Program.* Sept 2005 – August 2010. Title: Interdisciplinary Program in Nano- and Microfabricated Sensors for Chemical & Biochemical Applications. PI – Jordan Berg; Participant: Lauren S. Gollahon. Amount Requested: $3,399,978

14. Source of Support: TTU VPR – Research Development Funding
Total Award Amount: $624,987 Project Duration: Sept 2006 - August 2008
PI: Reynaldo Patino; Co-PIs: Lauren Gollahon, Nathan Collie, Kelvin Cheng, Mark Vaughn, Louisa Hope-Weeks, Jon Weidanz
Project Title: Nanotoxicology of Cadmium-based Quantum Dots Relevant to Human and Ecological Health

employment or research opportunities applied for and/or
received based on experience/training supported by this award.

Gollahon:
Sheree Case, graduated 2004. Currently a High School Biology Teacher in N.C

Joshua Balch, graduated 2004. Currently working as a laboratory Research Associate at TCU in Fort Worth, TX.
Uriyah Robinson, gradated 2005, currently working for Biotech industry in Dallas, Texas.
Nadia Bakdash, graduated 2002, just completed a Ph.D. at George Washington University in Cancer Biology, specializing in Breast Cancer. Currently applying for postdoctoral fellowships.
Marc Macaluso, graduated 2006, currently working in the lab as a research associate support - Receptor Logic Inc.
Rebecca Brousseau, graduated 2004, currently in graduate school at UT Southwestern Medical Center, Dallas, TX.

Collie:
David Keelen, graduated May 2004, currently a medical student at University of Texas Medical Branch at Galveston;

Gollahon:
DOD BCRP Panel Reviewer 2002 – present; Panels: MBG -2, Medical Genetics and Tumor pathobiology
DOD BCRP Concept Award Reviewer 2002 – present

Collie:
DOD BCRP Panel Reviewer 2006, Panel: Postdoctoral Multidisciplinary Research Program, Medical Genetics.

CONCLUSIONS:

Recent studies show CC cells stimulate tumorigenic genes [111-113]. In a CC of tumor cells and fibroblasts mimicking tumor-stroma interaction, the peritumoral fibroblast in the stromal compartment surrounding malignant breast cancer MDA-MB-231, produced tumor-associated MMP (matrix metalloproteinase)-1, MMP-2, MMP-3, and MMP-11 in breast, colon, lung, skin, and head and neck cancer [114]. Up-regulated tumor cell-associated extracellular matrix metalloproteinase inducer (EMMPRIN) stimulates matrix metalloproteinase expression in both tumor and stroma compartments [115-118]. Increased EMMPRIN and MMPs in both tumor and normal human dermal fibroblast stimulated transcription and translation of vascular endothelial growth factor (VEGF) to induce migration of endothelial cells away from the parental vessels [118-120]. Another study showed premalignant mammary epithelial cells exposed to senescent human fibroblast in mice irreversibly lose their differentiated properties, become invasive and undergo full malignant transformation in stromal-epithelial interactions [111, 113]. They suggest that senescent cells stimulate epithelial cell growth based on the evidence that senescent cells stimulate the migration and invasion (branching) of the epithelial cells through a collagen matrix. They identified MMP-3 as the major factor responsible for the effects of senescent fibroblasts on branching morphogenesis. In tumor-stroma interactions, breast cancer MCF10A derived human breast epithelial cells induce stromal fibroblasts to express MMP-9 via secretion of TNF-alpha and TGF-beta. Moreover, fibroblast derived from normal breast tissue, but not fibroblast from breast tumors, have been shown to inhibit the growth of breast cancer cells [20, 113].

Predicted results for differential gene reflect some of those presented in a study by Annab et al. [121]. This study investigated gene expression of corresponding fibroblast and epithelial cells during senescence, immortalization and various growth arrested states using microarray technology. This study was conducted on homogenous populations of mortal young and senescent cells as well as cells immortalized with human papillomavirus type 16 E6E7 (HPV 16E6E7) oncogenes or the human telomerase reverse transcriptase enzyme construct (hTERT). The results of the mortal cells showed that genes differentially upregulated in senescence included H2B histone, member Q serine proteinase inhibitor, serum ameloid A1, thrombospondin 2, integrin betalike-1 and plasminogen activator tissue. In addition, levels of bcl-2, p53, pRb, c-myc and associated cyclins were differentially expressed between cell types as predicted in the expected outcomes of the proposal. This confirms the rationale derived from results from previous studies of cellular senescence.

The results accumulated to date suggest there is a functional difference at the level of the organelles. This is based on the following evidence. Intracellular calcium **($Ca^{2+}$)** homeostasis is considered a signal of cell death and an activator of gene expression [122-124]. Maintaining intracellular $Ca^{2+}$ concentrations around 100 nM is essential to cell survival [96, 123, 124]. Membrane pumps in the endoplasmic reticulum **(ER),** mitochondria and plasma

membrane maintain these intracellular $Ca^{2+}$ levels [98, 122, 123, 125, 126]. Cells exposed to oxidative stress conditions [11, 122, 127-129], hydrogen peroxide [130, 131], or oxidants such as paraquat [124, 127] produce super-oxide ions. These intracellular oxygen-derived free radicals, also called reactive-oxygen intermediates **(ROI)** accumulate intracellularly, nicking the DNA causing single-strand breaks, or increased amounts of hydrogen peroxide $H_2O_2$ [130], bringing about an increase in the levels of free intracellular calcium. The majority of studies looking at intracellular $Ca^{2+}$ flux caused by ROI formation have shown that epithelial cells appear to have stress response pathways that trigger the release of proteins that reduce the free intracellular $Ca^{2+}$ toxicity levels by binding $Ca^{2+}$ [98, 123, 130, 132]. Some of these proteins are calreticulin [123, 133-139], glucose-regulated proteins (GRP94 and GRP78) [98, 123], and calnexin [98, 123, 140-142]. ER tolerance depends, in part, on maintaining cellular $Ca^{2+}$ homeostasis and preventing oxidative stress. The ER also releases stress proteins such as heat shock protein 72/70 in response to oxidative stress [98, 99, 123]. These proteins appear to have an active role in cellular $Ca^{2+}$ homeostasis and cell death as well as conferring tolerance to the ER to intracellular environmental changes. Thus, it may be that the ability of the ER to release or buffer intracellular $Ca^{2+}$ modulates cell death. We have observed some of these same proteins being expressed differentially between cell types.

One possible mechanistic link to cell specific differences may be the role of bcl-2 and the functional release of $Ca^{2+}$ ions into the cytoplasm. The bcl-2 protooncogene encodes an intracellular membrane associated protein localized to the nuclear membrane [96, 143], endoplasmic reticulum (ER) [25, 96, 97, 99], and mitochondrial membranes [25, 27, 96, 97, 126]. Previous results [124] show that cooperation between bcl-2 and c-myc alters the subcellular localization of p53 to the cytoplasm during $G_1$, and $G_2$/M rather than the nucleus. Other studies have also shown that bcl-2 and c-myc cooperate to completely overcome the growth inhibitory and cytotoxic effects of p53 [92, 144-148]. There is evidence to suggest that bcl-2 plays a role in an antioxidant pathway and this is consistent with the multiple membrane localization of the bcl-2 protein since ROIs are shown to be produced in the ER, nuclear envelope, and mitochondria [92, 99, 126, 146, 149]. It has also been shown that mitochondria from bcl-2 over-expressing cells have an increased capacity to accumulate $Ca^{2+}$ [92, 97, 122, 126], indicating a possible correlation between ER and mitochondrial $Ca^{2+}$ pools in cell death. A study by Hacki et al., [25] showed evidence of crosstalk between the ER and mitochondria modulated by bcl-2. Massive ER dilation was triggered by inhibiting secretion. Their data suggest that apoptotic agents perturbing ER functions induce this crosstalk between the ER and mitochondria that can be interrupted by ER-based bcl-2. If a lineage specific divergence exists, one way it may be demonstrated is by differences in the release of ER stress a response protein, regulation of free calcium generated from oxidative stress, superoxide anion formation and/or levels of $H_2O_2$ produced under hyperoxic conditions. Over-expression or re-expression of bcl-2 and possibly c-myc may also be specific to the cell lineage. Our functional siRNA assays planned for the coming months will confirm this as both bcl-2 and c-myc appear to be expressed at different levels between cell types.

C-myc is a 66kD protein whose expression is up regulated during cell proliferation and generally absent during quiescence. The c-myc protooncogene is a helix-loop-helix/leucine zipper transcription factor [150]. It is a potent transcription factor in activation and repression of specific genes. C-myc is also known to heterodimerize with other proteins such as Max, which can lead to further transcriptional regulation [151]. At several points in the cell cycle c-myc is required to perform particular functions. It is thought to push quiescent cells into the cell cycle, facilitate apoptosis – programmed cell death, and repress other proteins actively involved in inhibiting the progression of the cell cycle to name a few examples [152].

With respect to the cell cycle it has been shown that while not essential for cell proliferation, c-myc is needed for normal cell growth [153]. One of the more interesting regulatory roles in which c-myc is involved is the regulation of cyclin genes and their related cyclin-dependent kinases (cdks). Cyclins activate cdks making them capable of phosphorylating other gene products involved in regulating the cell cycle. The consequence of this action could be to inhibit or activate these proteins. It has been reported that c-myc levels correlate to the production of Cyclins D and E at the $G_1$/S interface of the cell cycle [153]. Both of these cyclins are thought to aid S phase entry through activation of cdks responsible for phosphorylating and consequently deactivating the retinoblastoma protein (pRb), the gatekeeper to the cell cycle. C-myc has also been shown to be a crucial factor in the decision between apoptosis and quiescence for cells under stress [150]. C-myc is integrally involved in the function of p53, pRb, and telomerase, both directly and indirectly.

The coordination of these four proteins (bcl-2, c-myc, p53 and pRb) along with many other associated proteins is important in regulation of the cell cycle. Cell cycle progression is stringently controlled and very sensitive to damage to any one component as evidenced by the upregulation of p53 and the differential expression of pRB between the cell types. However, controlling the cell cycle is not the only manner in which cells are prevented from proliferating indefinitely.

All mammalian cells contain 5'-TTAGGG-3' telomeric repeats on the ends of the chromosomes. There are generally 1000-2000 such repeats [154]. These sequence repeats help maintain genomic stability. The telomere interacts with several proteins that help regulate their length. Telomere Repeat Factor (TRF) 1 and TRF 2 are two such proteins. They maintain telomere length in cells and prevent end-to-end fusions with other chromosomes [155-158]. Due to the 3' end replication problem presented by linear genomes, telomeres lose between 50 - 200 BP during every DNA replication [159]. This gradual erosion causes genomic instability. Generally, cellular senescence follows and the cell is quiescent in $G_0$. Telomere loss can be prevented and in some cases, extended through the activation of the ribonucleoprotein enzyme telomerase. Telomerase consists of an internal RNA component, which acts as a primer and a catalytic subunit that acts as a reverse transcriptase. The human RNA and protein homologs were named human telomerase RNA (hTR) and human telomerase enzyme - reverse transcriptase (hTERT), respectively [160-162]. These two main telomerase components add the 5'-TTAGGG-3' repeats to the end of the telomere solving the 3'-end replication problem. hTERT is the rate-limiting component in this process. For a full review of telomerase refer to Blackburn [163]. The activity of telomerase is limited to germinal cells under normal conditions. Somatic cells do not possess detectable telomerase activity and likely utilize shortened telomeres as a signal to senesce. This signaling process, known as the Hayflick limit [159], is thought to be a "mitotic clock" preventing cumulative cell damage from progressing to tumorigenesis [164-166] and effectively limiting cancer formation.

Cancer progression relies on excessive and unlimited cell proliferation. Two events must occur in order for this to be possible. The cell-cycle machinery must become deregulated allowing rapid division, and telomeres must be maintained. This is the function of telomerase. Telomerase activity can be found in >85% of all cancers and over 90% of all advanced breast cancers (stages II-IV) .[167] The activity of telomerase in cancer biology has been intently examined in the last 10 years. The underlying hypothesis is that malignant cells lacking telomerase activity will not be capable of maintaining telomeres, losing their infinite replicative capabilities and the tumor cells will eventually senesce.

The activities of all these proteins are very relevant to human breast cancers. p53 activity is abrogated in half of all breast cancers [168, 169]. pRb is mutated in ~ 25% of tumor cells [170]. Telomerase activity is shown to be dramatically amplified in breast tumors with over 90% of carcinoma *in situ* and invasive breast cancers showing activity. Greater than 50% of fibroadenomas, conventionally considered a benign breast disease, also show some activity [171]. Even more compelling with respect to telomerase and breast cancer is the evidence that estrogen amplifies telomerase activity. This appears to occur through the interaction of the estrogen receptor (ER) and c-myc [58, 59]. C-myc has already been discussed as a transcription factor regulating p53 and pRb activities. C-myc is up regulated in 80% of all breast cancers as well [172-174]. Recent studies suggests that c-myc is a direct transcription factor for the hTERT gene [174]. The role of several genes as telomerase modulators is now known, [175-177]. This is significant because hTERT levels provide the rate-limiting link to telomerase activity [33, 161]. The combination of higher c-myc levels and possibly these other modulators as well as hTERT production are predictive of carcinogenesis.

There is some evidence that p53 and pRb interact with telomerase as well as with the telomeres. p53 has been shown to interact with human telomerase associated protein (hTEP1), which is part of the telomerase complex [178]. This regulation at the level of activity could diminish telomerase activity through interference with hTR or through modifying the conformation of hTERT [179]. p53 may also interact directly with the telomere itself [179]. A p53 directed cell cycle arrest has been shown to occur when telomeres shorten and there is a buildup of G rich DNA fragments indicative of the telomere sequence [154]. In addition, the activation of tetracycline inducible p53 cassettes in telomerase positive cell lines shows a dramatic decrease in telomerase activity over a 24h period [38]. These actions are counter to the action of c-myc. Less is know about pRb interaction with telomerase. One study showed that pRb inactivation is necessary for telomerase activity and subsequent cell immortalization[180].

Multi-drug resistance (MDR) to chemotherapy remains a significant impediment to effective cancer treatments, including Taxol therapy for breast cancer. One of the primary mechanisms by which tumor cells acquire resistance is to overexpress MDR transporters that expel anti-tumor drugs like Taxol from the cell. One way that MDR overexpressing cells manifest themselves is to exhibit elevated rates of Taxol accumulation. Hence, we developed a highly accurate multi-well assay for measuring Taxol accumulation per cell. This assay avoids some of the errors associated with static cell culture accumulation assays. Accurate measurements of Taxol transport rates are essential for determining whether the cellular mechanism of MDR lies at the level of plasma membrane efflux pumps. On-going and future work is directed at full development of our single-cell fluorescence flow assay because of the many advantages over culture plate-based assays in directly determining Taxol efflux in situ. Development of the latter will make possible the measurement of drug efflux in cells cultured under many different combinations that reflect more closely the in vivo growth conditions of breast tumors. Why are accurate measurements of drug efflux that reflect in vivo conditions important? Because such data permits calculation of the effective chemotherapy drug dose likely to kill particular tumors.

**Suggestions for improving the research.** Over the past three years, many studies have come out demonstrating different ways to visualize the tumors in vivo. However, there is no way to analyze inherent molecular differences in vivo at this time. Therefore those studies dealing with cell:cell interactions are still critical to understanding the effects of both patient/cell response and antitumor agent efficacy. Potential areas of improvement inludemicro-c0-culture systems that allow either the direct contact of cells or cells separated by biocompatible porous filters such as collagen. In addition, the micro-co-cultures can culture either stromal- epithelial, stromal- tumor, epithelial -tumor sets or any of those cell types with endothelial cells. In this manner not only will cell interactions be analyzed but also the ability for the antitumor agent to penetrate the endothelial barrier. Micro-co-cultures have the advantage of utilizing small volumes, small numbers of cells and they can be cultured short term. This allows fresh tissues from the patient to be mechanically disperse and co-cultured in numerous chip channels, each with a different treatment cocktail. This gives an almost immediate result of which cocktail would be most effective, or most targeted.

We will be continuing to look at the genetic profiles and start functional assays to determine mechanisms of resistance (in the case of the stromal cells) or sensitivity (in the case of the epithelial cells). Tumors with ER+ and ER- status will also be analyzed in the hope of elucidating pathways or genes that can be targeted for generating new treatments.

**So What?** To date, there is no other study that has investigated the effects of the physical interactions of cells in culture on differential gene expression. The data generated and being generated will elucidate important signaling pathways for cell responses to chemically-induced perturbations. The baseline data in the control sets will yield important information concerning cell lineage differences and how they may contribute to the risk of cancer progression. The results will give us a better understanding of the inherent differences in programmed cell differentiation and response to stress. This co-culture system will allow us to determine the effects of antitumor agents on different cell populations physically interacting. We do not make the claim that this simulates the in vivo environment. However, it is a first step towards building a synthetic environment from the patient's own cells to determine whether the target cells will be affected, what the most effective treatment regime will be and how quickly the normal cells can recover while insuring the destruction of the tumor cells. This system will not only allow us to design individualized treatment regimes, but also potentially allow us to predict the chances of recurrence based on the effectiveness of the treatment strategy applied.

The work by Nathan Collie establishes rigid control parameters to more accurately assess the uptake and efflux rates in each cell type. In addition, the ability to follow efflux and uptake on a per cell basis allows us to better understand why tumor cells are more resistant to chemotherapy agents than the normal epithelial cells.

REFERENCES:

1. Du, Z., et al., *Recognition and capture of breast cancer cells using an antibody-based platform in a microelectromechanical systems device.* Biomed Microdevices, 2007. **9**(1): p. 35-42.
2. Wankhede, S.P., et al., *Cell detachment model for an antibody-based microfluidic cancer screening system.* Biotechnol Prog, 2006. **22**(5): p. 1426-33.

3. Dean, M., A. Rzhetsky, and R. Allikmets, *The human ATP-binding cassette (ABC) transporter superfamily.* Genome Res, 2001. **11**(7): p. 1156-66.
4. Lin, J.H. and M. Yamazaki, *Role of P-glycoprotein in pharmacokinetics: clinical implications.* Clin Pharmacokinet, 2003. **42**(1): p. 59-98.
5. Loo, T.W. and D.M. Clarke, *Recent progress in understanding the mechanism of P-glycoprotein-mediated drug efflux.* J Membr Biol, 2005. **206**(3): p. 173-85.
6. Loo, T.W. and D.M. Clarke, *Determining the structure and mechanism of the human multidrug resistance P-glycoprotein using cysteine-scanning mutagenesis and thiol-modification techniques.* Biochim Biophys Acta, 1999. **1461**(2): p. 315-25.
7. Klein, I., B. Sarkadi, and A. Varadi, *An inventory of the human ABC proteins.* Biochim Biophys Acta, 1999. **1461**(2): p. 237-62.
8. Bart, J., et al., *The blood-brain barrier and oncology: new insights into function and modulation.* Cancer Treat Rev, 2000. **26**(6): p. 449-62.
9. Gottesman, M.M., T. Fojo, and S.E. Bates, *Multidrug resistance in cancer: role of ATP-dependent transporters.* Nat Rev Cancer, 2002. **2**(1): p. 48-58.
10. Ambudkar, S.V., et al., *P-glycoprotein: from genomics to mechanism.* Oncogene, 2003. **22**(47): p. 7468-85.
11. von Zglinicki, T., et al., *Mild hyperoxia shortens telomeres and inhibits proliferation of fibroblasts:A model for senescence?* Experimental Cell Research, 1995. **220**: p. 186-193.
12. von Zglinicki, T., R. Pilger, and N. Sitte, *Accumulation of single-strand breaks is the major cause of telomere shortening in human fibroblasts.* Free Radic Biol Med, 2000. **28**(1): p. 64-74.
13. Gollahon, L.S. and J.W. Shay, *Immortalization of human mammary epithelial cells transfected with mutant p53 (273his).* Oncogene, 1996. **12**: p. 715-725.
14. Shay, J.W., O.M. Pereira-Smith, and W.E. Wright, *A role for both RB and p53 in the regulation of human cellular senescence.* Experimental Cell Research, 1991. **196**(1): p. 33-39.
15. Shay, J.W., et al., *Spontaneous in vitro immortalization of breast epithelial cells from a patient with Li-Fraumeni syndrome.* Molecular & Cellular Biology, 1995. **15**(1): p. 425-432.
16. Shay, J.W., et al., *The frequency of immortalization of human fibroblasts and mammary epithelial cells transfected with SV40 large T-antigen.* Experimental Cell Research, 1993. **209**(1): p. 45-52.
17. Whitaker, N.J., et al., *Involvement of RB-1, p53, p16INK4 and telomerase in immortalisation of human cells.* Oncogene, 1995. **11**(5): p. 971-6.
18. Shay, J.W., et al., *E6 of human papillomavirus type 16 can overcome the M1 stage of immortalization in human mammary epithelial cells but not in human fibroblasts.* Oncogene, 1993. **8**(6): p. 1407-1413.
19. Adam, L., et al., *Selective interactions between mammary epithelial cells and fibroblasts in co-culture.* Int J Cancer, 1994. **59**(2): p. 262-8.
20. Dong-Le Bourhis, X., et al., *Effect of stromal and epithelial cells derived from normal and tumorous breast tissue on the proliferation of human breast cancer cell lines in co-culture.* Int J Cancer, 1997. **71**(1): p. 42-8.
21. Rossi, L., et al., *Fibroblasts regulate the migration of MCF7 mammary carcinoma cells in hydrated collagen gel.* Anticancer Res, 1994. **14**(4A): p. 1493-501.
22. Rossi, L., et al., *Co-culture with human fibroblasts increases the radiosensitivity of MCF-7 mammary carcinoma cells in collagen gels.* Int J Cancer, 2000. **85**(5): p. 667-73.
23. Gazdar, A.F., et al., *Characterization of paired tumor and non-tumor cell lines established from patients with breast cancer.* Int J Cancer, 1998. **78**(6): p. 766-74.
24. Zhang, Z., *A New Co-Culture Model of Breast Cancer-Cell Lines Labeled By Green Fluorescent Proteins*, in *Biological Sciences*. 2001, Texas Tech University: Lubbock, Texas. p. 37.
25. Hacki, J., et al., *Apoptotic crosstalk between the endoplasmic reticulum and mitochondria controlled by Bcl-2 [In Process Citation].* Oncogene, 2000. **19**(19): p. 2286-95.
26. Li, F.P. and J.F. Fraumeni, Jr., *Soft-tissue sarcomas, breast cancer, and other neoplasms. A familial syndrome?* Annals of Internal Medicine, 1969. **71**(4): p. 747-52.
27. Green, D.R. and J.C. Reed, *Mitochondria and apoptosis.* Science, 1998. **281**(5381): p. 1309-12.
28. Peereboom, D., et al., *Successful re-treatment with Taxol after major hypersensitivity reactions.* Jour Clin Oncol, 1993. **11**: p. 885-890.
29. Pazdur, R., et al., *The taxoids: Paclitaxel (Taxol) and Docetaxel (Taxotere).* Cancer Treatment Reviews, 1993. **99**(4): p. 351-386.
30. Khayat, D., E.C. Antoine, and D. Coeffic, *Taxol in the management of cancers of the breast and the ovary.* Cancer Invest, 2000. **18**(3): p. 242-60.

31. Jordan, M.A. and L. Wilson, *Microtubule Polymerization Dynamics, Mitotic Block, and Cell Death by Paclitaxel at Low Concentrations.* Americam Chemical Society, 1995: p. 138-153.
32. Herring, B., *Differential breast cell-lineage sensitivity to Taxol.*, in *Biological Sciences.* 2002, Texas Tech University: Lubbock, Texas. p. 53.
33. Takakura, M., et al., *Cloning of human telomerase catalytic subunit (hTERT) gene promoter and identification of proximal core promoter sequences essential for transcriptional activation in immortalized and cancer cells.* Cancer Res, 1999. **59**(3): p. 551-7.
34. Counter, C., et al., *Telomerase activity is restored in human cells by ectopic expression of hTERT (hEST2), the catalytic subunit of telomerase.* Oncogene, 1998. **16**(9): p. 1217-1222.
35. Jiang, X.R., et al., *Telomerase expression in human somatic cells does not induce changes associated with a transformed phenotype.* Nat Genet, 1999. **21**(1): p. 111-4.
36. Morales, C.P., et al., *Absence of cancer-associated changes in human fibroblasts immortalized with telomerase.* Nat Genet, 1999. **21**(1): p. 115-8.
37. McChesney, P.A., et al., *Telomere dynamics in cells with introduced telomerase: a rapid assay for telomerase activity on telomeres.* Mol Cell Biol Res Commun, 2000. **3**(5): p. 312-8.
38. Gollahon, L.S., et al., *Telomerase activity during spontaneous immortalization of Li-Fraumeni syndrome skin fibroblasts.* Oncogene, 1998. **17**(6): p. 709-17.
39. Takara, K., et al., *Molecular changes to HeLa cells on continuous exposure to cisplatin or paclitaxel.* Cancer Chemother Pharmacol, 2006.
40. O'Connell, P.A., et al., *Characterization of the microtubule proteome during post-diapause development of Artemia franciscana.* Biochim Biophys Acta, 2006. **1764**(5): p. 920-8.
41. Zhang, B., et al., *Microtubule-binding drugs offset tau sequestration by stabilizing microtubules and reversing fast axonal transport deficits in a tauopathy model.* Proc Natl Acad Sci U S A, 2005. **102**(1): p. 227-31.
42. Trojanowski, J.Q., et al., *Microtubule-stabilising drugs for therapy of Alzheimer's disease and other neurodegenerative disorders with axonal transport impairments.* Expert Opin Pharmacother, 2005. **6**(5): p. 683-6.
43. Foland, T.B., et al., *Paclitaxel-induced microtubule stabilization causes mitotic block and apoptotic-like cell death in a paclitaxel-sensitive strain of Saccharomyces cerevisiae.* Yeast, 2005. **22**(12): p. 971-8.
44. Wang, L. and R.C. MacDonald, *Effects of microtubule-depolymerizing agents on the transfection of cultured vascular smooth muscle cells: enhanced expression with free drug and especially with drug-gene lipoplexes.* Mol Ther, 2004. **9**(5): p. 729-37.
45. Suzaki, E., T. Suzaki, and K. Kataoka, *Use of taxol and collagenase for better three-dimensional visualization of microtubules in the enterocyte and Brunner's gland cell, with special reference to their relation to the Golgi apparatus.* J Electron Microsc (Tokyo), 2004. **53**(1): p. 79-86.
46. Panno, M.L., et al., *Evidence that low doses of Taxol enhance the functional transactivatory properties of p53 on p21 waf promoter in MCF-7 breast cancer cells.* FEBS Lett, 2006. **580**(9): p. 2371-80.
47. Park, S.J., et al., *Taxol induces caspase-10-dependent apoptosis.* J Biol Chem, 2004. **279**(49): p. 51057-67.
48. Roberts, J., et al., *Demonstration of cell cycle positions of Taxol-induced "asters" and "bundles" by sequential measurements of tubulin immunofluorescence, DNA content, and autoradiographic labeling of Taxol-sensitive and -resistant cells.* j. Histochem. Cytochem, 1989. **37**: p. 1659-1665.
49. Wahl, A.F., et al., *Loss of normal p53 function confers sensitization to Taxol by increasing G2/M arrest and apoptosis [see comments].* Nat Med, 1996. **2**(1): p. 72-9.
50. Zhang, Z., et al., *A germ-line p53 mutation accelerates pulmonary tumorigenesis: p53-independent efficacy of chemopreventive agents green tea or dexamethasone/myo-inositol and chemotherapeutic agents taxol or adriamycin.* Cancer Res, 2000. **60**(4): p. 901-7.
51. Doroshenko, P., V. Sabanov, and N. Doroshenko, *Cell cycle-related changes in regulatory volume decrease and volume-sensitive chloride conductance in mouse fibroblasts.* J Cell Physiol, 2001. **187**(1): p. 65-72.
52. Karbowski, M., et al., *Opposite effects of microtubule-stabilizing and microtubule-destabilizing drugs on biogenesis of mitochondria in mammalian cells.* J Cell Sci, 2001. **114**(Pt 2): p. 281-91.
53. Pasquier, E., et al., *Antiangiogenic activity of paclitaxel is associated with its cytostatic effect, mediated by the initiation but not completion of a mitochondrial apoptotic signaling pathway.* Mol Cancer Ther, 2004. **3**(10): p. 1301-10.
54. North, S. and P. Hainaut, *p53 and cell-cycle control: a finger in every pie.* Pathol Biol (Paris), 2000. **48**(3): p. 255-270.

55. Pockwinse, S.M., et al., *Microtubule-dependent nuclear-cytoplasmic shuttling of Runx2.* J Cell Physiol, 2006. **206**(2): p. 354-62.
56. Giessmann, D., et al., *Decreased gap junctional communication in neurobiotin microinjected lens epithelial cells after taxol treatment.* Anat Embryol (Berl), 2005. **209**(5): p. 391-400.
57. Mironov, S.L., M.V. Ivannikov, and M. Johansson, *[Ca2+]i signaling between mitochondria and endoplasmic reticulum in neurons is regulated by microtubules. From mitochondrial permeability transition pore to Ca2+-induced Ca2+ release.* J Biol Chem, 2005. **280**(1): p. 715-21.
58. Planas-Silva, M.D., et al., *Overexpression of c-Myc and Bcl-2 during progression and distant metastasis of hormone-treated breast cancer.* Exp Mol Pathol, 2007. **82**(1): p. 85-90.
59. Cericatto, R., et al., *Estrogen receptor-alpha, bcl-2 and c-myc gene expression in fibroadenomas and adjacent normal breast: association with nodule size, hormonal and reproductive features.* Steroids, 2005. **70**(3): p. 153-60.
60. Greider, C., et al., *BCL-x(L) and BCL2 delay Myc-induced cell cycle entry through elevation of p27 and inhibition of G1 cyclin-dependent kinases.* Oncogene, 2002. **21**(51): p. 7765-75.
61. Pasqualini, J.R., et al., *Transcriptional activation of the c-myc oncogene in the T-47D mammary cancer cells by conditioned media from embryonic mouse fibroblasts (BALB/c-3T3). Effect of the antiestrogen ICI 164,384.* Anticancer Res, 1995. **15**(3): p. 671-4.
62. Kyo, S., et al., *Estrogen activates telomerase.* Cancer Res, 1999. **59**(23): p. 5917-21.
63. Sutherland, G.R. and R.I. Richards, *The molecular basis of fragile sites in human chromosomes. [Review].* Current Opinion in Genetics & Development, 1995. **5**: p. 323-327.
64. Benlloch, M., et al., *Bcl-2 and Mn-SOD antisense oligodeoxynucleotides and a glutamine-enriched diet facilitate elimination of highly resistant B16 melanoma cells by tumor necrosis factor-alpha and chemotherapy.* J Biol Chem, 2006. **281**(1): p. 69-79.
65. Kumar Biswas, S., et al., *Down-regulation of Bcl-2 is associated with cisplatin resistance in human small cell lung cancer H69 cells.* Mol Cancer Ther, 2004. **3**(3): p. 327-34.
66. Makin, G.W., et al., *Damage-induced Bax N-terminal change, translocation to mitochondria and formation of Bax dimers/complexes occur regardless of cell fate.* Embo J, 2001. **20**(22): p. 6306-15.
67. Soucie, E.L., et al., *Myc potentiates apoptosis by stimulating Bax activity at the mitochondria.* Mol Cell Biol, 2001. **21**(14): p. 4725-36.
68. Bhatia, S.K., et al., *Use of thiol-terminal silanes and heterobifunctional crosslinkers for immobilization of antibodies on silica surfaces.* Anal Biochem, 1989. **178**(2): p. 408-13.
69. Breuninger, L.M., et al., *Expression of multidrug resistance-associated protein in NIH/3T3 cells confers multidrug resistance associated with increased drug efflux and altered intracellular drug distribution.* Cancer Res, 1995. **55**(22): p. 5342-7.
70. Drori, S., G.D. Eytan, and Y.G. Assaraf, *Potentiation of anticancer-drug cytotoxicity by multidrug-resistance chemosensitizers involves alterations in membrane fluidity leading to increased membrane permeability.* Eur J Biochem, 1995. **228**(3): p. 1020-9.
71. Ferreira, M.J., et al., *The effects of jatrophane derivatives on the reversion of MDR1- and MRP-mediated multidrug resistance in the MDA-MB-231 (HTB-26) cell line.* Anticancer Res, 2005. **25**(6B): p. 4173-8.
72. Gillet, J.P., et al., *Microarray-based detection of multidrug resistance in human tumor cells by expression profiling of ATP-binding cassette transporter genes.* Cancer Res, 2004. **64**(24): p. 8987-93.
73. Robey, R.W., et al., *Overexpression of the ATP-binding cassette half-transporter, ABCG2 (Mxr/BCrp/ABCP1), in flavopiridol-resistant human breast cancer cells.* Clin Cancer Res, 2001. **7**(1): p. 145-52.
74. Kruh, G.D., et al., *Expression complementary DNA library transfer establishes mrp as a multidrug resistance gene.* Cancer Res, 1994. **54**(7): p. 1649-52.
75. Spiropoulou, T., et al., *Effect of antineoplastic agents on the expression of human telomerase reverse transcriptase beta plus transcript in MCF-7 cells.* Clin Biochem, 2004. **37**(4): p. 299-304.
76. Mese, H., et al., *Inhibition of telomerase activity as a measure of tumor cell killing by cisplatin in squamous cell carcinoma cell line.* Chemotherapy, 2001. **47**(2): p. 136-42.
77. Ku, W.C., A.J. Cheng, and T.C. Wang, *Inhibition of telomerase activity by PKC inhibitors in human nasopharyngeal cancer cells in culture.* Biochem Biophys Res Commun, 1997. **241**(3): p. 730-6.
78. Mandal, M. and R. Kumar, *Bcl-2 Modulates Telomerase Activity.* The Journal of Biological Chemistry, 1997. **272**: p. 14183-14187.
79. Ambudkar, S.V., et al., *Biochemical, cellular, and pharmacological aspects of the multidrug transporter.* Annu Rev Pharmacol Toxicol, 1999. **39**: p. 361-98.

80. Krishna, R. and L.D. Mayer, *Multidrug resistance (MDR) in cancer. Mechanisms, reversal using modulators of MDR and the role of MDR modulators in influencing the pharmacokinetics of anticancer drugs.* Eur J Pharm Sci, 2000. **11**(4): p. 265-83.
81. Sauna, Z.E., et al., *The mechanism of action of multidrug-resistance-linked P-glycoprotein.* J Bioenerg Biomembr, 2001. **33**(6): p. 481-91.
82. Sharom, F.J., M.R. Lugo, and P.D. Eckford, *New insights into the drug binding, transport and lipid flippase activities of the p-glycoprotein multidrug transporter.* J Bioenerg Biomembr, 2005. **37**(6): p. 481-7.
83. Parekh, H. and H. Simpkins, *The transport and binding of taxol.* Gen Pharmacol, 1997. **29**(2): p. 167-72.
84. Karasov, W.H., et al., *Regulation of proline and glucose transport in mouse intestine by dietary substrate levels.* Proc Natl Acad Sci U S A, 1983. **80**(24): p. 7674-7.
85. Brown, R.S., Jr., et al., *Enhanced secretion of glycocholic acid in a specially adapted cell line is associated with overexpression of apparently novel ATP-binding cassette proteins.* Proc Natl Acad Sci U S A, 1995. **92**(12): p. 5421-5.
86. Letrent, S.P., et al., *P-glycoprotein-mediated transport of morphine in brain capillary endothelial cells.* Biochem Pharmacol, 1999. **58**(6): p. 951-7.
87. Crowe, A., *The influence of P-glycoprotein on morphine transport in Caco-2 cells. Comparison with paclitaxel.* Eur J Pharmacol, 2002. **440**(1): p. 7-16.
88. Walle, U.K. and T. Walle, *Taxol transport by human intestinal epithelial Caco-2 cells.* Drug Metab Dispos, 1998. **26**(4): p. 343-6.
89. Hoefel, D., et al., *A comparative study of carboxyfluorescein diacetate and carboxyfluorescein diacetate succinimidyl ester as indicators of bacterial activity.* J Microbiol Methods, 2003. **52**(3): p. 379-88.
90. Nordon, R.E., et al., *Analysis of growth kinetics by division tracking.* Immunol Cell Biol, 1999. **77**(6): p. 523-9.
91. Lyons, A.B., *Analysing cell division in vivo and in vitro using flow cytometric measurement of CFSE dye dilution.* J Immunol Methods, 2000. **243**(1-2): p. 147-54.
92. Ryan, J., et al., *c-myc and bcl-2 modulate p53 function by altering p53 subcellular trafficking during cell cycle.* Proc. Natl. Acad. Sci. USA, 1994. **91**: p. 5874-5882.
93. Shay, J.W., W.E. Wright, and H. Werbin, *Toward a molecular understanding of human breast cancer: a hypothesis. [Review].* Breast Cancer Research & Treatment, 1993. **25**(1): p. 83-94.
94. Wang, L.G., et al., *The effect of antimicrotubule agents on signal transduction pathways of apoptosis: a review.* Cancer Chemother Pharmacol, 1999. **44**(5): p. 355-61.
95. Salah-Eldin, A.E., et al., *An association of Bcl-2 phosphorylation and Bax localization with their functions after hyperthermia and paclitaxel treatment.* Int J Cancer, 2003. **103**(1): p. 53-60.
96. Akao, Y., et al., *Multiple subcellular localization of bcl-2: detection in nuclear outer membrane, endoplasmic reticulum membrane, and mitochondrial membranes.* Cancer Res., 1994. **54**: p. 2468-2471.
97. Krajewski, S., et al., *Investigation of the subcellular distribution of the bcl-2 oncoprotein: residence in the nuclear envelope, endoplasmic reticulum, and outer mitochondrial membranes.* Cancer Res., 1993. **53**(4701-4714).
98. Reddy, R.K., J. Lu, and A.S. Lee, *The endoplasmic reticulum chaperone glycoprotein GRP94 with Ca(2+)-binding and antiapoptotic properties is a novel proteolytic target of calpain during etoposide-induced apoptosis [In Process Citation].* J Biol Chem, 1999. **274**(40): p. 28476-83.
99. Lee, S.T., et al., *Bcl-2 targeted to the endoplasmic reticulum can inhibit apoptosis induced by Myc but not etoposide in Rat-1 fibroblasts.* Oncogene, 1999. **18**(23): p. 3520-8.
100. Maechler, P., L. Jornot, and C.B. Wollheim, *Hydrogen peroxide alters mitochondrial activation and insulin secretion in pancreatic beta cells [In Process Citation].* J Biol Chem, 1999. **274**(39): p. 27905-13.
101. Piwocka, K., et al., *A novel apoptosis-like pathway, independent of mitochondria and caspases, induced by curcumin in human lymphoblastoid T (Jurkat) cells.* Exp Cell Res, 1999. **249**(2): p. 299-307.
102. Gomez, A.M., B.G. Kerfant, and G. Vassort, *Microtubule disruption modulates Ca(2+) signaling in rat cardiac myocytes.* Circ Res, 2000. **86**(1): p. 30-6.
103. Yang, X., A. Pater, and S.C. Tang, *Cloning and characterization of the human BAG-1 gene promoter: upregulation by tumor-derived p53 mutants [In Process Citation].* Oncogene, 1999. **18**(32): p. 4546-53.
104. Kalechman, Y., et al., *Synergistic anti-tumoral effect of paclitaxel (Taxol)+AS101 in a murine model of B16 melanoma: association with ras-dependent signal-transduction pathways.* Int J Cancer, 2000. **86**(2): p. 281-8.
105. Shennan, D., *Mammary gland membrane transport systems.* Journal of Mammary Gland Biology and Neoplasia, 1998. **3**(3): p. 247-258.

106. Laupeze, B., et al., *Differential expression of the efflux pumps P-glycoprotein and multidrug resistance-associated protein in human monocyte-derived dendritic cells.* Hum Immunol, 2001. **62**(10): p. 1073-80.
107. Bart, J., et al., *The distribution of drug-efflux pumps, P-gp, BCRP, MRP1 and MRP2, in the normal blood-testis barrier and in primary testicular tumours*
*Quantitative assessment of P-glycoprotein function in the rat blood-brain barrier by distribution volume of [11C]verapamil measured with PET*
*An oncological view on the blood-testis barrier*
*P-glycoprotein at the blood-brain barrier and analysis of drug transport with positron-emission tomography*
*The blood-brain barrier and oncology: new insights into function and modulation.* Eur J Cancer, 2004. **40**(14): p. 2064-70.
108. Ambudkar, S.V., et al., *A novel way to spread drug resistance in tumor cells: functional intercellular transfer of P-glycoprotein (ABCB1).* Trends Pharmacol Sci, 2005. **26**(8): p. 385-7.
109. Cardarelli, C.O., et al., *Differential effects of P-glycoprotein inhibitors on NIH3T3 cells transfected with wild-type (G185) or mutant (V185) multidrug transporters.* Cancer Res, 1995. **55**(5): p. 1086-91.
110. Aziz, S.M., et al., *A unique interaction between polyamine and multidrug resistance (P-glycoprotein) transporters in cultured Chinese hamster ovary cells transfected with mouse mdr-1 gene.* Biochem Pharmacol, 1998. **56**(2): p. 181-7.
111. Sadlonova, A., et al., *Breast fibroblasts modulate epithelial cell proliferation in three-dimensional in vitro co-culture.* Breast Cancer Res, 2005. **7**(1): p. R46-59.
112. Fierro, F.A., et al., *Marrow-derived mesenchymal stem cells: role in epithelial tumor cell determination.* Clin Exp Metastasis, 2004. **21**(4): p. 313-9.
113. Lamb, C.A., et al., *Isolation of a stromal cell line from an early passage of a mouse mammary tumor line: a model for stromal parenchymal interactions.* J Cell Physiol, 2005. **202**(3): p. 672-82.
114. Airola, K. and N.E. Fusenig, *Differential stromal regulation of MMP-1 expression in benign and malignant keratinocytes.* J Invest Dermatol, 2001. **116**(1): p. 85-92.
115. Sier, C.F., et al., *EMMPRIN-induced MMP-2 activation cascade in human cervical squamous cell carcinoma.* Int J Cancer, 2006. **118**(12): p. 2991-8.
116. Tang, Y., et al., *Tumor-stroma interaction: positive feedback regulation of extracellular matrix metalloproteinase inducer (EMMPRIN) expression and matrix metalloproteinase-dependent generation of soluble EMMPRIN.* Mol Cancer Res, 2004. **2**(2): p. 73-80.
117. Kataoka, H., et al., *Role of cancer cell-stroma interaction in invasive growth of cancer cells.* Hum Cell, 2003. **16**(1): p. 1-14.
118. Caudroy, S., et al., *EMMPRIN-mediated MMP regulation in tumor and endothelial cells.* Clin Exp Metastasis, 2002. **19**(8): p. 697-702.
119. Tang, Y., et al., *Extracellular matrix metalloproteinase inducer stimulates tumor angiogenesis by elevating vascular endothelial cell growth factor and matrix metalloproteinases.* Cancer Res, 2005. **65**(8): p. 3193-9.
120. Noguchi, Y., et al., *Identification and characterization of extracellular matrix metalloproteinase inducer in human endometrium during the menstrual cycle in vivo and in vitro.* J Clin Endocrinol Metab, 2003. **88**(12): p. 6063-72.
121. Annab, L., et al., *Microarray analysis of gene expression of fibroblasts and epithelial cells during senescence, immortalization and various growth arrested states.* Proceeding from the 92nd Annual AACR Meeting, 2001. **42**(Abstract #2293).
122. Itoh, K., et al., *Regulatory mechanisms of cellular response to oxidative stress [In Process Citation].* Free Radic Res, 1999. **31**(4): p. 319-24.
123. Liu, H., et al., *Endoplasmic reticulum chaperones GRP78 and calreticulin prevent oxidative stress, CA2+ disturbances, and cell death in renal epithelial cells.* The journal of Biological Chemistry, 1997. **272 (35)**(August 29): p. 21751-21759.
124. Pombo, C., et al., *Activation of the Ste-like oxidant stress response kinase-1 duriing the initial stages of chemical anoxia-induced necrotic cell death.* Jour. Biol. Chem., 1997. **272**(46): p. 29372-29379.
125. Hayes, J.D. and L.I. McLellan, *Glutathione and glutathione-dependent enzymes represent a co-ordinately regulated defence against oxidative stress [In Process Citation].* Free Radic Res, 1999. **31**(4): p. 273-300.
126. Esposti, M.D., et al., *Bcl-2 and Mitochondrial Oxygen Radicals. New approaches with reactive oxygen species-sensitive probes.* J Biol Chem, 1999. **274**(42): p. 29831-29837.
127. Kennedy, C., et al., *Overexpression of hMTH1 mRNA: a molecular marker of oxidative stress in lung cancer.* FEBS Letters, 1998. **429**: p. 17-20.

128. Kazzaz, J., et al., *Cellular oxygen toxicity - Oxidant Injury without apoptosis.* The Journal of Biochemical Chemistry, 1996. **271**(June 21): p. 15182-75786.
129. Muschel, R., et al., *Induction of apoptosis at different oxygen tensions: Evidence that oxygen radicals do not mediate apoptotic signaling.* Cancer Ressearch, 1995. **55**: p. 995-998.
130. Weise, A., R. Pacifici, and K. Davies, *transient Adaptation to oxidative stress in Mammalian cells.* Archives of Biochemistry and Biophysics, 1995. **318**: p. 231-240.
131. Yuan, H., T. Kaneko, and M. Matsuo, *Relevance of oxidative stress to the limited replicative capacity of cultured human diploid cells: the limit of cumulative population doublings increases under low concentrations of oxygen and decreases in response to aminotriazole.* Mechanism of Ageing and Development, 1995. **81**: p. 159-168.
132. Reader, S., V. Moutardier, and F. Denizeau, *Tributyltin triggers apoptosis in trout hepatocytes: the role of Ca2+, protein kinase C and proteases.* Biochim Biophys Acta, 1999. **1448**(3): p. 473-85.
133. Zhu, N. and Z. Wang, *Calreticulin expression is associated with androgen regulation of the sensitivity to calcium ionophore-induced apoptosis in LNCaP prostate cancer cells.* Cancer Res, 1999. **59**(8): p. 1896-902.
134. Fadel, M.P., et al., *Calreticulin affects focal contact-dependent but not close contact- dependent cell-substratum adhesion.* J Biol Chem, 1999. **274**(21): p. 15085-94.
135. Nair, S., et al., *Calreticulin displays in vivo peptide-binding activity and can elicit CTL responses against bound peptides.* J Immunol, 1999. **162**(11): p. 6426-32.
136. Llewellyn, D.H. and H.L. Roderick, *Overexpression of calreticulin fails to abolish its induction by perturbation of normal ER function.* Biochem Cell Biol, 1998. **76**(5): p. 875-80.
137. McCool, D.J., et al., *Roles of calreticulin and calnexin during mucin synthesis in LS180 and HT29/A1 human colonic adenocarcinoma cells.* Biochem J, 1999. **341**(Pt 3): p. 593-600.
138. Michalak, M., P. Mariani, and M. Opas, *Calreticulin, a multifunctional Ca2+ binding chaperone of the endoplasmic reticulum.* Biochem Cell Biol, 1998. **76**(5): p. 779-85.
139. Basu, S. and P.K. Srivastava, *Calreticulin, a peptide-binding chaperone of the endoplasmic reticulum, elicits tumor- and peptide-specific immunity.* J Exp Med, 1999. **189**(5): p. 797-802.
140. Oliver, J.D., et al., *ERp57 functions as a subunit of specific complexes formed with the ER lectins calreticulin and calnexin [In Process Citation].* Mol Biol Cell, 1999. **10**(8): p. 2573-82.
141. Joseph, S.K., et al., *Biosynthesis of inositol trisphosphate receptors: selective association with the molecular chaperone calnexin [In Process Citation].* Biochem J, 1999. **342**(Pt 1): p. 153-61.
142. Gerner, C., et al., *Reassembling proteins and chaperones in human nuclear matrix protein fractions.* J Cell Biochem, 1999. **74**(2): p. 145-51.
143. Hockenberry, D., et al., *Bcl-2 is an outer membrane protein that blocks programmed cell death.* Nature (Lond), 1990. **348**: p. 334-342.
144. Froesch, B.A., et al., *Inhibition of p53 transcriptional activity by Bcl-2 requires its membrane-anchoring domain.* J Biol Chem, 1999. **274**(10): p. 6469-75.
145. Lock, R. and L. Stribinskiene, *Dual Modes of Death Induced by Etoposide in Human Epithelial Tumor Cells Allow Bcl-2 to Inhibit Apoptosis without Affecting Clonogenic Survival.* Cancer Research, 1996. **56**: p. 4006-4012.
146. Selvakumaran, M., et al., *The novel primary response gene MyD118 and the proto-oncogenes myb, myc, and bcl-2 modulate transforming growth factor b1-induced apoptosis of myeloid leukemia cells.* Molecular and Cellular Biology, 1994. **14**: p. 2352-2360.
147. Reed, J.C., *Bcl-2 and the regulation of programmed cell death.* Journal of Cell Biology, 1994. **124**: p. 1-6.
148. Korsmeyer, S., *Programmed cell death: Bcl-2.* Important Adv Oncol, 1993: p. 19-28.
149. D'Sa-Eipper, C. and G. Chinnadurai, *Functional dissection of Bfl-1, a Bcl-2 homolog: anti-apoptosis, oncogene-cooperation and cell proliferation activites.* Oncogene, 1998. **16**: p. 3105-3114.
150. Helbing, C., et al., *Quiesence versus apoptosis: Myc abundance determines the pathway of exit from the cell cycle.* Oncogene, 1998. **17**(12): p. 1491-1501.
151. Caassen, G. and S. Hann, *Myc-mediated transformation: the repression connection.* Oncogene, 1999. **18**(19): p. 2925-2933.
152. Pendergast, G., *Mechanisms of Apoptosis by c-Myc.* Oncogene, 1999. **18**(19): p. 2967-2987.
153. Obaya, A., M. Mateyak, and J. Sedivy, *Mysterious liasons: the relationship between c-myc and the cell cycle.* Oncogene, 1999. **18**(19): p. 2934-2941.
154. Griffith, J.D., et al., *Mammalian telomeres end in a large duplex loop [see comments].* Cell, 1999. **97**(4): p. 503-14.

155. Smith, S. and T. de Lange, *TRF1, a mammalian telomeric protein.* Trends in Genetics, 1997. **13**: p. 21-26.
156. van Steensel, B. and T. de Lange, *Control of telomere length by the human telomeric protein TRF1.* Nature, 1997. **385**: p. 740-743.
157. van Steensel, B., A. Smogorzewska, and T. de Lange, *TRF2 protects human telomeres from end-to-end fusions.* Cell, 1998. **92**: p. 401-413.
158. van Steensel, B., A. Smogorzewska, and T. de Lange, *TRF2 protects human telomeres from end-to-end fusions.* Cell, 1998. **92**(3): p. 401-13.
159. Hayflick, L., *The limited in vitro lifetime of human diploid cell strains.* Experimental Cell Research, 1965. **37**: p. 614-636.
160. Yi, X., et al., *Both transcriptional and posttranscriptional mechanisms regulate human telomerase template RNA levels.* Mol Cell Biol, 1999. **19**(6): p. 3989-97.
161. Kyo, S., et al., *Human telomerase reverse transcriptase as a critical determinant of telomerase activity in normal and malignant endometrial tissues.* Int J Cancer, 1999. **80**(1): p. 60-3.
162. Zhou, J.H., et al., *Relationship between telomerase activity and its subunit expression and inhibitory effect of antisense hTR on pancreatic carcinoma.* World J Gastroenterol, 2003. **9**(8): p. 1808-14.
163. Blackburn, E., *The telomeres and telomerase: How do they interact?* Mt Sinai J Med, 1999. **66**(5-6): p. 292-300.
164. Klingelhutz, A., *The roles of telomeres and telomerase in cellular immortalization and the development of cancer.* Anticancer Res, 1999. **19**(6A): p. 4823-4830.
165. Shay, J.W., W.E. Wright, and H. Werbin, *Defining the molecular mechanisms of human cell immortalization. [Review].* Biochimica et Biophysica Acta, 1991. **1072**(1): p. 1-7.
166. Harley, C.B., *Telomere loss: mitotic clock or genetic time bomb?. [Review].* Mutation Research, 1991. **256**(2-6): p. 271-282.
167. Shay, J.W. and S. Bacchetti, *A survey of telomerase activity in human cancer.* European Journal of Cancer, 1997. **5**: p. 787-791.
168. Boring, C., et al., *Cancer statistics 1994.* Cancer Association, 1994. **144**(1): p. 7-26.
169. Ioakim-Liossi, A., et al., *p53 protein expression in benign and amlignant breast lesions.* Acta Cytol, 1998. **42**(4): p. 918-922.
170. Varley, J., et al., *The retinoblastoma gene is frequently altered leading to loss of expression in primary breast tumors.* Oncogene, 1989. **4**(6): p. 725-729.
171. Pearson, S., et al., *Detection of telomerase activity in breast masses by fine needle aspiration.* Annals of Surgical Oncology, 1998. **5**(2): p. 186-193.
172. Kim, H.S., et al., *Immortalization of human embryonic fibroblasts by overexpression of c-myc and simian virus 40 large T antigen.* Exp Mol Med, 2001. **33**(4): p. 293-8.
173. Binder, C., et al., *Deregulated simultaneous expression of multiple glucose transporter isoforms in malignant cells and tissues.* Anticancer Res, 1997. **17**(6D): p. 4299-304.
174. Kurz, D.J., et al., *Fibroblast growth factor-2, but not vascular endothelial growth factor, upregulates telomerase activity in human endothelial cells.* Arterioscler Thromb Vasc Biol, 2003. **23**(5): p. 748-54.
175. Alonso, M.M., et al., *E2F1 and telomerase: alliance in the dark side.* Cell Cycle, 2006. **5**(9): p. 930-5.
176. Ohmichi, M., et al., *Molecular mechanism of action of selective estrogen receptor modulator in target tissues.* Endocr J, 2005. **52**(2): p. 161-7.
177. Goueli, B.S. and R. Janknecht, *Regulation of telomerase reverse transcriptase gene activity by upstream stimulatory factor.* Oncogene, 2003. **22**(39): p. 8042-7.
178. Toshikuni, N., et al., *Expression of telomerase-associated protein 1 and telomerase reverse transcriptase in hepatocellular carcinoma.* Br J Cancer, 2000. **82**(4): p. 833-7.
179. Li, H., et al., *Molecular interactions between telomerase and the tumor suppressor protein p53 in vitro.* Oncogene, 1999. **18**(48): p. 6785-94.
180. Garcia-Cao, M., et al., *A role for the Rb family of proteins in controlling telomere length.* Nat Genet, 2002. **32**(3): p. 415-419.

APPENDICES:

Metadata of the article that will be visualized in OnlineFirst

Recognition and capture of breast cancer cells using an antibody-based platform in a microelectromechanical systems device

Cell Detachment Model for an Antibody-Based Microfluidic Cancer Screening System

# Metadata of the article that will be visualized in OnlineFirst

| | | | |
|---|---|---|---|
| 1 | **Article Title** | **Recognition and capture of breast cancer cells using an antibody-based platform in a microelectromechanical systems device** | |
| 2 | | | |
| 3 | **Journal Name** | Biomedical Microdevices | |
| 4 | | Pre x | |
| 5 | | Family name | **Du** |
| 6 | **Author** | Particle | |
| 7 | | Given name | **Z.** |
| 8 | | Suf x | |
| 9 | | Degrees | |
| 10 | | Pre x | |
| 11 | | Family name | **Collie** |
| 12 | **Author** | Particle | |
| 13 | | Given name | **N.L.** |
| 14 | | Suf x | |
| 15 | | Degrees | |
| 16 | | Pre x | |
| 17 | | Family name | **Gollahon** |
| 18 | **Corresponding Author** | Particle | |
| 19 | | Given name | **L. S.** |
| 20 | | Suf x | |
| 21 | | Degrees | |
| 22 | | Organization | Texas Tech University |
| 23 | | Divison | Department of Biological Sciences |
| 24 | | Address | Texas, USA |
| 25 | | Pre x | |
| 26 | | Family name | **Cheng** |
| 27 | **Author** | Particle | |
| 28 | | Given name | **K.H.** |
| 29 | | Suf x | |
| 30 | | Degrees | |
| 31 | | Organization | Texas Tech University |
| 32 | | Divison | Department of Physics |
| 33 | | Address | Texas, USA |
| 34 | | Pre x | |
| 35 | | Family name | **Vaughn** |
| 36 | **Author** | Particle | |
| 37 | | Given name | **M.W.** |
| 38 | | Suf x | |
| 39 | | Degrees | |
| 40 | | Organization | Texas Tech University |
| 41 | | Divison | Department of Chemical Engineering |
| 42 | | Address | Texas, USA |

43 Received
44 **Schedule** Revised
45 Accepted

46 **Abstract**

Cancer is one of the most common diseases af icting humans. The use of biomarkers speci c for tumor cells has facilitated their identi cation. However, technology has not kept pace with the eld of molecular biomarkers, leaving their potential unrealized. Here, we demonstrate the ef cac y of recognizing and capturing cancer cells using an antibody-based, on-chip, micro uidic device. A cancer cell capture biochip consisting of microchannels of size 2.0 cm long and 500 $\mu$m was etched onto Polydimethylsiloxane. Epithelial membrane antigen (EMA) and Epithelial growth factor receptor (EGFR) were coated on the inner surface of the microchannels. The overall chip measured 2.0 cm $\times$ 1.5 cm $\times$ 0.5 cm. Normal and tumor breast cells in a phosphate buffered saline (PBS) suspension were o wed through the biochip channels at a rate of 15 $\mu$L/min. Breast cancer cells were preferentially captured and identi ed while most of normal cells passed through. The capture rates for tumor and normal cells were found to be $> 30\%$ and $< 5\%$, respectively. This preliminary cancer cell capture biochip design supports our initial effort of moving a BioMEMS device, from the bench top to the clinic.

47 **Keywords separated by '-'** Breast cancer – EMA – EGFR – Micro uidic system – Targeted cell capture

Biomed Microdevices
DOI 10.1007/s10544-006-9010-x

# Recognition and capture of breast cancer cells using an antibody-based platform in a microelectromechanical systems device

Z. Du · K.H. Cheng · M.W. Vaughn · N.L. Collie · L. S. Gollahon



**Abstract** Cancer is one of the most common diseases afflicting humans. The use of biomarkers specific for tumor cells has facilitated their identification. However, technology has not kept pace with the field of molecular biomarkers, leaving their potential unrealized. Here, we demonstrate the efficacy of recognizing and capturing cancer cells using an antibody-based, on-chip, microfluidic device. A cancer cell capture biochip consisting of microchannels of size 2.0 cm long and 500 $\mu$m was etched onto Polydimethylsiloxane. Epithelial membrane antigen (EMA) and Epithelial growth factor receptor (EGFR) were coated on the inner surface of the microchannels. The overall chip measured 2.0 cm × 1.5 cm × 0.5 cm. Normal and tumor breast cells in a phosphate buffered saline (PBS) suspension were flowed through the biochip channels at a rate of 15 $\mu$L/min. Breast cancer cells were preferentially captured and identified while most of normal cells passed through. The capture rates for tumor and normal cells were found to be $> 30\%$ and $< 5\%$, respectively. This preliminary cancer cell capture biochip design supports our initial effort of moving a BioMEMS device, from the bench top to the clinic.

**Keywords** Breast cancer · EMA · EGFR · Microfluidic system · Targeted cell capture

Z. Du · N. Collie · L. S. Gollahon (✉)
Department of Biological Sciences, Texas Tech University, Texas, USA

M. Vaughn
Department of Chemical Engineering, Texas Tech University, Texas, USA

K. Cheng
Department of Physics, Texas Tech University, Texas, USA

## 1 Introduction

Breast cancer is one of the most common malignancies in women (Chapman et al., 1999). About one in every eight women develops breast cancer (Cuello et al., 2002). Breast cancer progression is characterized by breast cells that grow out of control and invade nearby tissues or spread throughout the body (Sener et al., 2002). Theoretically, any type of the breast tissue can develop into cancer, but the majority of tumors develop from either the ductal or the glandular cells (Esch et al., 2001). Since breast cancer is considered an age associated disease, it may take years for a tumor to become large enough to be palpated. In a usual clinical setting, doctors screen for breast tumors using conventional mammogram, which has a size detection limit of 3 mm (Simon et al., 2002). If undetected and untreated, tumors in the breast grow and subsequently shed cancerous cells. Those cancer cells may spread (or metastasize) to other parts of the body through the bloodstream or the lymphatic system and may remain latent or undetected for years (Zhao et al., 2002).

Currently, there are standardized tests or examinations for the clinical diagnosis of breast cancer, e.g., palpation, mammography, ultrasonography and needle biopsy (Warnberg et al., 2001). Unfortunately, these standard examinations do not always detect abnormal cell growth until they have become cancerous and invaded nearby tissues. As a result, the cancer at that stage is too far advanced for effective interventions and treatments, and prognosis is generally poor. Therefore, early diagnosis is a critical factor in determining effective cancer treatments and survivorship. In addition, availability of the sensitive and quantitative method micrometastases detection, or detecting cancer cells circulating in the blood stream or body fluids, can significantly aid clinicians in designing cancer treatment plans that will

improve patient prognosis chance of survival and quality of life. To that end, we propose the use of an antibody-based micro uidics device for cancer cell detection in an aqueous suspension. Both normal and cancer cells came from a breast cell culture model system. We further developed a methodology to analyze the ef cac y of this device in screening for breast cancer cells, with the ultimate goal of applying it in a future clinical setting.

In developing a novel diagnostic technology to detect breast cancer cells on a biochip, the methodology of assembling surface immobilized, but functional, antibodies that are speci c to breast cancer cells and/or epithelial cells in a small volume, was needed. This was accomplished by covalently attaching the non-antigenic part of the antibodies onto the surface of etched microchannels embedded in a polymer chip. Small sample volumes were o wed through these channels at directed micro uidic rates. The cells that were bound to the immobilized antibodies were then collected and analyzed. Our cancer cell binding results suggest that this methodology would be useful in both the early detection of breast cancer as well as early detection of micrometastases from bone uid aspirates.

## 2 Materials and methods

### 2.1 Cell culture

The sample breast cancer cells referred to as TTU-1 (obtained from Joe Arrington Cancer Center, Lubbock, TX), were derived from an invasive ductal carcinoma. The normal cells were human mammary epithelial cells (HME). These were obtained from outside the margins of resection in a patient undergoing surgery for invasive ductal cancer. HME cells were maintained in serum free epithelial basal medium (SF170, Clonetics) supplemented with 0.4% bovine pituitary extract (Hammond Cell Technology), 0.5 $\mu$g/ml hydrocortisone (Sigma), 50 $\mu$g/ml gentamicin (Sigma), 5 $\mu$g/ml transferrin (Invitrogen), 10 ng/ml epidermal growth factor (Beckman) and 10 ng/ml insulin (Invitrogen). Tumor cells were maintained in Dulbecco's modi ed Eagle's medium (DMEM) supplemented with 10% fetal bovine serum and 50 $\mu$g/ml gentamicin (Sigma). Con uent cells were harvested for either subculturing or antibody-based capture using trypsin. The medium was aspirated and cells were rinsed with 10 mL of pre-warmed PBS. After rinsing, the PBS was aspirated and 2 ml pre-warmed trypsin-EDTA (50 $\mu$g/ml) (Invitrogen) was added to each ask. Cells were exposed to trypsin for 2 min at room temperature. Trypsin was then aspirated and the cells were incubated at 37°C for 5 min. Cells were then ushed off the ask using fresh medium, collected into a 15 cc tube and counted.

### 2.2 Immunocytochemistry

Antigen-antibody interactions were used to capture target cancer cells, employing surface antibodies selected for their speci c association with breast cancer cell phenotypes. Antibodies were immobilized on the luminal microchannel surface in order to capture the target cells. The antibodies used were:

(1) CA 15-3 (epithelial membrane antigen or EMA) (Vector Laboratories Inc). This monoclonal antibody was generated against an epithelial membrane antigen that belongs to a heterogeneous family of highly-glycosylated transmembrane proteins known as human milk fat globule (HMFG) membrane proteins (Fuqua and Cui, 2002). This antibody was used for recognition and capture of breast cells.
(2) Epidermal growth factor receptor (EGFR) (Chemicon International). This monoclonal antibody is directed against the antigenic site on the extracellular domain of the EGF receptor speci cally found on epithelial cells. This antibody is up regulated in 45% of breast tumors (Gion et al., 2001). EGFR was used to determine whether overexpression could be used as a capture criterion as well as novel antigen expression.
(3) Goat anti-mouse secondary antibody IgG uorescently-tagged with Rhodamine Red TM, (Molecular Probes, excitation 560 nm, emission 605 nm), was used to label the mouse anti-human primary monoclonal antibodies described above. Fluorescein isothiocyanate (FITC, Molecular Probes, excitation 490 nm, emission 530 nm), was initially utilized to test ef cac y of the PDMS chip surface modi cations, protein binding ef cienc y, and optimize visualization techniques. In addition, several of the primary antibodies were screened with a secondary antibody conjugated to FITC. However, Rhodamine Red proved to be better for uorescence microscopy.

Cells were plated in 4- chamber glass slides (Lab-Tek II) and allowed to attach for 24 h. After attachment, cold (−20°C) 100% methanol was added for 10 min to x the cells. The cells were then incubated with the primary antibody (EMA, CEA and EGFR) at 37°C for 1 h, rinsed, and then incubated for 1 h with the secondary antibody (goat anti-mouse IgG conjugated to Rhodamine Red) at 37°C. After a nal rinse, the chambers were removed, phosphate buffered saline (PBS) was added, the slides were cover-slipped, and results were visualized using an Olympus deconvolution microscope.

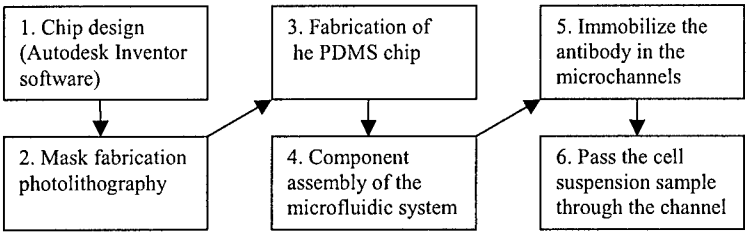


**Fig. 1** *The overall system production.* The o w chart identi es the major steps involved the micro uidic system used in this study. Each portion is described in following sections of the materials and methods

## 2.3 Design and fabrication of the on-chip micro uidic detection system

The micro uidic chips were fabricated for patterning silicon substrates by using chemistry and on-chip hydrodynamic focusing. A ow chart of the major steps in design and fabrication are shown in Fig. 1.

1. Chip design:
   Autodesk Inventor software was used to design the chip (Fig. 2).
2. Mask fabrication:
   The negative pattern to determine channel sizes was created using SU-8 as the photoresist solution by dispensing it from a viscous solution onto the chip surface in a resist spinner, following the techniques described in Saulius Juodkazis et al. (2005)
3. Fabrication of the PDMS chip:
   PDMS was mixed in a ratio of 10:1 base: curing agent. PDMS elastomer and curing agent (Sylgard 184, Dow Corning, Midland MI) was mixed with a stirring rod until homogeneous (about 5 min). The mixture was degassed to remove air bubbles. The mixture was poured on an acrylic mold that had been cast with a negative of the micro uidic channels. The mold containing the PDMS was placed in an oven at 60°C for 4 hr for curing. After curing, the PDMS was peeled from the mold and along with a clean, organic solvent-free glass slide, placed in a Plasma Cleaner (PDC-32F, Harrick Scienti c) for 1 min. The plasma treatment makes the PDMS surface highly hydrophilic or surface reactive. Immediately after removing from the plasma cleaner, the glass slide and PDMS chip are pressed together so the reactive PDMS forms a permanent bond with the glass slide (Chien and Parce, 2001). The overall channel length was 2.0 cm long, 500 $\mu$m in diameter, and 500 $\mu$m in depth.
4. Set up the micro uidic system:
   A modi ed micro uidic system prototype was assembled using a Sage$^{TM}$ M365 syringe pump (Fig. 3), with variable ow speed control from 1–30 $\mu$ L/min, depending on the syringe and tubing size used. In this study, a 10 $\mu$ L syringe (Hamilton Company) was used. The tubing and connectors were 3/16 in. ID. (World Precision Instruments).
5. Immobilizing the antibody onto the chip microchannel luminal surface:
   The surface of the PDMS chip was chemically modi ed by treating with a 2% solution of 3-mercaptopropyltrimethosilane (MTS) in toluene for 1 hr, dried, and then treated with 2 mM N-$\gamma$-maleimidobutyryloxy succinimide ester (GMBS) solution for 1 hr before rinsing with PBS (Stromberg et al., 2001). A solution of antibody plus bovine serum albumin (10% BSA) was introduced into the channels and incubated for 30 min at room temperature to react with the GMBS (Sia and Whitesides, 2003). The addition of BSA helped prevent nonspeci c cell binding and blocked unbound GMBS. Antibody : (Antibody + BSA) dilution ratios varied from 1:50 to 1:500, with the undiluted antibody concentration being 100 $\mu$g/ml (Caelen et al., 2000).

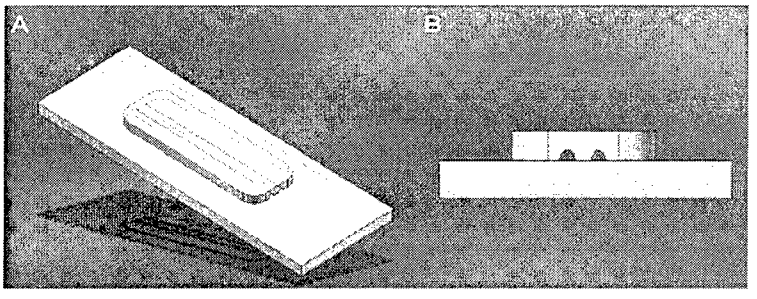


**Fig. 2** *PDMS chip design.* The chip pattern was designed using Autodesk Inventor. The micro uidic chips were fabricated using a PDMS elastomer and curing agent. Negative photolithography techniques were used to fabricate the mold (Juodkazis et al., 2005). The overall channel length was 2.0 cm long, 500 $\mu$m in diameter, and 500 $\mu$m deep. Panel A, top view and Panel B, front view

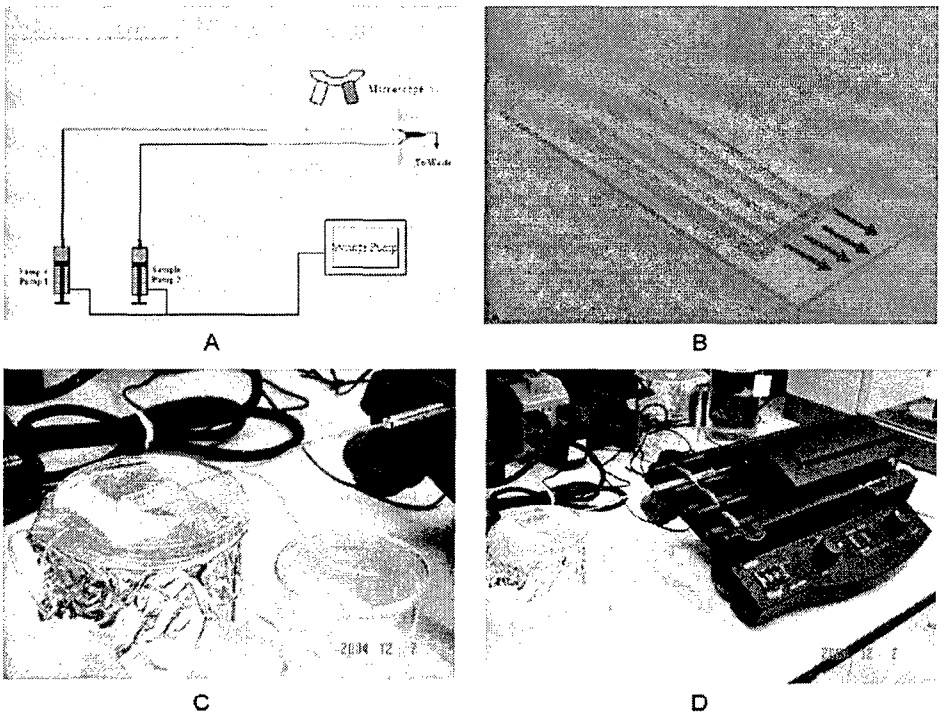


**Fig. 3** *PDMS chip design and microfluidic flow system.* (A) The overall micro uidic o w system included a syringe pump, micro uidic ow components and chip. The chip pattern was designed using Autodesk Inventor. (B) The micro uidic chips were fabricated using PDMS elastomer and curing agent (Sylgard 184, Dow Corning, Midland MI). Negative photolithography techniques were used to fabricate the mold. (C) The overall channel length was 2.0 cm long, 500 $\mu$m in diameter, and 500 $\mu$m deep. (D) Micro uidic ow was accomplished using a SageTM M365 syringe pump, tubing and connectors

6. Flowing the cell sample through the channels

Cells were harvested either for immunocytochemistry or antibody-based capture ow experiments. For each cell type, 20,000 cells were resuspended in phosphate buffered saline (PBS) and pumped through the chip. The number of cells captured was determined by counting 10 different regions of the channel under the microscope. Next, the bound cells were washed out by PBS. Captured cells harvested by ushing with PBS at a high o w rate (about 2000 $\mu$L/min) were collected and counted using a Coulter Counter (Beckman-Coulter). The number of cells counted by microscope and the number determined using the Coulter Counter was averaged, giving a nal capture rate. Complete cell detachment of the bound cells was con rmed by confocal microscopy.

## 3 Results

In order to effectively capture breast cancer cells, the antibodies should satisfy the following requirements: First, the antibody should be as speci c as possible or for target cells (e.g. breast cancer cells). Second, the antigen should be a membrane protein expressed at levels high enough on the tumor cells to allow discrimination between normal and target cells as well as to enhance binding. Using immunocytochemistry, EMA and EGFR were screened as potential capture antigens for breast cancer (Evron et al., 2001; Kumar et al., 2001) (Fig. 4). As seen in Fig. 4(A) and (B), the intensity of EMA is much greater in the tumor cells. It is also distributed evenly throughout the cell membrane. Z-stacks and 3-dimensional extrapolation using confocal microscopy con rmed this membrane localization.

Coupled with its excellent surface expression results, EMA has been shown to be expressed in a large portion of breast cancers. Sensitivity and speci city gures for the early detection of the relapse show wide variations. For EMA, speci cities range from 60% to 78% and sensitivities ranging from 33% to 78% (Fuqua and Cui, 2002). EMA can also detect "Missed" micrometastases that are reported as lymph node-negative (Gion et al., 2001). Epidermal growth factor receptor (EGFR) is the receptor for epidermal growth factor (EGF). It exist on the cell surface as inactive monomers and is activated through binding of its speci c ligands, including epidermal growth factor, transformation growth factor $\alpha$ (TGF$\alpha$), or others. EGFR is overexpressed in 14–90% of breast cancer, depending on the material tested and the method used to detect or quantitate the receptor (Ross et al.,

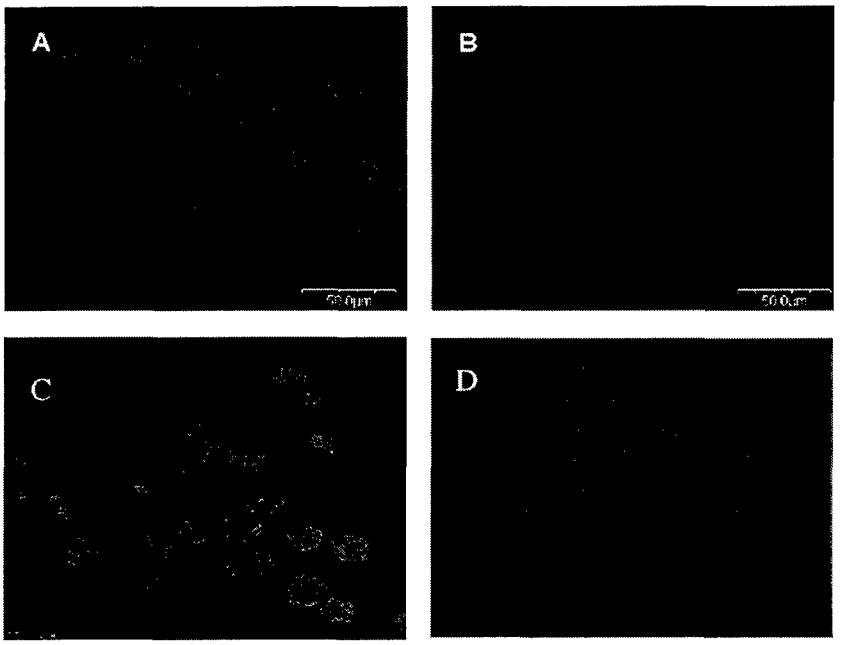


**Fig. 4** Relative expression of EMA and EGFR in breast tumor cells and normal HME cells. (A) Tumor cells stained for EMA, (B) Normal cells stained for EMA, (C) Tumor cells stained for EGFR, (D) Normal cells stained for EGFR. Blue: DAPI (345 nm excitation/459 nm emission) staining the nucleus; Red: Rhodamine (535 nm excitation/ 590 nm emission) bound to EMA. Green: FITC (485 nm excitation/517 nm emission) bound to EGFR. Magni cation: 400 ×

2003). EGFR has been shown to be overexpressed in about 45% of breast cancers (Evron et al., 2001). EGFR overexpression has been linked to adverse prognosis in a varity of tumors including breast cancer (Nicholoson et al., 1991; Castellani et al., 1994). In addition, those cancers found to express high levels of EGFR correlate with poor clinical prognosis.

Figure 4(C) and (D) show that like EMA, the intensity of EGFR was much greater in the tumor cells. Z-stacks and 3-dimensional extrapolation using confocal microscopy showed was localized to and distributed evenly throughout the cell membrane.

However, EGFR is expressed at low levels in the normal cells (Fuqua and Cui, 2002). These expression levels, although lower than the tumor cell levels (Gion et al., 2001), were high enough to yield greater background than that obtained using EMA. As a result, the capture rate of tumor cells with EGFR was only half as ef cient as EMA. Thus the signal to noise ratio when EGFR was the targeted antigen was lower, and the capture of tumor cells lower, compared to EMA.

Prior to manual o w through the channels, 20,000 cells in 100 $\mu$l of PBS were labeled with uorescent dyes to distinguish between cell types. Tumor cells were dyed with CellTracker$^{TM}$ Red CMTPX, a red dye, and normal HME cells were dyed with CellTracker$^{TM}$ Blue CMAC, a permeant blue dye (both from Molecular Probes). These two cell populations were mixed at 10,000 cells each in 100 $\mu$l of PBS and o wed through the microchannels using a Sage$^{TM}$ M365 syringe pump. Once in the microchannel, the sample was allowed to bind for 3 min, unbound cells were then rinsed out manually using PBS. Total number and percentage of cells bound to the surface were determined by two methods. Captured cells were rst counted and the percentage was determined by confocal microscopy. The second method involved counting the eluted captured cells as described earlier (Materials and Methods) based on color. The percent of captured cells for this study using EMA and EGFR is graphed in Fig. 6.

TTU-1 cells (20 k) were owed through at a rate of 15 $\mu$L/m for 3 min. This ow rate was observed to be optimal for capturing the target breast cancer cells (Fig. 5).

Figure 6 shows cells immobilized at different antibody dilutions of EMA. Although the binding rate at a dilution of 1:50 was only 30% for EMA, this could be attributable to the ow rate, the density of antigens, and distribution of antigens on the cell surface, or the speci city or avidity of different cancers. In other words, different cell surface antigens will express at different densities, and this will yield different capture rates. However, the background of normal cell capture was signi cantly lower at 2%.

The results show that the EMA antibody used enables this micro uidic system to detect breast cancer cell with high speci city and signi cantly low capture of normal cells. There are many factors that affect the results of this o w system (Taitt et al., 2004; Ngundi et al., 2005). The rst is the effect of o w rate. For each antigen-antibody pair, an optimum o w rate exists that is related to the dissociation constant of the antibody. Increasing the o w rate can cause both increased dissociation of labeled antigen and decreased antigen-antibody interaction time. The optimized o w rate in our system was 15 $\mu$L/min using the syringe pump.

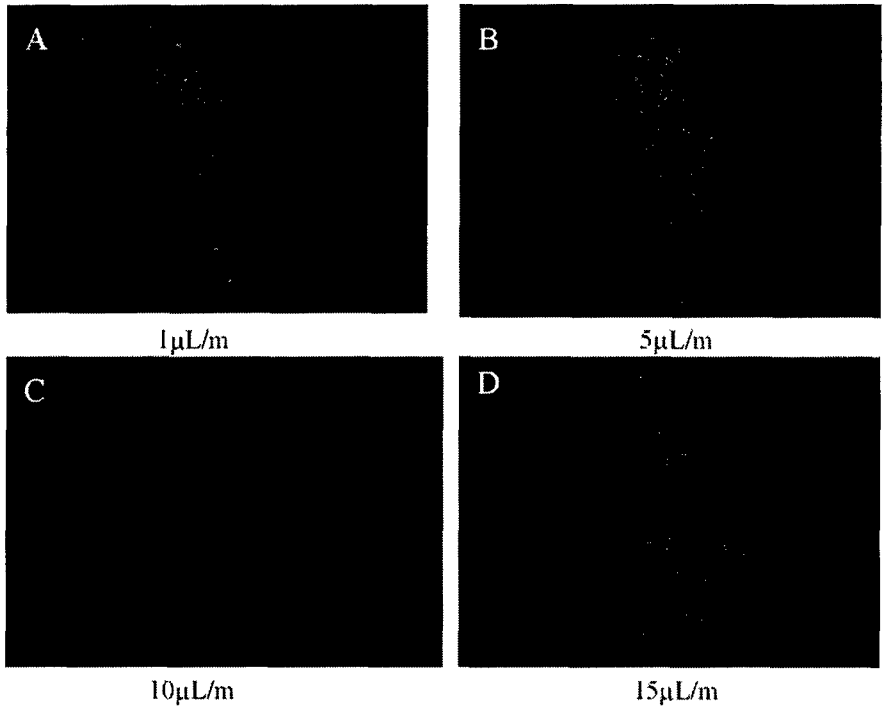


**Fig. 5** Immuno uorescent cell capture results as a function of the ow rate. Mixed cell samples ($10^4$ cells each of TTU-1 (red) and HME 50 (blue)) were pumped through channels coated with EMA antibody. The cell capture percent was determined by counting the captured cells. Panels (A–D) show the different o w rates from 1 to 15 $\mu$L/min. The antibody dilution was 1:50. With the EMA antibody, TTU-1 were captured more ef ciently than normal cells, therefore bound more strongly

The concentration of the antibody is another important factor in this capture system. Figure 6 showed that higher concentrations (shown as lower dilutions) improved capture results. More antibodies would be available to recognize the antigen on the surface of cancer cells resulting in more binding sites between the antigen and antibody. However, there is a point at which this relationship plateaus. Dilutions less than 1:50 were not observed to make a signi cant difference to the capture rates.

## 4 Discussion

Early detection is directly correlated to the success rates for breast cancer therapies. So capture and analysis of abnormal cells is high priority (Quinn et al., 2000). In addition, the ability to quickly and accurately identify micrometastases from small sample sizes is crucial for effective cancer treatment (O'Shannessy et al., 1992). The goal of this paper was to test whether design and fabrication of such a system based on antibody-antigen interactions and micro uidics could recognize and capture targeted cancer cells. In order to preferentially capture breast cancer cells, the antibody chosen was speci c for cancer-associated cell surface antigens. Alternatively, over-expressed surface antigens on cancer cells may also be useful for cell capture. Density may play an important role in discriminating from background.

Immunocytochemistry results (Fig. 4) showed strong binding interactions with breast cancer cells at the level of the plasma membrane of cells, whereas unaffected cells had low or negative reactivity. Quantitative analysis for antigen signal intensity demonstrated that breast cancer cells overexpress EMA on the cell surface (Fig. 4(A)). The intensity levels of signal in cancer cells were two- fold higher than in the normal cells. Furthermore, the signal was located on the cell membrane. Therefore, the cell-surface expression of the EMA antigen made an effective candidate for testing our antibody –based screening system (Daridon et al., 2001; Gao et al., 2001; Fiorini and Chiu, 2005; Shriver-Lake et al., 2004).

The most important factor determining successful capture and cancer cell identi cation may be the background. If very low numbers of normal cells are captured, the system has the exibility to lose some cancer cells because the captured population will be close to 100% pure. As observed with the TTU-1, lower dilutions of EMA antibodies have higher binding rates for target cells. For this reason, EMA antibody was the primary antibody used to capture target breast cancer cells in this study. Binding results for other candidate capture antibodies may reveal the best antigen to utilize in optimizing breast cancer cell detection.

An important consideration in micro uidic systems is microchannel diameter. If too wide, the cells will not encounter antibodies ef ciently , too narrow and the cells may block effective ow. Given that an average cell size ranges from 5–20 $\mu$m, a 100 $\mu$m-250 $\mu$m diameter microchannel under certain o w conditions is reasonable. Figure 6 shows that higher concentrations of EMA antibody increased the binding rate for target cells. These concentrations

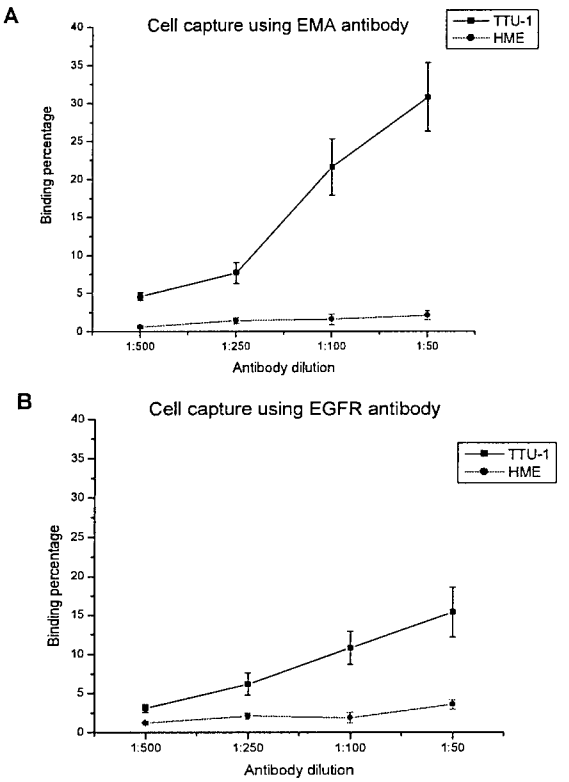


**Fig. 6** Results for breast cell capture by anti-EMA and anti-EGFR as a function of the dilution. Mixed cell samples (20 k cells each of TTU-1 and HME) were owed through the channels coated with EMA (Panel A) or EGFR (Panel B) antibody at a rate of 15 $\mu$L/min. Each run was performed in a freshly coated channel. Run time was 3 min. Cells that did not bind were rinsed and collected for further analysis. Bound cells were later ushed with PBS and counted. The binding results showed that TTU-1 cells were captured most ef ciently using EMA. EGFR was half as effective in target cell capture

have to be optimized for each antibody and microchannel geometry.

In addition, device cost is a factor. Not including instrumentation costs or microfabrication costs, the antibody alone is expensive. While lower dilutions of antibodies enhance binding, added to production costs, the overall volume used to coat the inner lumen is very small because of the micro uidic system. For example, the lowest dilution of 1:50, 10 $\mu$L of antibody was added to 490 $\mu$L BSA solution. This can be used to coat 4 microchannels. That translates into 2.5 $\mu$L of antibody per channel. If the total volume of the stock antibody is 1000 $\mu$L, this commercial antibody sample could be used for 400 microchannels at a 1:50 dilution. The cost of the antibody is approximately $300. The cost per channel calculates to about $0.75 per microchannel. Thus, antibody cost becomes economical by increasing the number of samples than can be analyzed using small antibody solution volumes per microchannel.

The advantage of the chips etched in PDMS is that they are small, with the patterned lanes having diameters in the micrometer' range (Folch et al., 2000; Watts and Lowe, 1994; Quan and Bornhop, 2001). Currently, PDMS chips in a ow system are being applied in our lab not only for target cell capture, but also for cell sorting. Application of this chip could signi cantly reduce the cost of separation instrumentation. Our fabrication and chip design in PDMS could be adapted for mass production. Our methodology demonstrates a potentially effective means for screening clinical samples. Given appropriate antibodies, this system has the potential to become a small, inexpensive and powerful device for cell sorting. This technique could have abroad range of utility in detecting a wide variety of cancer types.

By using antibodies speci c to breast cancer cells, these cells could potentially be captured and separated from ductal lavage samples and bone marrow uid aspirates. In addition, this technology could help facilitate diagnosis by its applicability to lymph uid. Therefore, lymphadenopathies could possibly be avoided, improving patient quality of life. Given the results that have been generated in this research, the chances of cell recognition and capture are high.

The proposed method is not only promising for cell capture and sorting, but also for application including drug screening, cell-cell communication studies and the production of cell-based biosensors. With the design of PDMS chips, one can use this micro uidic system to detect the target cells from the sample in a portal system in which uid o w is easily controlled. Although target cells can be detected by microscopy, we are currently developing an optical detection system to increase portability and alleviate the need for a microscope.

## 5 Conclusion

We have demonstrated that breast cancer cells can be captured and enriched by antibody binding in a micro uidic channel. EMA was used as a capture antibody bound to the channel surface. Tumor cells were captured ef ciently , and the capture rate and ef cienc y were found to be controlled by three important aspects: (1), the cell surface antigen expression or density; (2), ow rate through the microchannels; and (3), the concentration of antibody immobilized in the channels. If these 3 parameters are optimized, this would greatly facilitate diagnosis by pathologists through capturing and enriching speci c cell types. Our future work is currently focused on improving capture ef cienc y and enhancement by use of closed-loop recirculation to increase antigen-antibody interact on time, investigating breast cancer cell with different markers, and developing an on-chip micropump to make the unit self-contained.

**Acknowledgments** This work was supported by DOD US Army Breast Cancer Research Program Idea Award DAMD-17-02-1-0581, and Robert A. Welch Research Foundation (D-1158) given to KHC.

## References

I. Caelen, A. Bernard, D. Juncker, B. Michel, H. Heinzelmann, and E. Delamarche, Langmuir **16**, 9125 (2000).

R.Castellani, E.W. Visscher, and S. Wykes, Cancer **73**, 344 (1994).

J.W. Chapman, E.B. Fish, and M.A. Link, Br. J. Cancer **79**, 1508 (1999).

R.L. Chien and J.W. Parce, Fresenius J. Anal. Chem. **371**,106 (2001).

M.A. Cuello, M. Nau, and S. Lipkowitz, Breast Dis. **15**, 71 (2002).

A. Daridon, V. Fascio, J. Lichtenberg, R. Wutrich, H. Langen, E. Verpoorte, and N.F. De Rooij, Fresenius J. Anal. Chem. **371**, 261 (2001).

M.B. Esch, L.E. Locascio, M.J. Tarlov, and R.A. Durst, Anal. Chem. **73**, 152 (2001).

E. Evron, W.C. Dooley, C.B. Umbricht, and S. Sukumar, Lancet **357**, 1335 (2001).

G.S. Fiorini and D.T. Chiu, BioTechniques **38**, 429 (2005).

A. Folch, S. Mezzour, M. During, O. Hurtado, M. Toner, and R. Muller, Biochemical Microdevices 2 (2000).

S.A.W. Fuqua and Y. Cui, Breast Dis. **15**, 3 (2002).

S.A.W. Fuqua, Mol. Cell. Biol. **22**, 3373 (2002).

Q. Gao, V. Shi and S. Liu, Fresenius J. Anal. Chem. **371**, 137 (2001).

M. Gion, L. Peloso, R. Mione, and G. Cappelli, Breast Dis. **21**, 23 (2001).

S. Juodkazis, V. Mizeikis, K.K. Seet, M. Miwa, and H. Misawa, Nanotechnology **16**, 846 (2005).

R.R. Kumar, A. Meenakshi, and N. Sivakumar, Hum. Antibodies **10**, 143 (2001).

M.M. Ngundi, L.C. Shriver-Lake, M.H. Moore, M.E. Lassman, F.S. Ligler, and C.R. Taitt, Anal. Chem. **77**, 148 (2005).

S. Nicholoson, J. Richard, and C. Sainsbury, Br. J. Cancer **63**, 146 (1991).

D.J. O'Shannessy, M. Brigham-Burke, and K. Peck, Anal. Biochem. **205**, 132 (1992).

Z. Quan and D.J. Bornhop, In: *Lab Automation* (Palm Springs, CA. USA, 2001).

J.G. Quinn, S. O'Neil, A. Doyle, C. McAtamney, D. Diamond, B.D. MacCraith, and R. O'Kennedy, Anal. Biochem. **281**, 143 (2000).

J.S. Ross, G.P. Linette, J. Stec, E. Clark, M. Ayers, N. Leschly, W.F. Symmans, G.N. Hortobagyi, and L. Pusztai, Expert Rev. Mol. Diagn. **3**, 573 (2003).

S. F. Sener, B. Cady, and D. Merkel, Cancer Pract. **10**, 45 (2002).

L.C. Shriver-Lake, C.R. Taitt, and F.S. Ligler, J. AOAC Int. **87**, 1498 (2004).

S.K. Sia and G.M. Whitesides, Electrophoresis **24**, 3563 (2003).

M.S. Simon, D. Ibrahim, L. Newman, and M. Stano, Drugs Aging **19**, 453 (2002).

A. Stromberg, A. Karlsson, F. Ryttsen, M. Davidson, D.T. Chiu, and O. Orwar, Anal. Chem. **73**, 126 (2001).

C.R. Taitt, J.P. Golden, Y.S. Shubin, L.C. Shriver-Lake, K.E. Sapsford, A. Rasooly, and F.S. Ligler, Microb. Ecol. **47**, 175 (2004).

F. Warnberg, H. Nordgren, L. Bergkvist, and L. Holmberg, Br. J. Cancer **85**, 869 (2001).

H.J. Watts and C.R. Lowe, Anal. Chem. **66**, 2465 (1994).

B. Zhao, N.O. L. Viernes, J.S. Moore, and D.J. Beebe, J. Am. Chem. Soc. **124**, 5284 (2002).

# Cell Detachment Model for an Antibody-Based Microfluidic Cancer Screening System

**Swapnil P. Wankhede,[†] Zhiqiang Du,[‡] Jordan M. Berg,*[,†] Mark W. Vaughn,[§] Tim Dallas,[∥] Kwan H. Cheng,[⊥] and Lauren Gollahon[‡]**

Department of Mechanical Engineering and Nano Tech Center, Department of Biological Sciences, Department of Chemical Engineering, Department of Electrical Engineering and Nano Tech Center, and Department of Physics, Texas Tech University, Lubbock, Texas 79409

We consider cells bound to the floor of a microfluidic channel and present a model of their flow-induced detachment. We approximate hydrodynamic force and cell elastic response using static finite-element simulation of a single cell. Detachment is assumed to occur when hydrodynamic and adhesive forces are roughly equal. The result is extended to multiple cells at the device level using a sigmoidal curve fit. The model is applied to a microfluidic cancer-screening device that discriminates between normal epithelial cells and cells infected with human papillomavirus (HPV), on the basis of increased expression of the transmembrane protein α6 integrin in the latter. Here, the cells to be tested are bound to a microchannel floor coated with anti α6 integrin antibodies. In an appropriate flow rate range, normal cells are washed away while HPV-infected cells remain bound. The model allows interpolation between data points to choose the optimal flow rate and provides insight into interaction of cell mechanical properties and the flow-induced detachment mechanism. Notably, the results suggest a significant influence of cell elastic response on detachment.

## 1. Introduction

The progression of several epithelial cell cancers, including cervical cancer, is correlated with infection by human papillomavirus (HPV) (*1*). Infection with HPV is also known to correlate with up-regulation of the transmembrane protein *a6* integrin (*2*). Use of immunological assays based on unique biomarkers to capture cancer cells is well established (*3*). The technique considered here differs from the previous approach in that target cell detection and capture is based on discrimination between *levels* of a particular antigen. In particular, up-regulation of the cell membrane density of α6 integrin can be used to detect and concentrate HPV-infected cells using hydrodynamic forces. This principle has been demonstrated in a microfluidic device fabricated of glass and poly(dimethylsiloxane) (PDMS) (*4*). Antibodies against α6 integrin are bound to the glass floor of a glass/PDMS microchannel. When a mixture of HPV-infected and normal cells is introduced into the channel, infected cells, with a higher density of cell membrane antigens, adhere to the antibody-coated wall more strongly. Phosphate-buffered saline (PBS) is flowed through the microchannel at a specified rate, creating hydrodynamic forces that cause significantly more normal cells than HPV-infected cells to detach. The fraction of the cells that remain bound indicates the extent of HPV infection and in turn represents a potential positive cancer signal. The bound, potentially cancerous cells may subsequently be released by chemical, thermal, or mechanical processing for further testing, to reduce the incidence of false positives. The construction and performance of a prototype device implementing this assay is described in Section 2 below.

A critical parameter for proper functioning of the screening device is the flow rate. If too low, few cells of either type will detach, and selectivity for cancerous over noncancerous cells will be small. If too high, cancer cells as well as normal cells will detach, raising background levels to the point where reliable detection is no longer possible. If capture of potential cancer cells for further testing is desired, then low flow rates will cause large numbers of normal cells to be captured along with the desired cells, whereas high flow rates will give rise to very small sample sizes. Proper selection of the flow rate requires an understanding of both the hydrodynamic and adhesive forces acting on the cell.

A number of prior studies treat related problems. Goldman et al. (*5*, *6*) compute the hydrodynamic force on a single free-floating spherical cell. Hammer et al. (*7*−*9*) consider in detail the hydrodynamic and adhesive forces acting on a cell rolling across a planar surface. Tees and Goetz (*10*) relate ligand−receptor bond constants, cell size, and the hydrodynamic force on the cells adhered to the bottom of a microchannel. Brooks and Tozeren (*11*) determined the fluid force and fluid moment on an array of cells with various cell shapes and cell diameters. Gaver and Kute (*12*) consider a hemispherical cell in a narrow channel. These studies treat the cells as rigid bodies, while the current study considers the effects of cell deformation. These effects are seen to be significant. This is consistent with the conclusions of N'Dri et al. on leukocyte rolling (*13*). Konstantopoulos et al. (*14*) also examine the effects of cell deformability on hydrodynamic force and cell−substrate contact area during cell rolling. Chu et al. address the role of the cytoskeleton in

* To whom correspondence should be addressed. Email: jordan.berg@ttu.edu.
† Department of Mechanical Engineering and Nano Tech Center.
‡ Department of Biological Sciences.
§ Department of Chemical Engineering.
∥ Department of Electrical Engineering and Nano Tech Center.
⊥ Department of Physics.

10.1021/bp060127d CCC: $33.50 
Published on Web 08/09/2006 

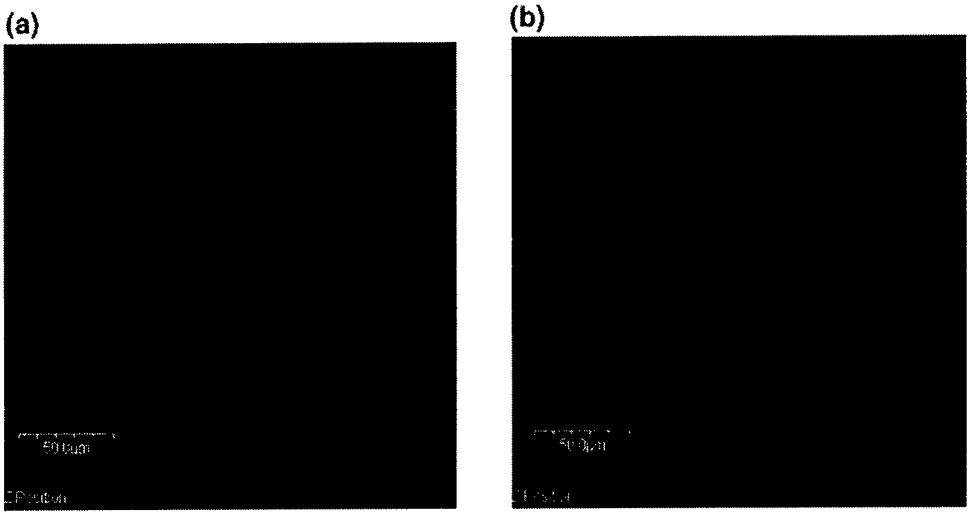


**Figure 1.** Cell surface α6 integrin levels visualized with rhodamine-labeled antibody for (a) HCCC and (b) HGEC. Confocal microscope image of cells after incubation with a primary antibody against the integrin α6 complex (MAb2254), followed by a fluorescently tagged secondary antibody (IgG). The higher intensity of fluorescence of the HCCC over that of HGEC indicates higher integrin levels.

cell elasticity (*15*). By treating the much simpler *detachment* problem, the current study can employ a simpler model, which appears to have significant predictive value. In particular, the model considered is a single elastic sphere, bound to a planar wall in a laminar flow. As described in Section 3, hydrodynamic forces and the elastic response are simulated for a *single* cell using finite-element analysis (FEA). Cell deformation is predicted to strongly affect the cell−substrate contact area, and therefore the cell binding force, while influencing hydrodynamic forces to a lesser extent.

The static analysis of a single cell is much less demanding of computational resources than transient simulation or simulation of a large number of interacting cells. Section 3 describes how the single-cell FEA model may be related to device level behavior through a sigmoidal-type function. This model is motivated by the following argument:

For a single cell, detachment will occur when the hydrodynamic force is roughly equal to the adhesive force. However, as a result of variations in cell properties such as diameter, stiffness, and surface antigen density, the flow rate at which this occurs will vary from cell to cell. The resulting *range* of detachment points may be represented by a *sigmoid*, with a transition width fit to experiment to account for the degree of variation in cell properties. The adhesion force is assumed proportional to cell/substrate contact area, with the constant of proportionality equal to the product of the antigen−antibody bond strength and the surface antigen density. At present, this proportionality constant is also fit to experimental data for each cell type, but if known it could be directly incorporated. Finally, the fraction of bound cells at zero flow rate is difficult to measure, because some cells that appear bound may rest atop other cells instead of the channel floor, and others may still be in suspension. This value is currently fit to data but is assumed independent of cell type. Thus for an experiment with two types of cells, the sigmoidal models inherently each contain one parameter to be fit to the data, with the present implementation requiring three additional parameters, for a total of five.

The fit of the sigmoidal model to experiment is found to be excellent, as described in Section 4. The model is also used to predict the ratio of surface antigen density between normal and cancer cells, giving a result consistent with fluorescence measurements.

The use of the detachment model results directly in flow rate selection is discussed in Section 5, which introduces an appropriate figure of merit, the "discrimination factor", to quantify performance in discriminating between and collecting cells of various types. Section 6 presents brief concluding remarks.

## 2. Experimental Section

Experimental cell detachment studies were carried out as described in ref 4. A microchannel 2.0 cm long by 500 $\mu$m wide by 500 $\mu$m deep was cast in PDMS (Sylgard 184, Dow Corning) using an acrylic mold, cured at 60 °C for 4 h, and peeled from the mold. The patterned surface of the PDMS and a clean glass microscope slide were exposed to an oxygen plasma for one minute, using a plasma cleaner (PDC-32F, Harrick Scientific). The treated surfaces were pressed together, resulting in a permanent bond. A syringe pump (Sage M365) controllable from 1 to 30 $\mu$L/min was connected to one end of the channel; an open tube was connected to the other end, and the output was collected for testing or disposal. The glass surface of the channels were readied for antibody binding as follows: (i) 1 h soak in a 2% solution of (3-mercaptopropyl) trimethoxysilane (MTS) in toluene, (ii) air dry, (iii) 1 h soak in 2 mM *N*-$\gamma$-maleimidobutyryloxy succinimide ester (GMBS), (iv) PBS rinse. A solution of anti α6 integrin antibody was then flowed into the channel and allowed to incubate for 30 min at room temperature. This procedure is known to effectively functionalize glass surfaces; the PDMS surfaces may also bind some antibodies, but the efficiency is markedly lower.

Testing was performed using cultures of normal human glandular epithelial cells (HGEC) and human cervical cancer cells (HCCC). Subsequently we also refer to the HGEC as "normal cells" and the HCCC as "cancer cells." The culturing protocols are described in detail in ref 4. A series of immunological tests confirm the presence of intracellular HPV in the HCCC and show that levels of α6 integrin are elevated on the surface of the HCCC versus the HGEC. Figure 1 shows a confocal microscope (Olympus IX-FV300) image of tagged anti α6 integrin antibodies (CD49*f*) for (a) HCCC and (b) HGEC. It can be seen that the α6 integrin not only is uniformly distributed over the cancer cell membrane but also exhibits a much higher fluorescence signal. The antigen surface density

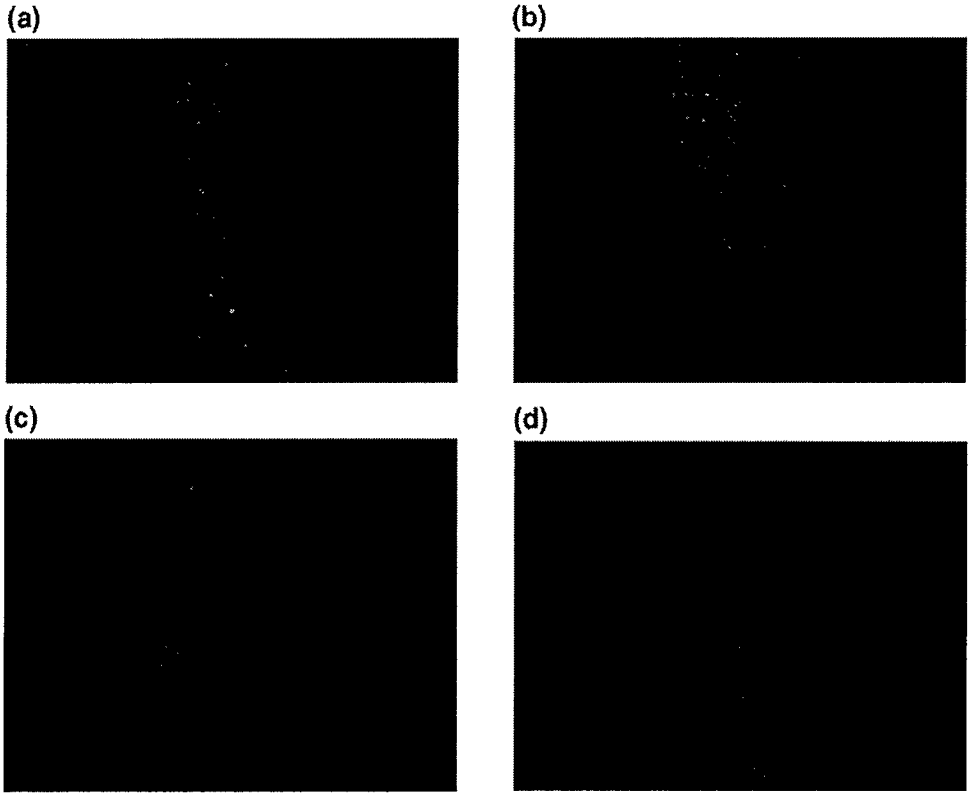


**Figure 2.** Fluorescent confocal microscope images of mixed cell samples (initially $10^4$ cells each of HGEC (blue) and HCCC (red)) bound to the microchannel floor after 3 min of flow at rates of (a) 0, (b) 10, (c) 15, and (d) 20 $\mu$L/min. The increase in the preferential binding of the cancer cells at the higher flow rates is evident.

ratio, HCCC:HGEC, estimated from the fluorescence intensity ratio was 2.3. This value was determined as follows. Images were processed using *ImageJ* software (*16*). After the images were converted to gray scale, the background fluorescence from the cell free region was subtracted from each image. The intensity was integrated over the cell surfaces. Cell surface area was determined using the "Analyze Particles" feature of *ImageJ*. This area was verified by visual comparison with differential interference contrast images of the cells and by counting the area after conversion to binary black and white images.

To facilitate imaging for device characterization, the HGEC and HCCC were labeled with fluorescent molecular probes, CellTracker Blue CMAC 353/466 (Invitrogen) and CellTracker Red CMTPX 577/602 (Invitrogen), respectively. These dyes pass through the cell membrane and so do not interfere with antibody−antigen interactions at the cell surface. For these tests a mixture of 10,000 normal cells and 10,000 cancer cells were suspended in 100 $\mu$L of PBS, flowed into the channel, and allowed to settle under gravity for 5 min. All testing was performed using freshly coated channels. Since only the glass surface is known to bind large quantities of antibodies, the glass wall of the channel was always chosen to be the bottom surface. This is also convenient since the microscope is configured to image through the bottom of a glass slide. The fixtures used to make fluid connections to the channels sit on top of the PDMS layer, making any other orientation inconvenient. After 5 min the syringe pump was used to flow the cell mixture at rates between 4 and 28 $\mu$L/min for 3 min. At the end of that time the number of normal and cancer cells remaining was determined using fluorescence confocal microscopy. Three runs were made at each flow rate. Figure 2 shows confocal fluorescent microscopy images of the resulting cell distributions at four flow rates. Figure 3 shows the resulting data normalized to the cell count

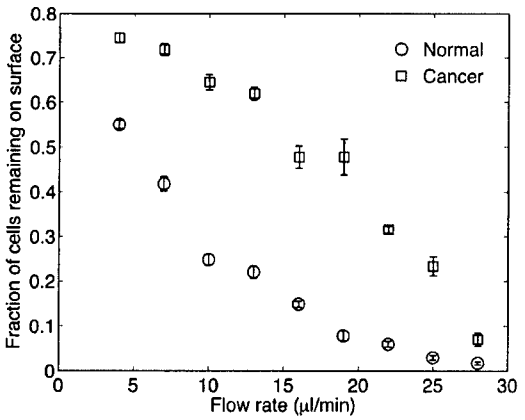


**Figure 3.** Normalized fraction of cells remaining after 3 min of flow, as a fraction of the initial number of cells, versus flow rate: (○) normal cells; (□) cancer cells. Error bars are standard deviation about the mean value ($N = 3$).

before initiation of flow. This value does not reliably represent the number of initially bound cells because without flow, cells that are resting on other cells or cells that have not settled out of suspension may appear to be bound. The error bars are the standard deviation about the mean value at each flow rate ($N = 3$). Note that the fraction of cancer cells remaining at 19 $\mu$L/min is, within experimental uncertainty, indistinguishable from that at 16 $\mu$L/min, whereas one might expect it to be significantly lower. As discussed below, the proposed model explains this counterintuitive behavior.

## 3. Theoretical Basis

**Cell Detachment Modeling.** The primary goal of this study is to develop a cell detachment model that can be used to design

and optimize microfluidic systems for cancer cell detection and concentration. Here we demonstrate the use of the model to pick an appropriate flow rate for the system and to provide physical insight into the flow rate dependence. We propose a simple model based on the ratio between the adhesive force ($F_A$) holding the cell to the channel wall and the hydrodynamic force ($F_H$) pulling the cell away. The model is

$$\frac{N}{N_0} = P_a\left(\frac{F_H}{F_A}\right) \tag{1}$$

where $N$ is the number of cells remaining, $N_0$ is the initial number of cells, and $P_a$ is the sigmoid function:

$$P_a(x) = \frac{1}{1 + e^{a(x-c)}} \tag{2}$$

where $a$, $c > 0$ are adjustable parameters. The function (eq 2) decreases monotonically from one to zero as $x$ increases. When $a$ is very large, $P_a(x)$ approaches a step function behavior, being approximately 1 for $x < c$, approximately zero for $x > c$, and transitioning rapidly as $x$ passes through $c$. For smaller values of $a$, $P_a(0)$ is less than 1, and the transition region around $x = c$ is more gradual. For any value of $a$, eq 2 is always exactly 0.5 at $x = c$. For the purposes of this paper, we will take $c = 1$. That is, the model predicts that 50% of the cells will detach when the adhesive and hydrodynamic forces, as predicted by the FEA, are equal.

Figure 4 shows the behavior of eq 2 for $c = 1$ and increasing values of $a$. In the context of cell detachment the parameter $a$ may be thought of as describing variability in the forces seen by individual cells. If all cells of a particular type are acted upon by uniform forces, then $a$ will be large, and the model predicts that all of the cells will detach in a narrow flow range. On the other hand, if these forces can deviate widely from the average, then $a$ will be smaller, and some cells will detach at significantly lower flow rates and others at significantly higher flow rates. Sources for such nonuniformity would include variations in cell size, cell elasticity, surface antigen density, and possibly the local flow velocity. Implied in this model is the assumption that all of the cell attachment occurs during the 5 min settling period and during the flow period cells only detach. As a consequence of this assumption, PBS could replace the cell suspension for the flow phase in future devices. This would have the advantage of reducing the required analysis sample size.

**Finite Element Analysis.** While the model based on eq 2 seems straightforward, the hydrodynamic and adhesion forces depend on the flow rate in a complex way. FEA captures these effects, particularly those due to cell deformation. The model in this study was generated on the basis of the following assumptions: the cell surface was assumed to be smooth, the effect of the presence of other cells on fluid force was neglected, and cells were assumed to be of uniform size. Hydrodynamic forces and cell deformation were then computed using the finite-element package CFD-ACE+ (*17*). The first step in such an analysis is geometry and grid generation. Figure 5 shows a single cell model generated using the preprocessor CFD-GEOM (*17*). Normal and cancerous epithelial cells typically have diameters in the 7−14 $\mu$m range (*19*). The analysis assumed a 10 $\mu$m diameter; this was based on the average size of HCCC and HGEC captured and counted (*4*). When in suspension, the cytoskeletal microfibers contract and the cells assume a spherical shape (*19*). The cell size when plated increased by a factor of

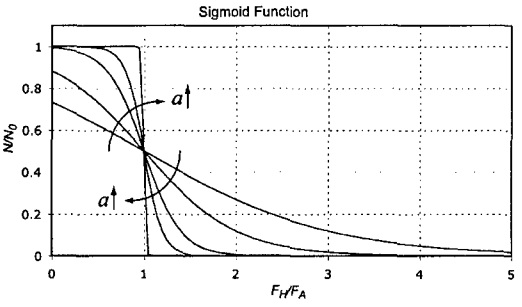


**Figure 4.** Sigmoid functions for $c = 1$ and $a = 1, 2, 5, 10, 100$.

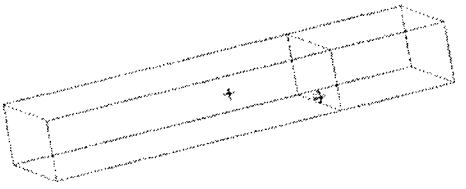

**Figure 5.** CFD-GEOM model of a single cell, modeled as a 10 $\mu$m diameter sphere, bound to the wall of a 50 $\mu$m × 50 $\mu$m square channel. The channel inlet is to the left. About 57,000 elements are used to mesh the fluid; about 3,000 are used for the elastic sphere.

2 due to plate adhesion. It is assumed that this shape change has not occurred in the brief settling period that begins this experiment.

The use of a single cell for simulation suggests that flow interaction between cells will not be accurately captured. The mean velocities considered in this study range from 1.9 to 13 mm/s. the corresponding velocities at a height of 10 $\mu$m from the channel wall are 0.22−1.6 mm/s. Thus the highest Reynolds number, based on cell diameter and velocity at the cell, is about 0.02. A recent study computes interaction forces between spheres bound to a wall in low Reynolds number Poiseuille flow (*18*). For channel heights that are large compared to the sphere diameter, the interaction forces drop off quickly with the distance between spheres. For example, for downstream distances of 2, 5, and 10 diameters, the interaction forces are 15%, 1.6%, and 0.2% of the hydrodynamic drag force (*18*, Figure 6). In the experiments described in Section 2, cells are sparsely bound to the channel floor. The distribution is irregular and apparently random, but the smallest distance between neighboring cells is about 50 $\mu$m. Therefore the assumption of noninteracting cells is valid in this device. For higher Reynolds numbers or more densely packed cells, this assumption will need to be revisited.

The initial contact area must be chosen for the simulation. Following, for example, ref 20, we assume all bonds within a specified cutoff distance of the surface are active. For leukocyte rolling this cutoff height is typically assumed to be on the order of 40 nm or about twice the equilibrium bond length (*20*), though some studies assume cutoff distances up to 100 nm (*14*). To accommodate some flattening of the cell during the settling period, as well as stretching of established bonds (*21*), we have used a cutoff height of 200 nm. With this choice, the initial contact area is about 6.3 $\mu$m$^2$, with a radius of 1.4 $\mu$m. This is about 2% of the total cell surface area. Implementation in simulation is by slicing the bottommost 200 nm from the spherical cell model and constraining the resulting circular surface to the bottom of the microchannel.

Although the cross-section of the channel under study is 500 $\mu$m × 500 $\mu$m, for computational efficiency the simulated channel cross-section is only 50 $\mu$m × 50 $\mu$m. Also for computational efficiency, although the entire cross-section of the channel must be simulated, a more highly refined mesh is

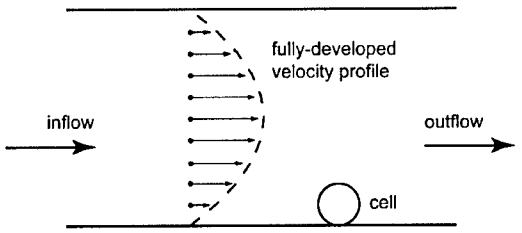


**Figure 6.** Cell in fully developed laminar flow with nonslip boundaries experiences a parabolic velocity profile. Near the channel floor velocities are much lower than the mean across the entire channel.

used around the cell than elsewhere in the channel. The mean velocity in the simulation is set to $U_{mean} = Q_{exp}/A_{exp}$, where $Q_{exp}$ is the experimental volume flow rate and $A_{exp}$ is the cross-sectional area of the experimental channel. This normalization procedure allows channels of different dimensions to be accommodated without additional simulations.

A plug flow with uniform velocity $U_{mean} = Q_{exp}/A_{exp}$ is applied at the inlet. The distance to the cell is sufficient for a steady laminar flow profile to fully develop. Figure 6 shows the resulting parabolic velocity distribution. Because the influence of the cell on the flow extends upstream as well as downstream, for a distance on the order of the cell diameter, the velocity profile immediately upstream of the cell itself will differ somewhat (neither this length nor the length required for a steady flow profile to develop are shown to scale). However some important qualitative observations are possible, including that at the wall the flow velocity is zero, hence the more a body flattens to the wall, the lower average flow velocity and therefore lower hydrodynamic force it experiences.

The cell is modeled as an isotropic, linear, elastic body. The change of shape in response to the flow will depend on the elastic properties, which differ for normal and cancer cells. Normal cells are more elastic than pre-metastatic cancer cells (*22*). For this study a Young's modulus of 3,000 N/m$^2$ was used for normal cells and 10,000 N/m$^2$ for cancer cells (*23*, *24*). The CFD-ACE solver (*17*) was used to obtain steady-flow solutions, including contact modeling between the cell and the channel wall. The CFD-VIEW postprocessor (*17*) was used to extract the hydrodynamic forces acting on the cell (including the effects due to deformation) and the contact area between the deformed cell and the channel wall. Figure 7 shows the cell deformation for normal and cancer cells at three different flow rates. The analyses took between 3 and 10 min at each flow rate, running on a Pentium 4 with 1 GB of RAM.

Figure 8 shows the hydrodynamic forces acting on the cell for a solid sphere, a normal cell, and a cancer cell. The effect of cell deformation can be seen, as the more elastic the cell, the more it flattens out as flow rate increases, thus bringing the cell center of pressure nearer the wall, resulting in reduced average flow velocity. The dependence in each case is nearly linear in the flow rate, as expected from analytical considerations, but the effect of cell deformation is to reduce the hydrodynamic force experienced by as much as 30%, for the normal cell as compared to the rigid cell.

While the effect of cell deformation on the hydrodynamic forces is significant, the effect on adhesive forces is much greater. Figure 9 shows the increase in contact area as a function of flow rate. It can be seen that the more elastic normal cell increases its contact area by more than a factor of 4 over the test flow rate range, and the cancer cell by a factor greater than 2.5. The cell adhesion model assumes that the cell membrane antigens are evenly distributed over the cell surface and that the bound antibody density on the channel walls is also uniform and much greater than the antigen density, $\rho_A$. Then the adhesive force of the cell to the wall is

$$F_A = f_b \rho_A A_c \tag{3}$$

where $f_b$ is the force of each antigen–antibody bond, and $A_c$ is the contact area. Thus the adhesive force is directly proportional to the cell contact area. Also of interest are the shapes of the curves in Figure 9. For both the normal and the cancer cell there is a narrow flow region in which the contact area increases rapidly. For the normal cell this occurs between 6 and 12 $\mu$L/min. For the cancer cell this occurs between 16 and 20 $\mu$L/min. The physical cause of the "knee" in the curves is not clear. We hypothesize that if the hydrodynamic and elastic forces were appropriately nondimensionalized, the normal and cancer cells would show identical deformation behavior. That is, assuming the cells are the same size and shape initially, we believe the reason that the jump in area occurs at a higher flow rate in cancer cells is entirely due to their higher stiffness. However, rigorously testing this hypothesis will require extensive further simulation of cells of a variety of size and stiffness and is beyond the scope of the present paper.

Use of the model (eqs 1 and 2 requires knowledge of the ratio of hydrodynamic to adhesive force, and a value for the "nonuniformity" parameter $a$. (Recall that $c$ is set to 1.) The finite-element simulation gives $F_H$ and $A_c$ as functions of flow rate and a reasonable value of 40 pN for $f_b$ is found in the literature (*21*, *25*), but at present we lack a priori knowledge of $\rho_A$ and $a$. Therefore these values are fit to match the data. Furthermore, as mentioned earlier, the number of initially bound cells $N_0$ is not reliably known and is fit to the data as well. Thus five parameters are simultaneously fit to the data shown in Figure 3. These are $\rho_{A_n}$ and $a_n$ for the normal cells, $\rho_{A_c}$ and $a_c$ for the cancer cells, and $N_0$, which is assumed the same for both types of cells.

## 4. Results

The five free parameters in the sigmoidal model were fit using nonlinear least squares minimization, via the Levenberg–Marquardt algorithm, as implemented in the function lsqnonlin in the Matlab software package (*26*). The search was terminated when subsequent iterations changed the residual value by an absolute difference of less than $10^{-6}$. The Euclidean norm of the combined experimental data vector is 1.8, and the sum square error was 0.13, giving a relative modeling error of 7.2%. Based on an antigen–antibody bond strength of 40 pN, the estimated values of $\rho_{A_c}$ and $\rho_{A_n}$ are 9.52 and 3.26 $\mu m^{-2}$, respectively. These values correspond to average spacing between antigens of 0.32 $\mu$m for cancer cells and 0.55 $\mu$m for normal cells. The estimated values of $\rho$ are sensitive to the assumed bond strength and differences between the FEA and actual cell geometry, but the ratio $\rho_{A_c}/\rho_{A_n}$ should be more robust. We estimate this as 2.92, which compares well with the value of 2.3 estimated from the fluorescence images in Section 2. Because of the uncertainty of background contributions and of the cell area, there can be considerable uncertainty in the fluorescence-based estimate. Direct measurement of the surface antigen densities is planned for the near future. The values of $a_n$ and $a_c$ are found to be 3.8 and 9.3, respectively. The initial cell coverage $N_0$ is estimated to be 72%.

The resulting cell detachment model is shown versus the modeled force ratio in Figure 10a and versus flow rate in Figure 10b. Here hydrodynamic force and contact area values at flow rates between simulated points are interpolated using cubic

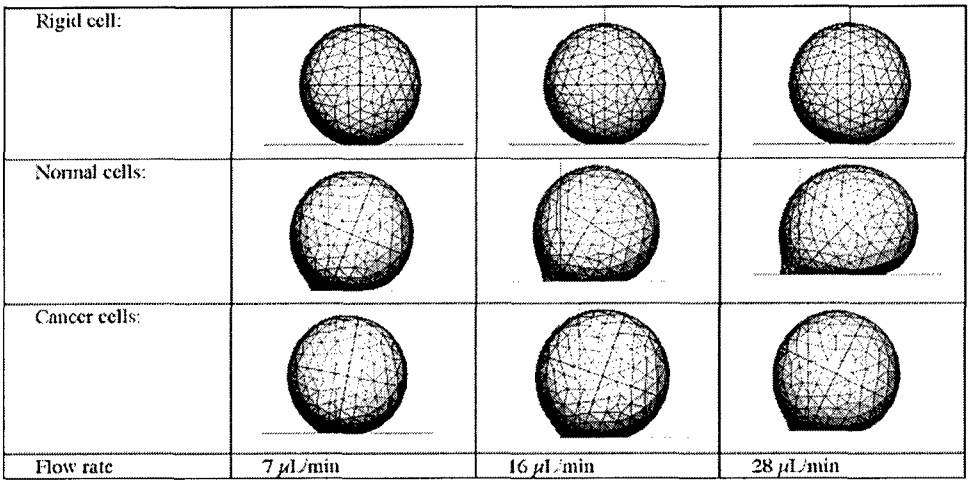


**Figure 7.** Side view of initially spherical cell showing flow-induced deformation. Cancer cells are more than three times stiffer than normal cells.

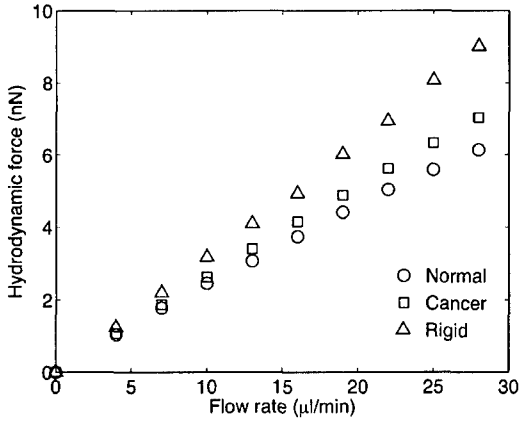


**Figure 8.** Simulated hydrodynamic forces for (△) rigid, (○) normal, and (□) cancer cells.

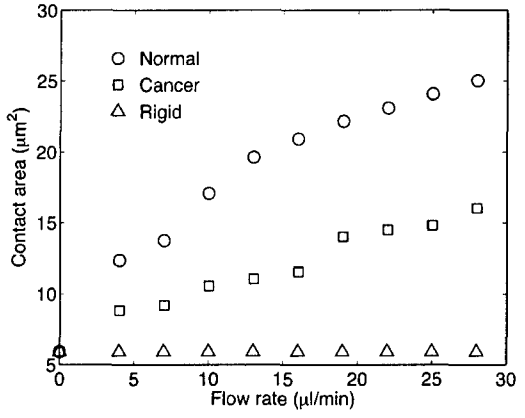


**Figure 9.** Simulated contact area as a function of flow rate for (△) rigid, (○) normal, and (□) cancer cells.

splines, as implemented using the "pchip" option in the Matlab function interp1 (*26*).

The potential of the model is evident when considering the behavior of the cancer cells in the 16−20 $\mu$L/min flow range, where the number of detached cells actually drops as the flow rate increases. From the data it is unclear whether this counterintuitive result is real or an artifact of experimental variation or measurement error. However the model predicts the same increase, and here we can investigate the cause from first principles. The phenomenon is seen to be due to the rapid increase in contact area in this flow range, which causes an increase in adhesion force that more than counteracts the increase in hydrodynamic force. The normal cell has an even greater contact area change in the 6−12 $\mu$L/min flow range, but because the value of $\rho_A$ is smaller for normal cells, the force change is not enough to decrease cell detachment. (The normal cells increase their contact area twice as much as the cancer cells, but the cancer cells have almost three times the surface antigen density.) However, the effect is visible even in the normal cells as a flattening of the detachment versus flow rate curve.

## 5. Discussion

To use the cell detachment model for device design and optimization, it must be incorporated into an appropriate figure of merit to quantify performance. The operational principle of this cancer-screening assay is to remove normal cells while retaining cancerous cells. Thus a high fraction of cells remaining after the flow phase indicates the presence of cancerous (or at least HPV-infected) cells. Furthermore, those cells may then be captured for subsequent testing. This suggests the following formula, which we refer to as the "discrimination factor":

$$D = \frac{N_{cf}}{N_{ci}} - \frac{N_{nf}}{N_{ni}} \tag{4}$$

where $N_{c_i}$ and $N_{c_f}$ are the initial and final number of bound cancer cells, and $N_{n_i}$ and $N_{n_f}$ are the initial and final number of bound normal cells. If the device works perfectly, removing all normal cells and preserving all cancer cells, $D = 1$. If the device actually acts against the desired result, by eliminating all cancer cells and preserving all normal cells, we have $D = -1$. Between these extremes of performance, $D$ will also vary, with the case in which no processing at all is done on the sample giving a discrimination factor of zero.

The discrimination factor has a simple representation in terms of the cell detachment model presented above:

$$D = P_{a,c}\left(\frac{F_{H,c}}{F_{A,c}}\right) - P_{a,n}\left(\frac{F_{H,n}}{F_{A,n}}\right) \tag{5}$$

where the additional subscript distinguishes between values for normal and cancer cells. The discrimination factor can be plotted versus flow rate from the experimental data directly using eq

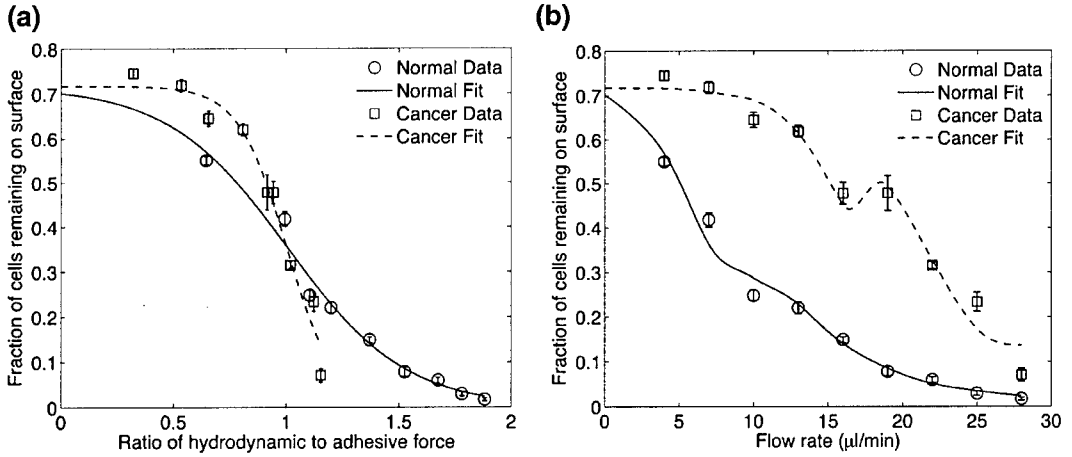


**Figure 10.** Sigmoidal fit of cell detachment model to experimental data. (a) Fit versus predicted force ratio shows a simple sigmoidal form. (b) Fit versus flow rate shows a more complex dependence arising from interplay of predicted hydrodynamic force and elastic deformation.

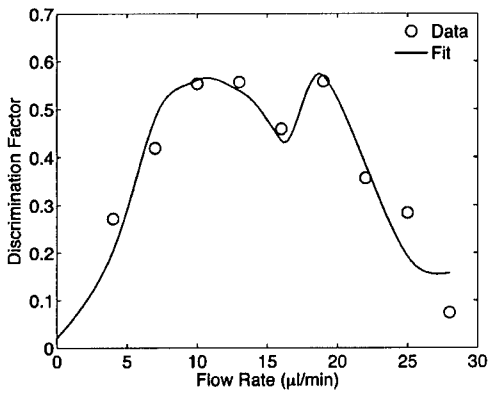


**Figure 11.** Comparison of experimental (4) and modeled (5) discrimination factor.

4. After curve fitting, eq 5 can be used to predict $D$ versus flow rate. Figure 11 compares the experimental and model-based curves.

The model captures the counterintuitive "double-peaked" behavior of the experimental data and provides an explanation for the effect. As was discussed for the detachment behavior of the cancer cells, the second peak is due to the rapid increase in cancer cell contact area in the 16−20 $\mu$L/min range. This improves cancer cell adhesion and increases retention, while the normal cells continue to detach. The normal cells have a large increase in contact area in the 6−12 $\mu$L/min range. Because of their lower surface antigen density, the force ratio is not reduced as significantly as for the cancer cells, but this effect contributes to the trough at 16 $\mu$L/min.

The flow rate should be chosen to maximize the discrimination factor. Figure 11 shows that this is a nonconvex objective, so some design tradeoffs may be considered. In this case there are two peaks with similar maximum values, one at 10.8 $\mu$L/min and the other at 18.7 $\mu$L/min. There are several ways to choose between them. One is to note that the lower-flow peak is broader, and hence device performance should be less sensitive to errors in the flow rate in this region. Another is to note that the higher-flow peak corresponds to lower overall numbers of cells, and therefore follow-up testing may be more difficult. Both of these favor the lower-flow peak. However the higher flow rate could also be chosen on the basis of its slightly higher discrimination factor. Finally, a two-part assay could be used, with the first run at the higher flow rate to provide maximum sensitivity and, if positive, a second run at the lower flow rate to gather cells for additional independent testing.

Another potential use of the model is to provide a *quantitative* measurement of the level of HPV infection, by estimating the surface antigen density directly from the detachment behavior. This would require better knowledge of the relationship between elasticity and HPV infection, but the result could provide not only a flag for cervical cancer but also an indication of the progression of the disease. Such a test would have significant clinical and research value.

## 6. Conclusions

A simple cell detachment model based on static hydrodynamic and elastic FEA of a single cell shows excellent agreement with experimental results when applied to a prototype microfluidic assay for cervical cancer. This approach is more practical and more computationally tractable than transient and/or multicell simulations. The model provides physical insight, explaining apparently counterintuitive features of the prototype assay data. It may be incorporated directly into a device level figure-of-merit, for use in interpolating predicted performance and choosing design parameters. Finally, further refinements of the model might allow a quantitative measure of surface adhesive forces, with the potential to greatly enhance the value of the basic assay.

## Acknowledgment

The authors gratefully acknowledge the support of the National Science Foundation under grants 0087902 (S.P.W., J.M.B., T.D., L.G.) and 0134594 (M.W.V.) and the Welch Foundation under grant D-1158 (K.H.C.). The authors thank Prof. Sukalyan Bhattacharya of Texas Tech University for help in quantifying cell-cell interactions.

## References and Notes

(1) Follen, M.; Tortolero-Luna, G.; Wright, T.; Sarkar, A.; Richards-Kortum, R.; K Hong, W.; Schottenfeld, D. Cervical human papillomavirus infection and intraepithelial neoplasia: A review. *J. Natl. Cancer Inst. Monogr.* **1996**, no. 21.

(2) Yoon, C. S.; Kim, K. D.; Park, S. N.; Cheong, S. W. Alpha (6) integrin is the main receptor of human papilloma virus type 16 VLP. *Biochem. Biophys. Res. Commun.* **2001**, *283*, 668−673.

(3) Follen, M.; Richards-Kortum, R. Emerging technologies and cervical cancer. *J. Natl. Cancer Inst.* **2000**, *92* (Mar 1), no. 5.

(4) Du, Z.; Colls, N.; Cheng, K. H.; Vaughn, M. W.; Gollahon, L. Microfluidic-based diagnostics for cervical cancer cells. *Biosens. Bioelectron.* **2006**, *21*, 1991−1995.

(5) Goldman, A. J.; Cox, R. G.; Brenner, H. Slow viscous motion of a sphere parallel to a plane wall. I. Motion through quiescent fluid. *Chem. Eng. Sci.* **1967**, *22*, 637−651.
(6) Goldman, A. J.; Cox, R. G.; Brenner, H. Slow viscous motion of a sphere parallel to a plane wall. II. Couette flow. *Chem. Eng. Sci.* **1967**, *22*, 653−660.
(7) Hammer, D. A.; Apte, S. M. Simulation of cell rolling and adhesion on surfaces in shear flow: General results and analysis of selectin-mediated neutrophil adhesion. *Biophys. J.* **1992**, *63*, 35−57.
(8) Hammer, D. A.; Lauffenburger, D. A. A dynamic model for receptor-mediated cell adhesion to surfaces. *Biophys. J.* **1987**, *52*, 475−487.
(9) Hammer, D. A.; Dembo, M.; Torney, D. C.; Saxman, K. The reaction-limited kinetics of membrane-to-surface adhesion and detachment. *Proc. R. Soc. London, Ser. B* **1988**, *234*, 55−83.
(10) Tees, D. F. J.; Goetz, D. J. Leukocyte adhesion: An exquisite balance of hydrodynamic and molecular forces. *News Physiol. Sci.* **2003**, *18*, 186−190.
(11) Brooks, S. B.; Tozeren, A. Flow past an array of cells that are adherent to the bottom plate of a flow channel. *Comput. Fluids* **1996**, *25* (8), 741−757.
(12) Gaver, D. P., III; Kute, S. M. A theoretical model study of fluid stresses on a cell adhering to a microchannel wall. *Biophys. J.* **1998**, *75* (Aug), 721−733.
(13) N'Dri, N. A.; Shyy, W.; Tran-Soy-Tay, R. Computational model of cell adhesion, movement using a continuum-kinetics approach. *Biophys. J.* **2003**, *85* (4), 2273−2286.
(14) Jadhav, S.; Eggleton, C. D.; Konstantopoulos, K. A 3D computational model predicts that cell deformation affects selectin-mediated leukocyte rolling. *Biophys. J.* BioFAST, published on October 15, 2004 as doi 10.1529/biophysj.104.051029.
(15) Chu, Y. S.; Dufour, S.; Thiery, J. P.; Perez, E.; Pincet, F. Johnson−Kendall−Roberts theory applied to living cells. *Phys. Rev. Lett.* **2005**, *94* (2):028102.
(16) Image J documentation. National Institutes of Health: Washington, DC; http://rsb.info.nih.gov/ij.
(17) *CFD-ACE(U) Module Manual*, Version 2002; CFD Research Corporation: Huntsville, AL, June 2002.
(18) Bhattacharya, S.; Blawzdziewicz, J.; Wajnryb, E. Hydrodynamic interactions of spherical particles in Poiseuille flow between two parallel walls. *Phys. Fluids*, in press.
(19) Freshney, R. I. *Culture of Animal Cells: A Manual of Basic Techniques*, 4th ed.; Wiley-Liss: New York, 2000.
(20) Chang, K.-C.; Tees, D. F. J.; Hammer, D. A. The state diagram for cell adhesion under flow: Leukocyte rolling and firm adhesion. *Proc. Natl. Acad. Sci. U.S.A.* **2000**, *97*(21), 11262−11267.
(21) Fritz, J.; Katopodis, A. G.; Kolbinger, F.; Anselmetti, D. Force-mediated kinetics of single P-selectin/ligand complexes observed by atomic force microscopy, *Proc. Natl. Acad. Sci. U.S.A.* **1998**, *95* (6), 12283−12288.
(22) Mittelman, L.; Levin, S.; Verschueren, H.; De Baetselier, P.; Korenstein, R. Direct correlation between cell membrane fluctuations, cell filterability, and the metastatic potential of lymphoid cell lines. *Biochem. Biophys. Res. Commun.* **1994**, *203*, 899−906.
(23) Knight, M. M.; van de Breevaart Bravenboer, J.; Lee, D. A.; van Osch, G. J.; Weinans, H.; Bader, D. L. Cell and nucleus deformation in compressed chondrocyte-alginate constructs: Temporal changes and calculation of cell modulus. *Biochim. Biophys. Acta* **2002**, *1570* (1), 1−8.
(24) Braet, F.; Seynaeve, C.; De Zanger, R.; Wisse, E. Imaging surface and submembranous structures with the atomic force microscope: a study on living cancer cells, fibroblasts and macrophages, *J. Microsc.* **1998**, *190*, 328−338.
(25) Bell, G. I. Models for the specific adhesion of cells to cells. *Science* **1978**, *200*, 618−627.
(26) *Matlab User's Guide*, Release 14, Service Pack 3; The MathWorks: Natick, MA, 2005.

Received April 24, 2006. Accepted July 11, 2006.

BP060127D